

AD628803

AFWL-TR-65-146

AFWL-TR
65-146

INVESTIGATION OF EQUATION OF STATE OF POROUS EARTH MEDIA

G. D. Anderson
G. E. Duvall
J. O. Erkman
G. R. Fowles
C. P. Peltzer

Stanford Research Institute
Menlo Park, California
Contract AF29(601)-6427



TECHNICAL REPORT NO. AFWL-TR-65-146

February 1966



AIR FORCE WEAPONS LABORATORY
Research and Technology Division
Air Force Systems Command
Kirtland Air Force Base
New Mexico

CLEARINGHOUSE FOR FEDERAL SCIENTIFIC AND TECHNICAL INFORMATION			
Hardcopy	Microfiche		
\$5.00	\$1.00	177pp	as
ARCHIVE COPY			

PROCESSING COPY

BLANK PAGE

2

1994

INVESTIGATION OF EQUATION OF STATE OF
POROUS EARTH MEDIA

G. D. Anderson
G. E. Duvall
J. O. Erkman
G. K. Fowles
C. P. Peltzer

Stanford Research Institute
Menlo Park, California
Contract AF29(601)-6427

TECHNICAL REPORT NO. AFWL-TR-65-146

Distribution of this document
is unlimited.

FOREWORD

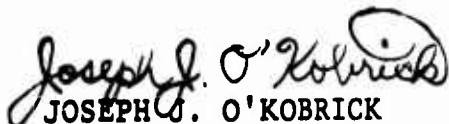
This report was prepared by Stanford Research Institute, Menlo Park, California, under Contract AF29(601)-6427. The research was performed under Program Element 7.60.08.01.D, Project 5710, FERRIS WHEEL, and was funded by the Defense Atomic Support Agency (DASA).

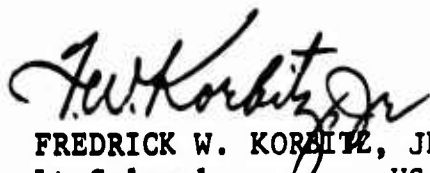
Inclusive dates of research are 15 June 1964 to 26 July 1965. The report was submitted in December 1965 by the AFWL Project Officer, Captain Joseph J. O'Kobrick, (WLDC).

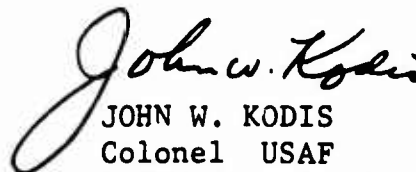
The contractor's number is SRI Project No. GSU-5059.

The principal investigator on this project was G. R. Fowles. Experiments were conducted by G. D. Anderson, J. T. Rosenberg, and A. L. Fahrenbruch. The theoretical techniques for extrapolating the equation of state to pressure and temperature regimes beyond the experimental range were derived by C. P. Peltzer, and the shock calculations were carried out by J. O. Erkman. G. E. Duvall and V. Horie, of Washington State University, carried out the theoretical work on the effects of phase changes on shock propagation under subcontract to Stanford Research Institute.

This report has been reviewed and is approved.


JOSEPH J. O'KOBRIK
Captain USAF
Project Officer


FREDRICK W. KOBITZ, JR.
Lt Colonel USAF
Chief, Civil Engineering Branch


JOHN W. KODIS
Colonel USAF
Chief, Development Division

ABSTRACT

Earlier experimental work has been extended to evaluate the effect of moisture on the Hugoniot of playa. For engineering applications the Hugoniot of moist playa can be predicted with sufficient accuracy from the Hugoniot of dry playa and water and the assumption of pressure equilibrium.

Isentropic release data were obtained for moist and dry playa. The steep release curve (in the P-V plane) from high pressure implies an irreversible phase change. Some low pressure data in the elastic-plastic region are presented.

A theoretical discussion of various forms of the Mie-Grüneisen equation and the physical basis of asymptotic statistical models is presented.

Shock stability is reviewed. Phase transitions in which $\Delta V < 0$ are classified according to the signs of the slopes of the coexistence curves. Relative slopes of Hugoniots and isentropes in the mixed phase region are calculated. The results of the theoretical discussion are applied to transitions in bismuth, iron, and quartz. Agreement of values of dP/dT deduced from shock data and measured directly are good for bismuth and poor for quartz and iron.

Calculations of spherical shock propagation in a hypothetical medium that undergoes a phase change are presented. The calculations show qualitatively some types of pulse shapes that may be expected in a transforming medium.

It is concluded that the proper treatment of phase changes is an outstanding problem in predicting equations of state for earth materials.

This page intentionally left blank.

CONTENTS

1.	INTRODUCTION	1
2.	SUMMARY	5
3.	EXPERIMENTS	9
	A. Introduction	9
	B. Sample Preparation	10
	C. High Pressure Shock Wave Experiments	13
	D. Data and Results	23
	E. Low Pressure Shock Wave Experiments	42
4.	THEORY	51
	A. Introduction	51
	B. Derivation of Equations of State (EOS)	53
	C. Some Thermodynamics of EOS	54
	D. Derivation of a Semiempirical EOS	60
	E. Semiempirical EOS for SiO_2	63
	F. Conclusions and Recommendations	68
5.	EFFECTS OF A PHASE TRANSITION ON THE PROPAGATION OF FINITE AMPLITUDE WAVES	71
	A. Introduction	71
	B. Stability of Shock Waves	72
	C. Thermodynamic Functions in the Coexistence Region	78
	D. Examples	105
	E. Discussion	112
6.	FLOW CALCULATIONS	115
	A. Introduction	115
	B. Equations of State	117
	C. Spherical Piston	122
	D. Results of Calculations	124
	E. Conclusions	135

CONTENTS

APPENDIX	HIGH DENSITY MODELS FOR SEMIEMPIRICAL COLD EQUATIONS OF STATE FOR SOLIDS	143
REFERENCES		169
DISTRIBUTION		173

ILLUSTRATIONS

Fig. 3-1	Experimental Assembly to Measure Release Isentropes of NTS Playa	15
Fig. 3-2	Smear Camera Still and Arrival Record of Shock Passing through Adiabatic Shot	19
Fig. 3-3	Pressure Vs. Particle Velocity in NTS Playa	29
Fig. 3-4	Pressure Vs. Particle Velocity in NTS Playa	30
Fig. 3-5	Pressure Vs. Particle Velocity in NTS Playa	31
Fig. 3-6	Pressure Vs. Particle Velocity in NTS Playa	32
Fig. 3-7	Pressure Vs. Particle Velocity in NTS Playa	33
Fig. 3-8	Hugoniot and Release Isentropes for NTS Playa	34
Fig. 3-9	Hugoniot and Release Isentropes for NTS Playa	35
Fig. 3-10	Release Isentropes for NTS Playa	37
Fig. 3-11	Release Isentropes for NTS Playa	38
Fig. 3-12	Gun and Target Assembly	43
Fig. 3-13	Details of Shot Assembly Showing Sample and Gage	45
Fig. 3-14	Oscilloscope Records Showing the Pressure-Time Profile for Quartz Gage Shots	48
Fig. 5-1(a)	Assumed R-H Curve	73
Fig. 5-1(b)	Compression Profile for Assumed Instability at A	73
Fig. 5-2	Compression of Slopes at a Point of Instability	78
Fig. 5-3	Definition of the Transition Parameter X	80
Fig. 5-4	Relative Positions of Phase Boundaries in S-T Plane; $\Delta V < 0$	84
Fig. 5-5	Relative Slopes of Isotherm, Phase Boundary and Adiabatic in P-V Plane	88
Fig. 5-6	Triply-Mapped Region in the P-V Plane for Type 1	89
Fig. 5-7	Equation of State Surface in P-V-T Space	90
Fig. 5-8	Phase Boundaries in S-T and P-V Planes	91

ILLUSTRATIONS

Fig. 5-9	Adiabat in the Coexistence Region	92
Fig. 5-10	Relative Slopes at the Phase Boundary	96
Fig. 5-11	Second Shock Originating at a Phase Boundary	97
Fig. 5-12	Calculation of Hugoniot in C-Region	97
Fig. 5-13	Anomalous R-H Curve for Type 1 Transition	102
Fig. 5-14	Adiabats and Hugoniot for Type 3 Transition	103
Fig. 5-15	Coexistence Region for BiI - BiII	109
Fig. 5-16	Phase Diagram for Bismuth	110
Fig. 5-17	Phase Diagram for Iron ($\alpha \rightarrow \text{hcp}$)	111
Fig. 6-1	Cold Isotherm for Quartz and Stishovite	118
Fig. 6-2	Single Function Representation of Phase Change, Zero-Degree Isotherm	120
Fig. 6-3	Multifunction Representation of Phase Change, Zero-Degree Isotherm	121
Fig. 6-4	Schematic of Reversible and Irreversible Phase Change	123
Fig. 6-5(a)	Pressure Vs. Distance from Center of Cavity	125
Fig. 6-5(b)	Particle Velocity Vs. Distance from Center of Cavity	126
Fig. 6-6(a)	Pressure Vs. Distance from Center of Cavity	127
Fig. 6-6(b)	Particle Velocity Vs. Distance from Center of Cavity	128
Fig. 6-7(a)	Pressure Vs. Distance from Center of Cavity	130
Fig. 6-7(b)	Particle Velocity Vs. Distance from Center of Cavity	131
Fig. 6-8(a)	Pressure Vs. Distance from Center of Cavity	132
Fig. 6-8(b)	Particle Velocity Vs. Distance from Center of Cavity	133
Fig. 6-9(a)	Pressure Vs. Distance from Center of Cavity	135
Fig. 6-9(b)	Particle Velocity Vs. Distance from Center of Cavity	136
Fig. 6-10	Time of Arrival of Peak Pressure Based on Quartz Equation of State	138
Fig. 6-11	Time of Arrival of Peak Pressure Based on Stishovite Equation of State	139
Fig. 6-12	Peak Pressure as Function of Radius Based on Quartz Equation of State	140
Fig. 6-13	Peak Pressure as Function of Radius Based on Stishovite Equation of State	141

TABLES

Table 3-I	Hugoniot Data for NTS Playa	24
Table 3-II	Hugoniot Data for NTS Playa	25
Table 3-III	Hugoniot Data for NTS Playa	26
Table 3-IV	Hugoniot Data for NTS Playa	27
Table 3-V	Hugoniot Data for NTS Playa	28
Table 3-VI	Release Isentrope for NTS Playa	36
Table 3-VII	Low Pressure Data for Dry NTS Playa	49
Table 5-I	Classification of Polymorphic Transitions $\Delta V < 0$, $(\partial V / \partial T)_{P_1} > 0$, $C_{P_1} > 0$	83
Table 5-II	Physical Data on Phase Transition	107

This page intentionally left blank.

1-INTRODUCTION

The goal of this program is to measure in some detail the equation of state of Nevada Test Site playa, to extrapolate the results to pressure and temperature regimes beyond the experimental range using existing theoretical methods, and to examine the sensitivity of shock propagation in spherical geometry to reasonable variations and uncertainties in the equation of state.

In the previous year's work Hugoniot measurements were obtained on dry samples of playa of two different porosities, of initial densities 1.55 and 1.95 g/cm³ (crystal density, 2.66 g/cm³) in the pressure range 40 to 500 kbar. These results showed several interesting features: (1) the differences in thermal pressure due to differences in initial porosity are small and imply a small value (< 1) of the effective Grüneisen parameter, (2) the pressure-volume curve appears to be multivalued in the 200- to 400-kbar range. This result shows that a simple Mie-Grüneisen equation of state with Γ a function of volume only is inadequate and probably implies the existence of polymorphism--presumably the quartz-stishovite transition, which is known to occur in this pressure range.

During the current effort these results were extended in three directions:

1. The effects of moisture were examined by measuring Hugoniot states of samples of the same initial (dry) density as before, viz., 1.55 and 1.95 g/cm³, but with approximately 10 percent by weight of water added. In addition, samples containing as large a fraction of moisture as possible consistent with controllable sample quality were tested.

2. The experiments also determined several points on the release isentropes from shocked states. For earth materials particularly, experimental determination of these curves is just as important as determination of Hugoniots because of the possibility of irreversible phase transitions and because of uncertainties in the proper theoretical treatment of the effects of

moisture. Both of these problems severely complicate the derivation of isentropes from Hugoniot so that customary procedures used, for example, for metals and simple ionic solids are of questionable validity. Some unexpected peculiarities were in fact observed at higher pressures.

3. Preliminary experiments were also performed in the very low pressure range to investigate the pressure region in which compaction to crystal density occurs. Unfortunately, insufficient effort could be devoted to this problem to give clearly reliable results. Some measurements were obtained, but the results should be regarded as tentative.

The experimental methods and results are described in Section 3.

In Section 4 a general discussion of various approaches to predicting equations of state is given. Also in that section is a comprehensive review of the thermodynamics of the Mie-Grüneisen equation of state and a discussion of the different forms in which it is used by various authors.

The physical bases for theories of high pressure asymptotic forms of equation of state are reviewed in the appendix in elementary form to assist the nonspecialist to understand the assumptions underlying these theories and to assist him in appreciating the difficulties in assessing their validity.

Clearly one of the most difficult and potentially important problems in constructing an equation of state is that of phase changes, including polymorphism, melting, and vaporization. The existence of polymorphism, the location of phase boundaries, and the relevant thermodynamic parameters describing transitions must at present be determined experimentally, and measurements in most cases are lacking. Moreover, the effects of phase changes on Hugoniot and isentropic forms of equation of state and on shock propagation has so far received little attention.

The work reported in Section 5 is a fundamental and general treatment of the thermodynamics of phase changes with particular reference to their effects on the Hugoniot. Application of this theory to existing shock measurements in iron and quartz shows substantial discrepancies between theory and experiment--possibly due to nonequilibrium effects.

In Section 6 the results of spherical shock calculations for an equation-of-state model containing the major elements of a phase transition are presented. These show the qualitative shock structure to be expected for a reversible phase change. A summary of the results of parameter variation studies, including the previous year's effort, is also given in that section.

This page intentionally left blank.

2-SUMMARY

This report describes an extension of work reported previously on the equation of state of playa from Area 5 of the Nevada Test Site. As in the previous effort the work was concerned with (1) experimental determination of the equation of state, (2) theoretical interpretation of the experimental data, and extrapolation by semitheoretical means to pressure and temperature regimes beyond the experimental range, and (3) shock calculations to indicate the sensitivity of spherical shock propagation to reasonable variations in the equation of state.

The experimental work was extended to include the determination of release isentropes from shocked states in both dry and moist playa. These curves appear relatively uncomplicated where the peak pressure is less than 100 kbar, indicating only some degree of compaction by the fact that the free-surface velocity is less than twice the shock particle velocity.

The release curves from a shock pressure of about 270 kbar, however, shows two interesting features. For dry playa the initial slope (high pressure) of the isentrope is very steep in both the $P-u$ and $P-V$ planes. The fact that it is steeper than the Hugoniot in the $P-V$ plane is clear evidence of some form of change of state since such behavior for a simple fluid would violate the shock stability condition. The most reasonable explanation, consistent with other independent observations, is that the quartz component of the playa is converting irreversibly to stishovite. At lower pressures the isentrope from 270 kbar becomes shallow, possibly due to reconversion of stishovite to quartz.

The isentropes for moist playa also appear to be uncomplicated from shock pressures of about 100 kbar. For the higher shock pressures the free-surface velocity is appreciably higher than twice the shock particle velocity.

It seems likely that this is due to vaporization of the water on release of pressure, and resulting rapid expansion of steam ahead of the surface of the solid. The experiments also determined the Hugoniot curves for moist playa. These results show that the effect of water on the Hugoniot can be predicted accurately enough for engineering applications by assuming that the solid and the liquid are shocked along their respective Hugoniots and that pressure equilibrium is obtained. The question of thermal equilibrium is thereby ignored, and the model is clearly oversimplified. Nevertheless, it is found empirically that satisfactory agreement is obtained.

A few shock experiments at very low pressures were performed to investigate the region in which compaction to crystal density occurs. The results should be regarded as tentative, but indicate a precursor wave of about 0.1 kbar amplitude traveling at a velocity of 0.5 km/sec. More thorough investigation of this pressure range should be conducted before definite conclusions are drawn.

The theoretical work during this period presents a general review of approaches to the problem of predicting an equation of state. It also presents a thorough treatment of the thermodynamics of the general Mie-Grüneisen formulation and shows the differences in the forms used by different authors. Finally, an elementary description is given of the assumptions upon which asymptotic high pressure and temperature forms are based.

Because of the evidence for polymorphism in the solid constituents and vaporization of moisture in the playa, and because these effects cannot now be easily treated theoretically, a considerable effort was devoted to the effects of a phase change on both the equation of state and on shock propagation. Comparison of the predicted Hugoniots in the coexistence region for iron and quartz with experimental measurements shows substantial discrepancies. These may be due to incorrect interpretation of the data, or to nonequilibrium effects. The results for bismuth agree reasonably with theory.

Shock propagation calculations were extended to include in a qualitative way the major features of a phase transition, and typical pressure profiles and decay curves are shown.

In general, the two-year program has established the Hugoniot equation of state from 40 to 500 kbar including the effects of variable porosity and moisture content. Some release isentropes were measured and preliminary measurements in the very low pressure region obtained. A relatively simple theoretical equation of state was developed that, in the absence of phase changes, appears adequate for playa and perhaps other earth materials. A major remaining difficulty, however, is the prediction and proper treatment of phase changes; progress was made in the application of thermodynamics to this problem. Shock calculations for a simple energy source and spherical geometry showed that peak pressures as a function of radial distance are not highly dependent on uncertainties or variations in the equation of state and some insight into reasons for this insensitivity was gained. Of potential importance to interpretation of field measurements are the pulse shapes associated with phase changes because it is often tacitly assumed that the peak pressure is closely associated with the first shock arrival.

Possible directions for extension of this work include:

- 1) More thorough investigation of the very low pressure range where the material is not completely compacted.
- 2) Further investigation of phase changes, due to polymorphism and to vaporization, theoretically and experimentally.
- 3) Model tests in which shock propagation and decay can be compared with predictions based on the equation of state as established thus far.

AFWL-TR-65-146

This page intentionally left blank.

3-EXPERIMENTS

G. D. Anderson, J. T. Rosenberg, and A. L. Fahrenbruch

A. INTRODUCTION

The purpose of the experimental program to be discussed is to gather shock wave data on Nevada Test Site playa which can be combined with existing theory to yield an equation of state suitable for machine flow calculations. The current experimental phase is a continuation of a program which was begun in mid 1963. The explosive systems and streak camera techniques used in obtaining Hugoniot data were described in an earlier report¹ which summarized the work at the end of the first year. During the first year the effort was directed toward gathering Hugoniot data on dry playa. It was found that it was necessary to reconstitute samples by pressing sifted soil in order to obtain satisfactory streak camera records. The native material contained inhomogeneities in density which were large on the scale of the experiments. These inhomogeneities lead to irregular or "ragged" shock fronts passing through the samples which destroyed the necessary precision. Samples which were pressed from soil which had been sifted proved to be quite satisfactory. X-ray analysis and streak camera records both indicated a uniform density. The initial densities of the dry material were 1.95 g/cm^3 and 1.55 g/cm^3 . The fully completed crystal density was measured to be 2.65 g/cm^3 . The densities of the pressed samples studied were greater than the native dry density of the soil (1.39 g/cm^3) as it was found to be necessary to press to higher densities in order to obtain samples which were mechanically strong enough to be used in experiments. The two densities were chosen so as to generate two Hugoniots for the purpose of estimating the role of thermal pressure. No large difference between

Hugoniot was observed. In the course of the present work the measurement of the Hugoniot of dry material has been repeated with good agreement with earlier data.

The work of the first year, which has just been briefly summarized, was expanded in three directions during the second year. Each of the three new phases brought new problems which required technique development. The three phases were the measurement of the Hugoniot of moist playa and evaluation of the effect of water, the study of release isentropes including free-surface velocity, and the study of the low pressure behavior of dry playa in the 1 kbar region where compaction may not be complete and nonhydrostatic behavior is expected. The Hugoniot measurements of moist playa presented the fewest experimental problems as the tests relied heavily upon techniques developed during the first year's effort. The isentrope measurements and the low pressure studies involved new types of experiments. As the work on these phases progressed it became clear that extensive studies would require an effort much larger than the present one. However, significant progress was made toward the perfection of the new techniques and some preliminary data were obtained.

B. SAMPLE PREPARATION

During the current phase of this program an effort has been made to improve the existing techniques of dry sample preparation and to develop a method of constructing high quality samples of uniform moisture content and density. For reasons already discussed, the playa as it is received from the field is unsuitable for small scale shock wave tests.

The initial step in preparing a soil stock from which to construct test samples is to shake the soil through a series of sieves. All that passes through a No. 50 sieve (297 micron openings) is recovered. The material at this stage contains 5 to 6 percent moisture by weight. A portion of this soil is dried in an oven at 105°C to be used at a later time as a diluent to a high moisture content stock in the preparation of specimens of various intermediate moisture contents.

(1) Control of Moisture Content

To prepare homogeneous high moisture soil, a weighed amount of the ambient soil is placed in a 400- to 600-ml beaker, leveled, and covered with four or five layers of filter paper cut to fit snugly in the beaker. It is important that the height to diameter ratio of the soil does not exceed one. The filter papers are then covered with several layers of paper towel. Water is added to the paper towel which absorbs the moisture and allows it to slowly diffuse down through the filter paper into the soil. No more than 8 to 10 g of water should be added at one time and not more than 1/8 of the total water should be added in any 12 to 24 hour period. After addition of the water the beaker is sealed and allowed to stand for at least one day. Before more water is added, the soil is poured into a larger beaker and thoroughly stirred. It is then replaced in the smaller beaker and covered with the filter paper and towels prior to adding more water. This slow process of water addition is repeated until the desired moisture content is achieved. Upon completion of this process the moist soil is stored in stoppered flasks. Soil samples of intermediate moisture content are made by mixing the moist material just described with the oven dried soil in the appropriate proportions and storing for one day in a stoppered flask.

(2) Sample Pressing

Since the low density samples are fragile and require some external support after removal from the pressing die, they are pressed in steel rings of 1/8-inch wall thickness. Prior to pressing, one face of the ring is covered with 0.0007-inch Mylar which is aluminized on one side. The Mylar is bonded to the ring to form a seal and then the assembly is weighed. The Mylar covered ring is bolted in the pressing die so that the ring and die axes are parallel. A predetermined quantity of soil is then poured into the die and spread uniformly with a leveling tool. At the time of pressing, all soil contains some moisture since it has been found that samples pressed from dry material crack upon pressure release. Dry samples are pressed from soil initially containing a small amount of moisture and then dried in an oven at 105°C for several hours after pressing. The density is controlled by pressing a weighed amount of soil into a given volume fixed by a series of stops on the pressing die.

All samples are weighed immediately after pressing and those to be dried are then placed in an oven. Moist samples are sealed in the rings by 0.0003-inch Mylar to prevent moisture loss, reweighed, and mounted on the driver plate. Moist samples are not made until just prior to shooting in order to minimize moisture loss which would occur during long periods of storage.

Samples of density less than 1.9 g/cm^3 are pressed in steel rings which serve a dual purpose. They provide lateral support for the samples which at low densities are relatively fragile. Also they are a convenient support point at which to glue the aluminized Mylar which covers the playa to hermetically seal it and to record the arrival of the shock wave. The pressing process assures that the playa will be in intimate contact with this aluminized Mylar top. Similarly, care is taken that there will be good surface to surface contact between the bottom of the sample and the lapped 2024 aluminum driver plate by pressing the sample to a thickness several mils greater than that of the support ring. In the case of dry samples, which may be kept free of moisture during delays between pressing and mounting on the shot assembly by storage either in an oven or a desiccator, the playa could be mounted in direct contact with the aluminum driver surface.

Samples of density greater than 1.9 g/cm^3 require no lateral support and are pressed free standing. In the shot assembly a plastic ring, again thinner than the sample, is used as an anchor to which to attach the aluminized Mylar. These samples are not stored between pressing and mounting, hence both dry and moist specimens are attached directly to the driver plate surface with no intermediate layer of Mylar.

C. HIGH PRESSURE SHOCK WAVE EXPERIMENTS

(1) Hugoniot Experiments

The Hugoniot data for all samples were obtained by the impedance match method² which is described quite completely in Section 3.B (2) of Reference 1. This method permits determination of a point on the Hugoniot of an unknown material from knowledge of the shock velocity alone, if the shock is introduced into the unknown through a standard material whose Hugoniot and relief cross curves are well known. 2024 Aluminum was used as a standard; its Hugoniot and calculated isentropic relief curves were obtained by private communication from Dr. R. G. McQueen at Los Alamos Scientific Laboratory.

The 2024 aluminum driver plate used as a standard on the Hugoniot experiments is nominally 8 inches in diameter and 3/8 inches thick, the dimensions varying somewhat from shot to shot. A plane shock wave is induced into the driver either by detonation of an explosive train in contact or by impact of an explosively driven flying plate as described in Section 3.B. (1) of Reference 1. The measurements necessary to apply the impedance mismatch method -- (free-surface velocity of the aluminum driver plate and shock velocity in the play sample) -- are made in the manner described in Reference 1. Some detail refinements have been made in order to attain a higher degree of precision in these measurements. For example, each experiment includes two independent measurements of the free-surface velocity of the driver. The thickness of shims used to protect gapped mirrors from air shock has been reduced from 0.006 to 0.004 inches with the result that perturbations upon the values of velocities measured by these mirrors is negligibly small after corrections. No samples or arrival mirrors are located at the center of the aluminum driver in experiments involving flying plates since it has been noted that in some cases the shock wave arriving at the front surface of the driver plate has a small radially symmetric dimple, in both pressure and shape. The precision of the playa pressing process has been increased during the course of

the project. The results of the Hugoniot measurements, in the form of graphs and tables, are presented and discussed in a later section of this report.

(2) Release Isentrope Experiments

The problem of determining release isentropes for playa necessitated the development of new techniques. The method chosen is again based on the impedance mismatch principle. A shock of known strength in a standard aluminum driver plate is used to introduce a shock into the playa sample in the same manner as in the Hugoniot experiments. However in the adiabat shots a material of lower shock impedance than soil is mounted in contact with the front surface of the soil. As porous playa is of relatively low shock impedance, the only suitable materials of lower shock impedance are liquids. The initial shock propagates through the driver and playa as before until it reaches the playa-liquid interface. There a rarefaction is reflected back into the soil, and a shock is transmitted into the liquid. If the Hugoniot of the liquid is known, a measurement of the shock velocity is sufficient to specify the state in the liquid behind the shock. As the boundary conditions require continuity of pressure and particle velocity at the playa-liquid interface, this state in the liquid must be a pressure and particle velocity state on the release isentrope of soil. The zero pressure point on the release isentrope is determined by observing the free-surface velocity of the playa which is constrained to remain at essentially zero pressure.

Experimentally it is much more difficult to obtain the measurements necessary to determine adiabats than Hugoniots. All adiabat measurements are made after the shock has passed through the playa specimen thereby increasing the number of uncertainties which may enter the problem. In the Hugoniot experiments an aluminum driver is used, whereas in the adiabat shots one can think of the shock being introduced into the liquid by a playa driver.

The final experimental design chosen for the release isentrope experiments is shown in Fig. 3-1 and will be described below. Each assembly yields a Hugoniot point and three points on the release isentrope from that Hugoniot point. For shots in which the explosive is in contact with the driver plate, the

driver thickness is $3/4$ inch. For shots in which a flyer plate with a free run is used to initiate the shock, the driver thickness is $1/8$ inch. The reasons for this difference in driver thickness and the explosive systems used in each case will be discussed later in this section. The smear camera trace from slit 1 gives two independent records of the free-surface velocity in the driver at approximately the same radial distance from the center of the driver plate as the observations on the state in the playa and liquids are taken. For each of these measurements the shock arrival at the free surface is recorded, and the transit time of the free surface across a $1/8$ -inch air gap is measured. The recording surface of the gapped¹ mirror, the side toward the driver plate, is protected from premature arrivals such as air shock by a 0.004-inch iron shim. Since the Hugoniot of iron is known, it is possible through application of the impedance mismatch method in an iterative manner, to correct the observed transit time for the presence of the shim. In actual calculations the correction is small, less than 2 percent, as the shim thickness is small compared to the gap.

The points defining the release isentrope are taken from slits 2 and 3. The playa sample of diameter $2-5/8$ inches is covered with aluminized Mylar to record shock arrival and planarity at the front surface of the specimen. On the upper two quadrants of the cell are $1/8$ -inch gapped free-surface arrival mirrors, protected by 0.004-inch iron shims as before, to measure the playa free-surface velocity. The lower two quadrants of the cell are covered by water and ethyl ether, both transparent liquids, to a depth of $1/8$ inch. The transparent covers of the liquid cells have a $1/4$ -inch-wide reflecting stripe, protected by the customary 0.004-inch iron shim, to record the arrival of the shock at the liquid free surface. On the middle slit two shock arrival mirrors are mounted on the driver surface in order to be able to monitor the shock velocity in the playa. This measurement is used as a consistency check only since knowledge of the playa Hugoniot, determined in the earlier research period, and measurement of the state in the aluminum driver are sufficient information to specify the state in the playa by the impedance match method.

The gapped mirrors above the aluminum driver surface are supported by means of 1/8-inch hardened steel dowel pins whose diameters are held to tolerances of 0.0001 inch. The dowel pin-shim-mirror assembly, which is glued directly to the driver surface, is shown in Fig. 3-4 of reference 1. The final uncertainty in gap thickness with such an assembly is less than 0.0002 inch and hence is negligible.

The playa specimens are supported by a steel ring of 1/8-inch height and wall thickness. Lucite rings of the same diameter and wall thickness are mounted concentrically on top of the playa support ring. The Lucite rings are divided into quadrants by Lucite cross members. This assembly is hand lapped, checked for parallelism of top and bottom, and held to maximum deviations in thickness of 0.0005 inch. The entire assembly is covered on top by a circular piece of slide glass with 1/4-inch-wide aluminized stripes oriented as shown in Fig. 3-1 and mounted facing the playa specimen. Each of the two liquid cells is checked for leaks between quadrants or to the outside by filling with air at a pressure of at least 10 psi. Using air rather than liquids to check for leaks prevents contamination of the cells and reduces the possibility that either of the liquids used may attack any component of the cell assembly. It is thought that water may cause the aluminized Mylar to relax or deteriorate at a very slow rate, and similarly that ethyl ether may attack Lucite at an equally slow rate. It has been determined that neither of these processes occurs during the time intervals involved in the course of firing these experiments.

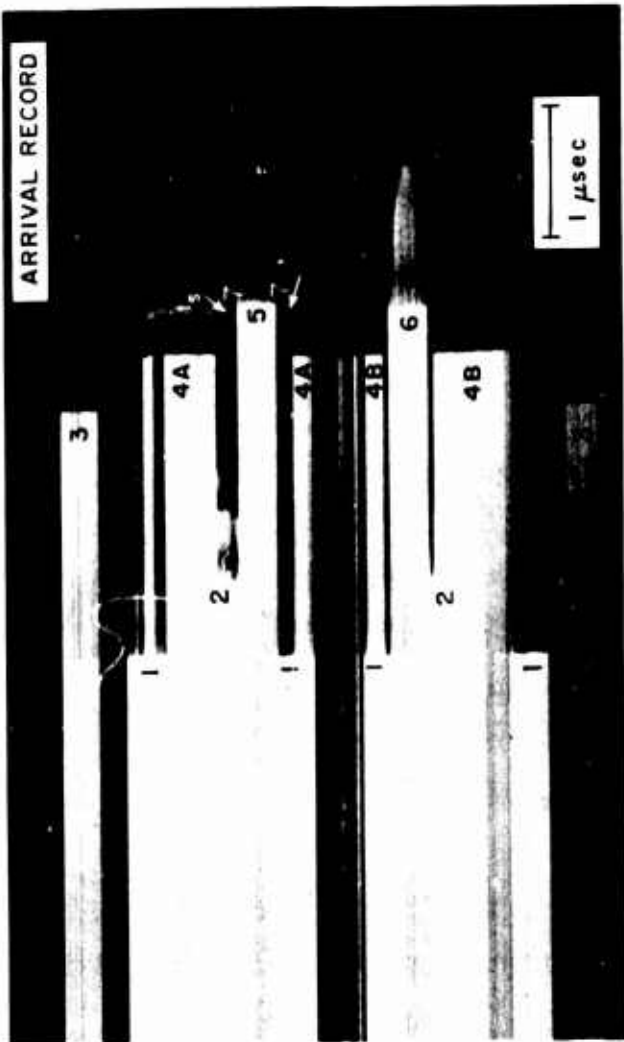
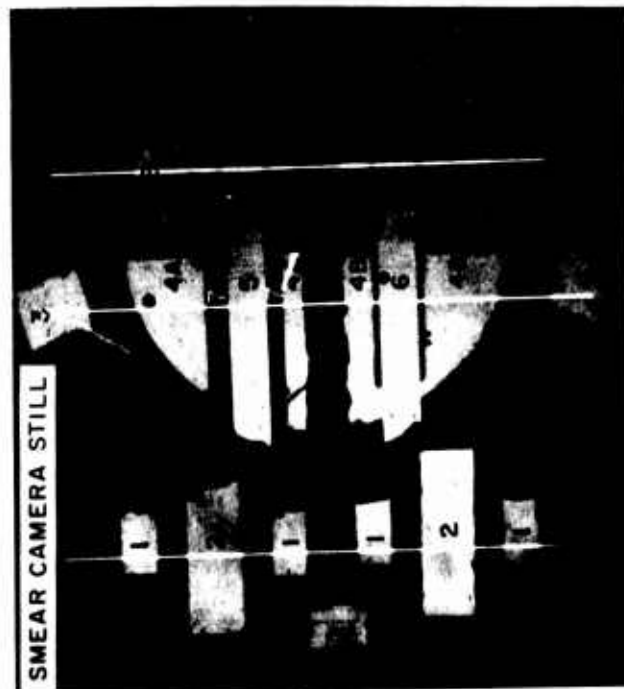
It has been observed that on some previous experiments the aluminized Mylar covering the playa has pulled away from the playa surface. This is thought to be caused by the fact that the experiments are constructed in temperature controlled environment and fired at the test site where the ambient temperature may typically be 20°F higher. Hence the gases filling the pores of the sample and trapped there may expand and lift the Mylar from the surface of the playa. To avoid such situations a system of applying an overpressure of approximately one pound per square inch to the top surface of the aluminized Mylar has been developed. This is accomplished by filling the two liquid cells, opening passages to the upper two quadrants, and applying the overpressure by means of a balloon to the entire Lucite assembly which is still

hermetically sealed from the outside. It is apparent from visual observations when the Mylar has been pressed into contact with the playa surface, and hence it is possible to apply only the minimum overpressure required. This overpressure is in all cases taken to be so small as not to effect the initial densities of either liquid.

A typical smear camera record from such an experiment is shown in Fig. 3-2. Fig. 3-2(a) is a still photograph of the shot face with the image of the streak camera slits exposed over it. The streak camera record is shown in Fig. 3-2(b). The record from slit 1 yields the transit time of the aluminum driver free surface across a 1/8-inch gap. The record from slits 2 and 3 yield the release isentrope data. The measurement of shock velocity through the playa from slit 2 is not as precise as the shock velocity measurements from shots designed to determine playa Hugoniot points. This loss of precision occurs because the samples used for isentrope measurement are of large diameter to permit all measurements for a single isentrope to be taken from the same sample raised to a uniform Hugoniot state by the initial shock. Due to the large diameter of the samples, shape and arrival time of the shock at the driver playa interface on slit 2 are not well known. However, the accuracy of the measurement is sufficient for a consistency check on the state in the playa.

The measurement of playa free-surface velocity is complicated by the fact that playa, being a porous material, is subject to jetting as the shock arrives at the free surface. The effect of such jetting is to cause the free-surface arrival recording mirrors to yield jagged free-surface arrivals with a corresponding high degree of uncertainty in interpretation. In order to smooth the jagged arrivals a shim is mounted directly on the surface of the playa. If the shock impedance of the shim material is greater than that of playa and if the release isentrope of playa from a doubly shocked state is not significantly different from that for the singly shocked playa, then it can be shown that the shim will achieve the playa free-surface velocity, through a series of wave reflections at the playa-shim and shim-air interfaces. If the time in which the shim accelerates to the playa free-surface velocity through the wave reflections is small, then its presence will have a negligible effect upon the value measured

SHOT 11,458



KEY

- 1 SHOCK ARRIVAL MIRRORS ON DRIVER, SLIT 1.
 - 2 FREE SURFACE ARRIVAL MIRRORS ABOVE DRIVER.
 - 3 SHOCK ARRIVAL MIRRORS ON DRIVER, SLIT 2.
 - 4 ALUMINIZED MYLAR ON PLAYA SURFACE: (A) VIEWED THROUGH AIR GAP.
(B) VIEWED THROUGH LIQUID CELL.
 - 5 FREE SURFACE ARRIVAL MIRROR ABOVE PLAYA.
 - 6 SHOCK ARRIVAL MIRROR COVERING LIQUID CELL.
 - 7 EDGES OF 0.003" ALUMINUM SHIM MOUNTED ON PLAYA FREE SURFACE.
 - 8 REPLICA OF ADJACENT SLIT.
- t_s DIFFERENCE IN TRANSIT TIME ACROSS THE AIR GAP FOR THE PLAYA FREE SURFACE WITH AND WITHOUT THE 0.003" ALUMINUM SHIM.

GP-5058-13

FIG. 3-2 SMEAR CAMERA STILL AND ARRIVAL RECORD OF SHOCK PASSING THROUGH ADIABAT SHOT

for the playa free-surface velocity. On slit 2 of Fig. 3-2(a), a 0.003-inch aluminum shim was used and on slit 3 no shim was used on the playa free surface. Aluminum is a more suitable material for such a shim than iron or steel since it is of lower impedance thereby introducing a smaller perturbation on the state of the playa. Since the shock and rarefaction velocities of aluminum are higher than in iron, it will reach equilibrium in shorter time. Also, fewer wave reflections are required to achieve equilibrium because of the closer impedance match to playa. The free-surface record from slit 2 provides direct experimental examination of the shim effect. The shim was purposely cut wider than the free-surface arrival mirror number 5. The shim, labeled 7, can be seen protruding from either side of mirror 5 on Fig. 3-2(a). Along the free-surface quadrant there is a distinct line at approximately the same point in time at which the free surface impacts its arrival mirror. This is due to air trapped between the playa free surface and the glass cover of the Lucite cell luminescing as shocks reflect back and forth raising its temperature. The record shows quite clearly a time interval, t_g , between the luminescence due to the arrival of the accelerated shim and due to the unobstructed free surface. The shim arrives later. When the total transit time of the shim on the free surface is corrected by this factor there is very satisfactory agreement between the two free-surface cells. This effect will be discussed further when the data are presented. The designations A and B are used on mirrors number 4 in Fig. 3-2(a) to point out that the aluminized Mylar on the playa is being observed through an air gap and a liquid cell respectively.

(3) Explosive Assemblies for Hugoniot Release Isentrope Experiments

The explosive assemblies used to initiate the shock in the driver for the Hugoniot experiments are discussed in section 3.B. (1) of reference 1. The only change made during the experimental period is that the free run distance of the 1/8-inch stainless steel flying plates is reduced from 1-1/2 inches to 1 inch. For the adiabat shots, however, the problem of attenuation of the shock amplitude with distance as the wave progresses through the experiment is more severe since measurements are made over twice as long an interval from the driver surface as in Hugoniot experiments. For shots in which the explosive is in contact with the back surface of the driver plate one would like

to use a configuration which gives a long, relatively flat, pressure pulse at the front of the driver. It has been shown in this laboratory³ that a slowly decaying pressure pulse can be obtained in an aluminum plate from an explosive train of plane-wave lens, Comp B, and Baratol, if the ratio of the thickness of Baratol to that of Comp B is 2 to 1 and the aluminum plate is at least 1/2 inch thick. Such a system is used and produces a shock of approximately 180 kbar in aluminum with planarity of breakout at the front surface on the order of 0.01 μ sec variation along a 3-inch slit length. Shock attenuation, which is inevitable due to the inherent characteristics of an explosive detonation, is not monitored directly, but by Gregson's report should not be a source of difficulty.

Wave initiation by flying plates seems desirable for two reasons. Higher shock amplitudes are possible than for in-contact shots since the flyer plate receives momentum gradually over its free run and then gives it up rapidly on impact thereby delivering an impulse in a short time resulting in high pressures. In addition to higher pressures, it is in principle possible to achieve flatter topped pressure profiles via the impact mechanism of a flying plate. According to hydrodynamic theory the wave should be perfectly flat until the trailing rarefaction from the rear of the flying plate overtakes the original shock, as discussed in reference 1. The difficulty in designing flying plate assemblies is that not enough information is known to accurately compute the point at which the overtaking will occur. On the basis of early results in the adiabat program it is felt that such attenuation was taking place in the region in which measurements were being made. Hence a new system designed to minimize the possibility of attenuation has been designed. This involves increasing the ratio of flyer to driver plate thickness from 1/3 to 2 and changing the flyer material to be identical with that of the driver. Earlier experiments to obtain Hugoniot data made use of a steel flyer with an aluminum driver plate. Increasing the flyer-to-driver-thickness ratio creates two problems. As the driver is made thinner it becomes more difficult to machine to the necessary degree of flatness and planarity, and as the flyer is made thicker it becomes more massive and hence achieves lower velocities. The first problem is really one of economics and has been met simply by increasing the care taken in the machining process

and rejecting all unsatisfactory plates. The second problem is partially solved by changing the flyer material to aluminum which is approximately $1/3$ the density of steel. However, since the shock impedance of aluminum is less than that of steel, aluminum must be accelerated to a greater velocity than steel to produce the same target pressure upon impact. The maximum pressure attained with the new system is 500 kbar in the driver whereas 700 kbar is easily attained using $1/8$ -inch steel flyer plates, however, 500 kbar is adequate for the purposes of the current release isentrope program. Previous work has shown that shock attenuation occurs in aluminum flying plate experiments earlier than is predicted on the basis of hydrodynamic calculations. The premature attenuation is attributed to elastic relaxation due to elastic relief waves propagating at velocities approximately 20 percent higher than hydrodynamic values. Taking this 20 percent velocity increase into consideration, time-distance analysis of the wave propagation in flyer and driver indicates that the present systems should be free of attenuation within the driver-playa-liquid assembly. The fact that the flyer and driver are of the same material means that there is no impedance mismatch at this interface and hence the driver may be made as thin as is desired without new disturbances originating when reflected waves from the playa-driver interface reach driver-flyer interface. The advantages of this are reflected in the above mentioned calculation placing the attenuation region well beyond the time interval in which adiabat measurements are made.

Two explosive trains are used with the new flyer plates. For intermediate pressures the Composition B-Baratol system is used, and for high pressures a plane-wave generator and an HMX pad are used. With the first system driver pressures of 265 kbar are reached with maximum deviation from planarity at the front of the driver being $0.03 \mu\text{sec}$ over a 3 inch diameter. Because of the flatness of the pulse produced by this particular explosive system at the back of the flyer, spalling of the flyer, which could introduce premature attenuation, is unlikely. The HMX system gives driver pressures of 500 kbar and planarities of $0.01 \mu\text{sec}$ over a 3 inch diameter at the front of the driver. The observed high degree of planarity is very satisfactory.

D. DATA AND RESULTS

(1) Hugoniot Experiments

Hugoniots for NTS playa in five different initial states have been experimentally determined. Two porosities of dry playa, $\rho_0 = 1.55 \text{ g/cm}^3$ and $\rho_0 = 1.95 \text{ g/cm}^3$, were selected for study during the first year of the program in order to ascertain the effects of thermal pressure on the equation of state. Some Hugoniot work for dry playa of these densities has been repeated in this experimental period to serve as a consistency check. As playa in situ is moist, two new densities of playa containing approximately 10 percent moisture, $\rho_0 = 1.71 \text{ g/cm}^3$ and $\rho_0 = 2.14 \text{ g/cm}^3$, were studied. These two densities were obtained by requiring that the samples, in addition to containing approximately 10 percent moisture by weight, have the same pore volume as the corresponding dry samples. Thus if a moist sample of density 2.14 g/cm^3 were to be dried, the resulting sample would have a density of 1.95 g/cm^3 . Finally, playa of moisture content 19 percent and initial (wet) density 1.55 g/cm^3 was examined in order to observe the effect on the Hugoniot of having the pores filled to a high degree with water. This represents the highest moisture content it was possible to introduce in samples of wet density 1.55 g/cm^3 . It corresponds to 56 percent of saturation. It should be remembered when comparing Hugoniots of dry and moist samples of the same density that there is necessarily a variation in pore volume between the two.

The results of the Hugoniot experiments are presented in Tables 3-I to V and, as pressure-particle velocity plots, in Figs. 3-3 to 7. The tables are divided into direct-contact and flyer-plate shots on the basis of the manner in which the shock is introduced into the driver. It should be noted that for some of the very low pressure shots it was necessary to replace the standard aluminum driver plate with one of brass. As the Hugoniot of brass is steeper than that of aluminum, application of the impedance match method will show that the pressure achieved in some specimen material through use of a given explosive material and a brass driver is lower than that achieved using the same explosive material and the standard aluminum driver. Also some shots were fired in vacuum in order to determine if air in the pores of the playa

Table 3-1

HUGONIOT DATA FOR NTS PLAYA

$$\rho_0 = 1.55 \pm 0.02 \text{ g/cm}^3$$

$$\text{Moisture Content (M.C.)} = 0 \text{ percent} \pm 0.2$$

SHOT NO.	DRIVER DATA		PLAYA DATA					
	Explosive System	2024 Aluminum Driver Pressure (kbar)	Specimen No.	Shock Velocity (mm/ μ sec)	Free-Surface Velocity (mm/ μ sec)	Particle Velocity (mm/ μ sec)	Pressure (kbar)	Final Volume (cm ³ /g)
10,584	Direct contact P-60 +							
	2" Comp B	285	10 $\Delta 15$	4.01 3.92	3.21 --	2.08 2.09	129 128	0.310 0.300
10,997	2" Comp B	275	56	3.85	3.19	2.05	122	0.302
10,605	--	138	32	2.58	1.37	1.23	49	0.338
10,996	--	137	57	2.49	1.46	1.23	47.5	0.327
10,606	--	165*	31	1.90	0.852	0.821	24.4	0.367
10,698	--	166*	7	1.86	0.849	0.819	24	0.359
1/8" stainless steel flyer plates P-80 +								
10,549	3" IMX	660	12	6.38	6.13	3.64	357	0.281
11,053	3" IMX	602	68	6.35	--	3.40	334	0.301
11,131	3" IMX	612	71	5.85	--	3.52	318	0.257
			69	5.84	--	3.52	318	0.256
11,173	4" IMX [§]	550	74	5.54	--	3.28	282	0.263
11,174	2" Comp B	491	75	5.38	--	3.02	252	0.283
			73	5.34	--	3.04	251	0.279
10,945	2" Comp B	478	36	5.25	4.79	2.99	244	0.277
10,699†	2" Comp B	476	8	5.14	5.24	2.97	239	0.271
			16	5.12	--	2.98	238	0.270
10,586	2" Comp B	445	$\Delta 9$	5.02	4.90	2.85	220	0.282

* Brass driver.

† Vacuum shot.

§ 1/16" stainless steel flyer plate.

Table 3-11
HUGONIOT DATA FOR NTS PLAYA

$$\rho_0 = 1.95 \pm 0.02 \text{ g/cm}^3$$

$$\text{Moisture Content (M.C.)} = 0 \text{ percent} \pm 0.2$$

SHOT NO.	DRIVER DATA		PLAYA DATA					
	Explosive System	2024 Aluminum Driver Pressure (kbar)	Specimen No.	Shock Velocity (mm/ μ sec)	Free-Surface Velocity (mm/ μ sec)	Particle Velocity (mm/ μ sec)	Pressure (kbar)	Final Volume (cm ³ /g)
10,467	Direct contact P-60 + 2" Comp B	288	E5 D1	4.55 4.68	3.13 --	1.93 1.92	172 176	0.296 0.304
10,468	--	158	E1 D2	3.35 3.34	1.66 --	1.26 1.26	82 82	0.321 0.323
10,548	--	163.4*	D18 D12	2.57 2.52	0.895 --	0.772 0.775	39 38	0.355 0.354
	1/8" stainless steel flyer plates P-80 +							
10,585	3" IMX	610	Δ 3	6.27	4.76	3.22	394	0.250
10,469	2" Comp B	503	E7	5.65	--	2.84	314	0.255
10,690†	2" Comp B	476	4	5.48	--	2.74	295	0.256

* Brass driver.

† Vacuum shot.

Table 3-III

HUGONIOT DATA FOR NTS PLAYA

$$\rho_0 = 1.70 \pm 0.01 \text{ g/cm}^3$$

$$\text{Moisture Content (M.C.)} = 9.6 \text{ percent} \pm 0.4$$

SHOT NO.	DRIVER DATA		PLAYA DATA					
	Explosive System	2024 Aluminum Driver Pressure (kbar)	Specimen No.	Shock Velocity (mm/ μ sec)	Free-Surface Velocity (mm/ μ sec)	Particle Velocity (mm/ μ sec)	Pressure (kbar)	Final Volume (cm ³ /g)
10,584	Direct contact P-60 +							
	2" Comp B	285	4 525	4.44 4.43	3.39 --	1.98 1.99	150 149	0.325 0.325
10,605	--	138	34	2.99	1.56	1.17	59.5	0.358
10,698	--	166*	3	2.36	1.19	0.795	32	0.390
10,606	--	165*	1	2.36	0.950	0.797	32	0.389
	1/8" stainless steel flyer plates P-80 +							
10,549	3" HMX	660	2	6.58	6.46	3.50	393	0.274
10,586	2" Comp B	445	5	5.40	--	2.72	250	0.291

* Brass driver.

Table 3-IV
HUGONIOT DATA FOR NTS PLAYA

$$\rho_0 = 2.14 \pm 0.01 \text{ g/cm}^3$$

$$\text{Moisture Content (M.C.)} = 9.4 \text{ percent} \pm 0.2$$

SHOT NO.	DRIVER DATA		PLAYA DATA					
	Explosive System	2024 Aluminum Driver Pressure (kbar)	Specimen No.	Shock Velocity (mm/μsec)	Free-Surface Velocity (mm/μsec)	Particle Velocity (mm/μsec)	Pressure (kbar)	Final Volume (cm ³ /g)
10,467	Direct contact P-60 +	288						
	2" Comp B		G8 G3	5.00 4.72	3.18 --	1.82 1.86	196 187	0.295 0.282
10,468	--	158	G10 G2	3.86 3.78	1.67 --	1.18 1.18	97 95.5	0.325 0.321
	--		ω7 ω3	3.52 3.60	-- 1.36	0.727 0.724	55 55.9	0.370 0.372
10,548	1/8" stainless steel flyer plates P-80 +	163*						
10,585	3" IMX	610	ω10	6.81	6.26	3.04	444	0.260
10,469	2" Comp B	503	G6	6.20	5.01	2.68	359	0.264

* Brass driver.

Table 3-V

HUGONIOT DATA FOR NTS PLAYA

$$\rho_0 = 1.55 \pm 0.01 \text{ g/cm}^3$$

$$\text{Moisture Content (M.C.)} = 18.9 \text{ percent} \pm 0.2$$

SHOT NO.	DRIVER DATA		PLAYA DATA					
	Explosive System	2024 Aluminum Driver Pressure (kbar)	Specimen No.	Shock Velocity (mm/ μ sec)	Free-Surface Velocity (mm/ μ sec)	Particle Velocity (mm/ μ sec)	Pressure (kbar)	Final Volume (cm ³ /g)
	Direct contact P-60 +							
10,997	2" Comp B	275	79A	4.55	2.53	1.96	138	0.366
10,860	--	139	45	3.22	1.95	1.17	58.5	0.410
10,996	--	137	85	3.09	1.67	1.18	57	0.399
	1/8" stainless steel flyer plates P-80 +							
11,130	3" HMX	639	70A 83A-1	6.60 6.51	-- --	3.52 3.54	360 357	0.301 0.295
11,053	3" HMX	602	81A-1	6.08	5.86	3.44	324	0.280
10,861	2" Comp B	475	32	5.70	6.50	2.91	257	0.315
10,945	2" Comp B	478	82	5.66	6.20	2.93	257	0.311

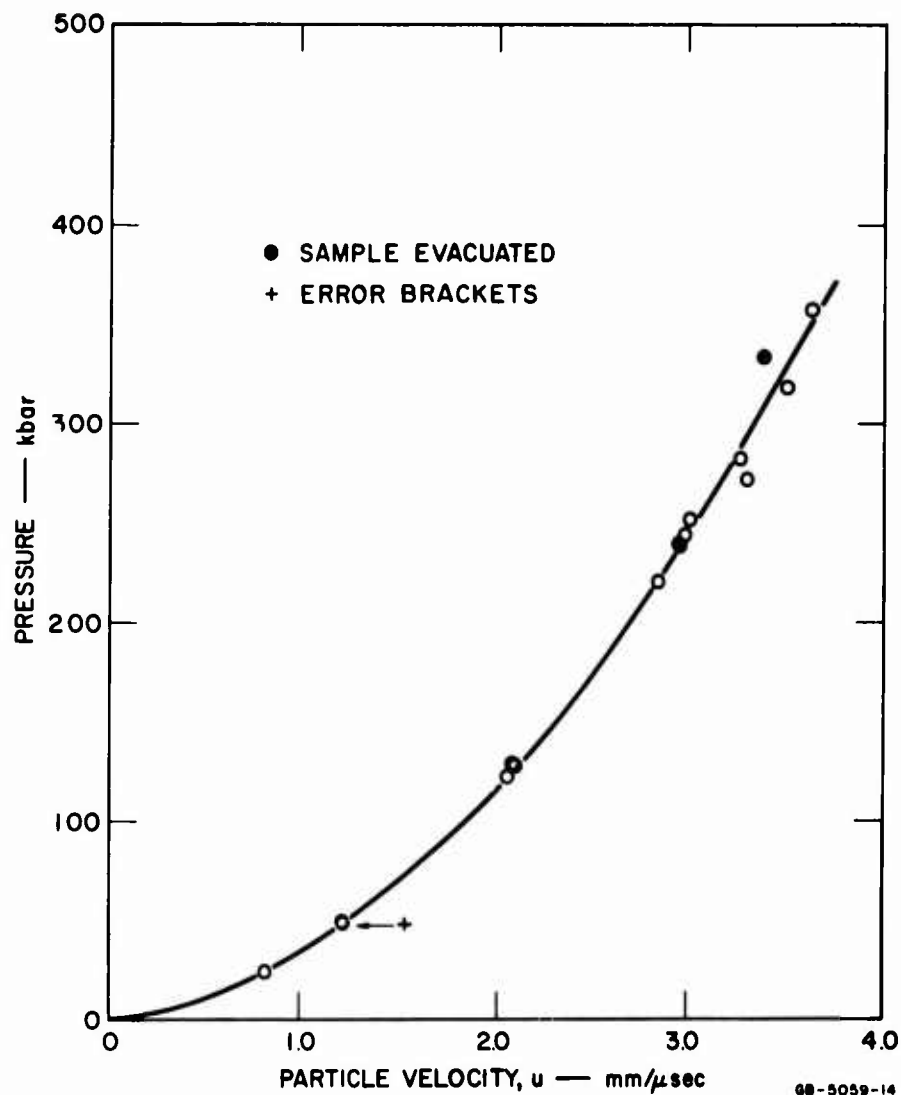


FIG. 3-3 PRESSURE vs. PARTICLE VELOCITY IN NTS PLAYA
 ($\rho_0 = 1.55 \text{ g/cm}^3$, moisture content = 0 percent)

affects the Hugoniot. These shots are appropriately marked in the tables. On the basis of the results it appears that any effects due to air in the pores is smaller than experimental error.

The densities and moisture contents which specify the initial conditions of the playa are recorded at the top of each of the tables. The quoted tolerances in densities refer to the maximum deviations that were actually observed. The value of the average density of any given sample is measured to within 1/4 percent. The tolerances in moisture content are estimates based upon observations

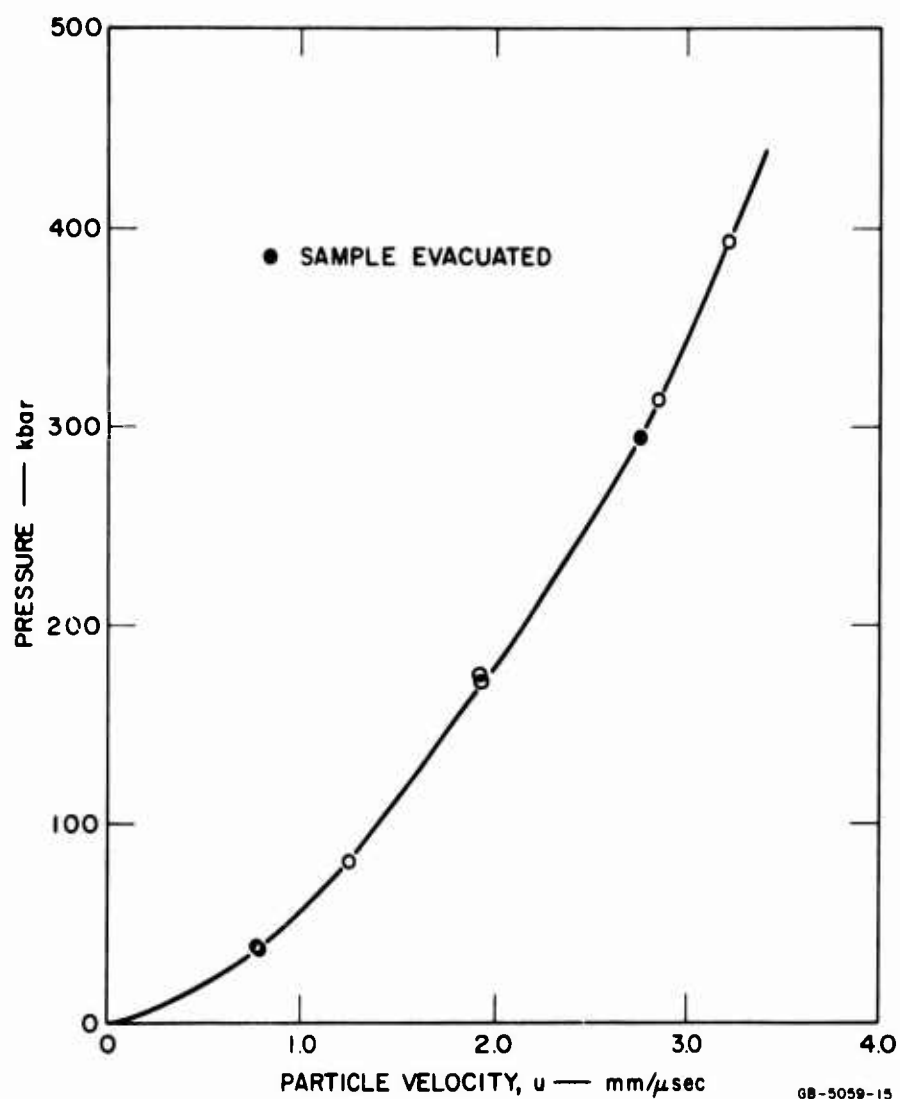


FIG. 3-4 PRESSURE vs. PARTICLE VELOCITY IN NTS PLAYA
($\rho_0 = 1.95 \text{ g/cm}^3$, moisture content = 0 percent)

of the rates at which dry and moist playa gain and lose moisture, and upon known variations in the moisture content of the stocks from which nominally similar samples were pressed.

Playa free-surface velocities have been measured in many of the Hugoniot experiments. The purpose of these measurements is to give insight into the qualitative behavior of the free-surface velocity as a function of pressure. Inclined mirrors rather than gapped mirrors are used since inclined mirrors monitor free-surface velocity continuously, and are able to observe any structure which the shock might have such as a double wave induced by a phase transition. Iron shims are used on the free surface whereas in the more

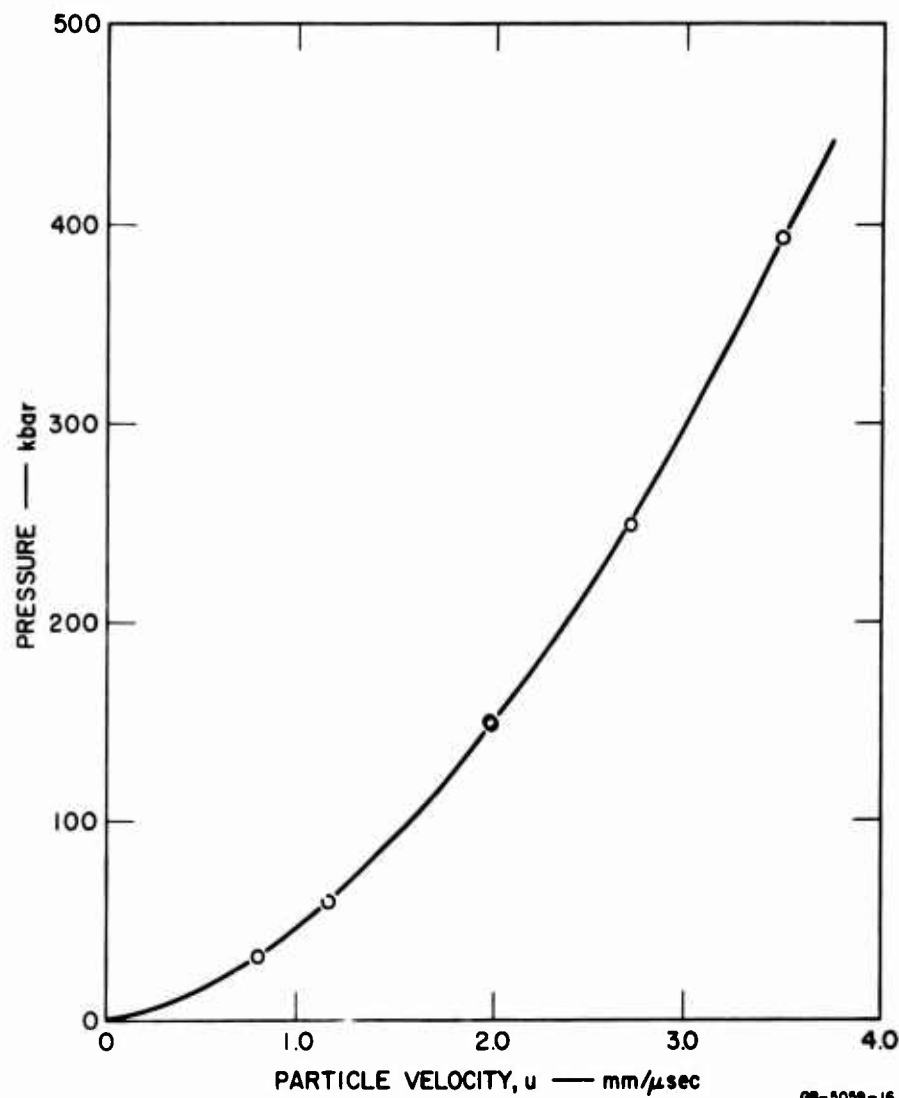


FIG. 3-5 PRESSURE vs. PARTICLE VELOCITY IN NTS PLAYA
($\rho_0 = 1.70 \text{ g/cm}^3$, moisture content = 9.6 percent)

sophisticated adiabat experiments aluminum shims were used as described in a previous section. Free-surface velocities measured using aluminum shims indicate that the free-surface velocities measured earlier using iron shims were systematically low. The variation is on the order of 10 percent at 100 kbar, and less than 2 percent above 300 kbar. This variation is probably due to shock attenuation as the wave passes through the experiment and to the nonnegligible time required for the shim to accelerate to the playa free-surface velocity. In addition, the random error is greater for measurements made with inclined mirrors than gapped mirrors since the inclined are more sensitive to shock tilt and curvature. The resulting free-surface velocity measurements are useful for

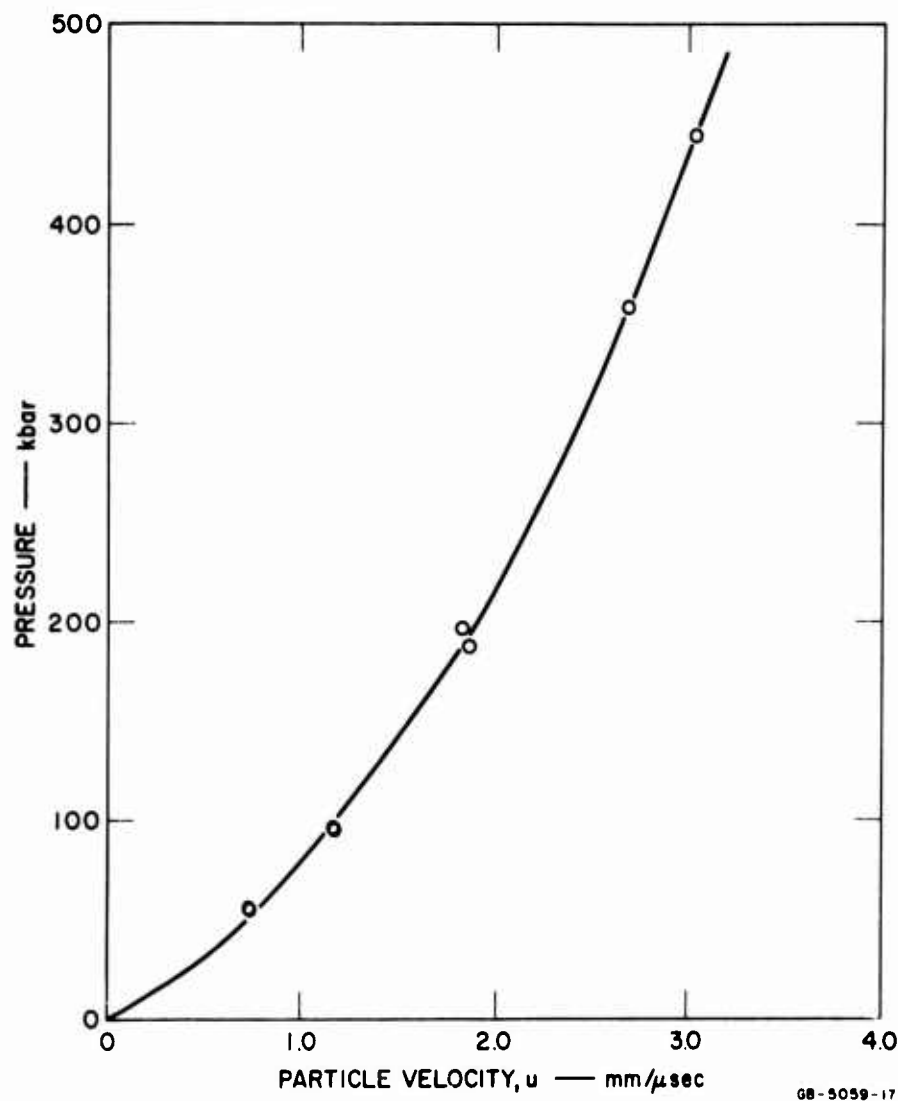


FIG. 3-6 PRESSURE vs. PARTICLE VELOCITY IN NTS PLAYA
 $(\rho_0 = 2.14 \text{ g/cm}^3, \text{ moisture content} = 9.4 \text{ percent})$

giving the general nature of free-surface velocity dependence on parameters such as shock velocity or pressure, and for showing the relative changes in free-surface velocity with the variation of the density and moisture content.

Figures 3-3 to 3-9 show the experimental results in the form of five pressure, particle-velocity plots, and two pressure specific volume plots for playa in the various initial states. Figure 3-3, $\rho_0 = 1.55 \text{ g/cm}^3$, moisture content = 0 percent, has error brackets on two typical points. These are representative of the errors to be associated with points in the high and low pressure ranges of each of the Hugoniot. They are probable random error, rather than maximum error, calculated from estimates of the uncertainty in

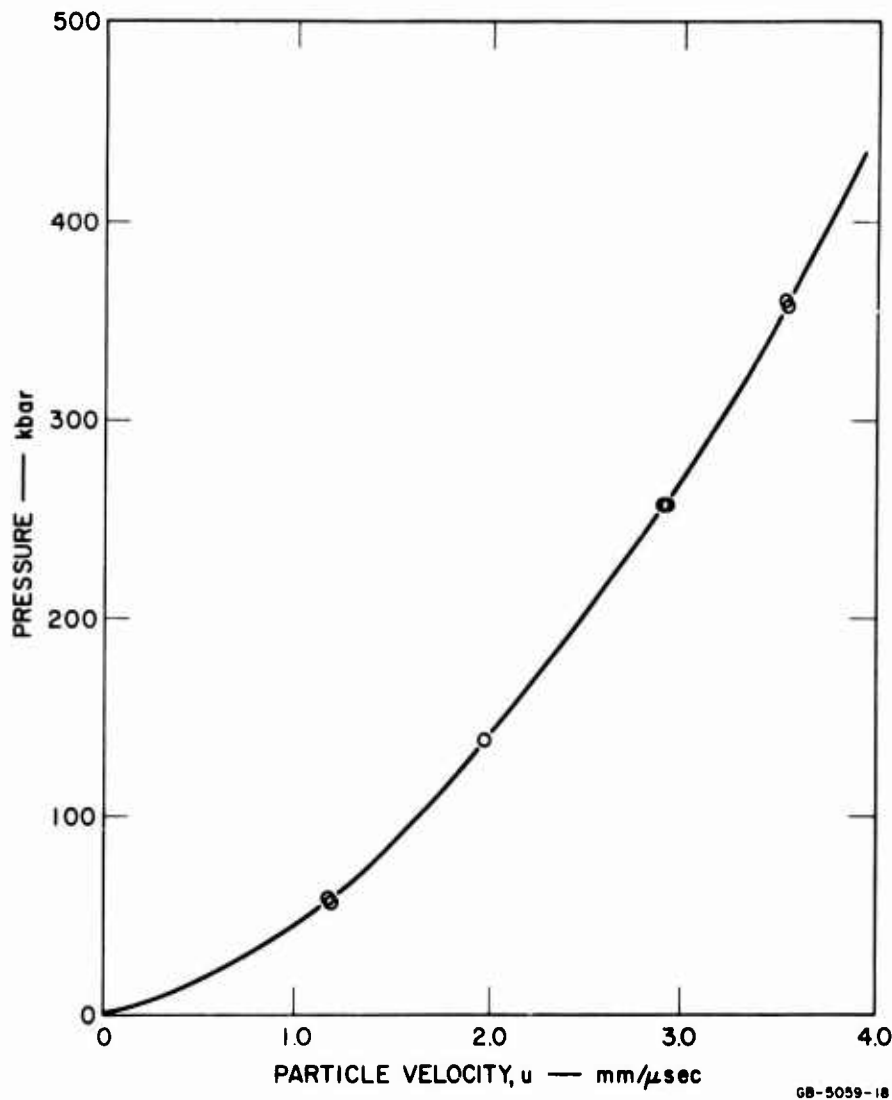


FIG. 3-7 PRESSURE vs. PARTICLE VELOCITY IN NTS PLAYA
 $(\rho_0 = 1.55 \text{ g/cm}^3, \text{ moisture content} = 18.9 \text{ percent})$

sample density, shock path length, shock curvature, and shock transit time as recorded by the smear camera. The error estimate is lower than in the previous year partially because of technique refinements, but primarily because of the availability of a new film reader having considerably better resolution than that which was previously attainable.

The five Hugoniot are distinct in the pressure, particle-velocity plane mostly because of the variation in initial densities. The data presented in the thermodynamic plane, pressure-specific volume, are less sensitive to the initial density and the various Hugoniot are much closer. In fact, after initial

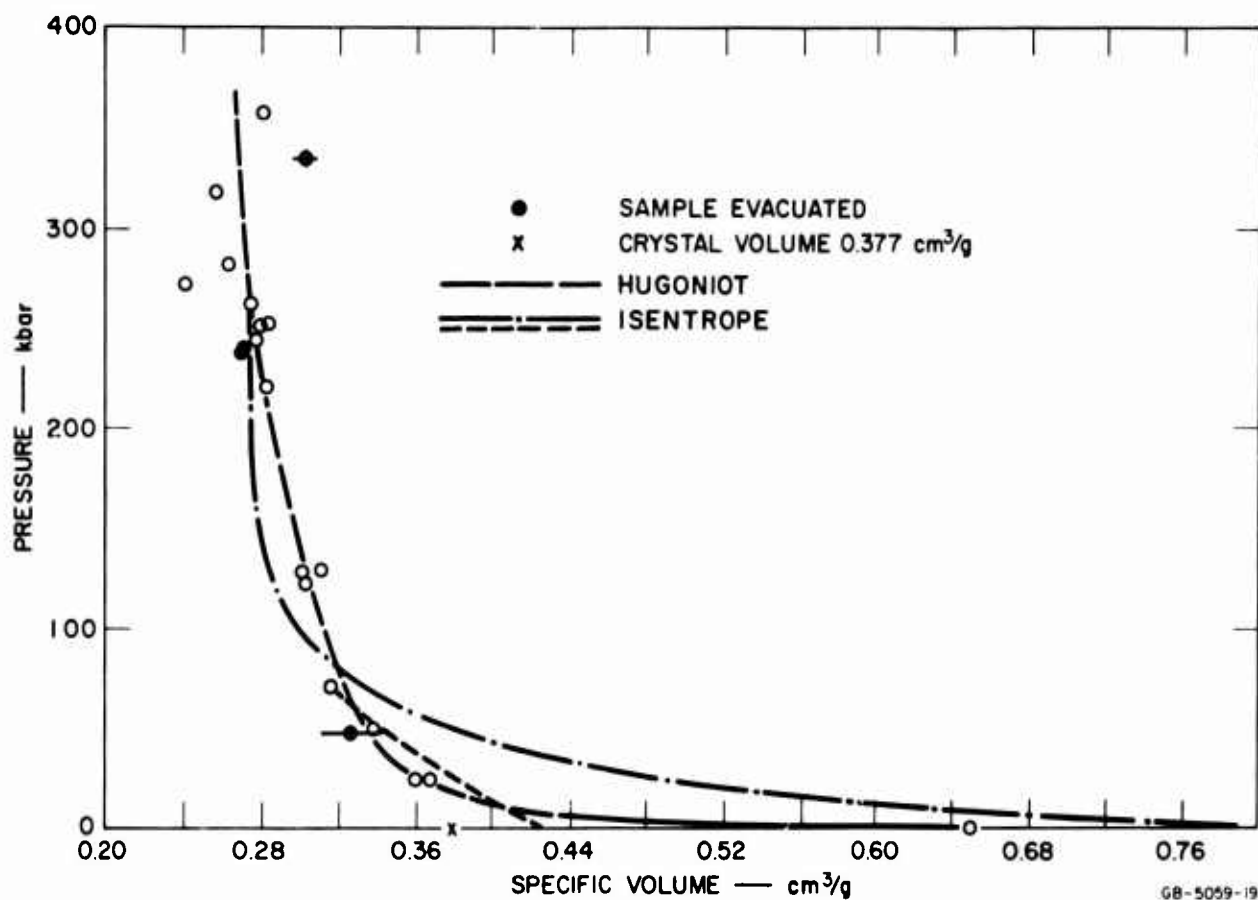


FIG. 3-8 HUGONIOT AND RELEASE ISENTROPES FOR NTS PLAYA
 ($\rho_0 = 1.55 \text{ g cm}^{-3}$, moisture content = 0 percent)

porosity has been removed, the only significant difference between the various samples is due to the moisture content and is relatively small. It is interesting to note that in the P-V plane it is possible to generate the Hugoniot of moist playa, $\rho_0 = 1.55 \text{ g/cm}^3$, moisture content 19 percent, in the intermediate pressure region quite closely from the Hugoniots of water and of dry playa of the same density. This is done by making the simple assumption that the water and playa making up a moist sample act independently and are at the same pressure behind the shock. Differences in temperature are neglected. Since both Hugoniots are known, one can add together the specific volumes of playa and water at various pressures, in the relative proportions which each are present in the sample, to obtain specific volumes of moist playa at those pressures. In this way a Hugoniot may be generated which agrees quite closely with the measured one. This model for moist playa is certainly a gross oversimplification of the actual material, hence it is interesting that calculations

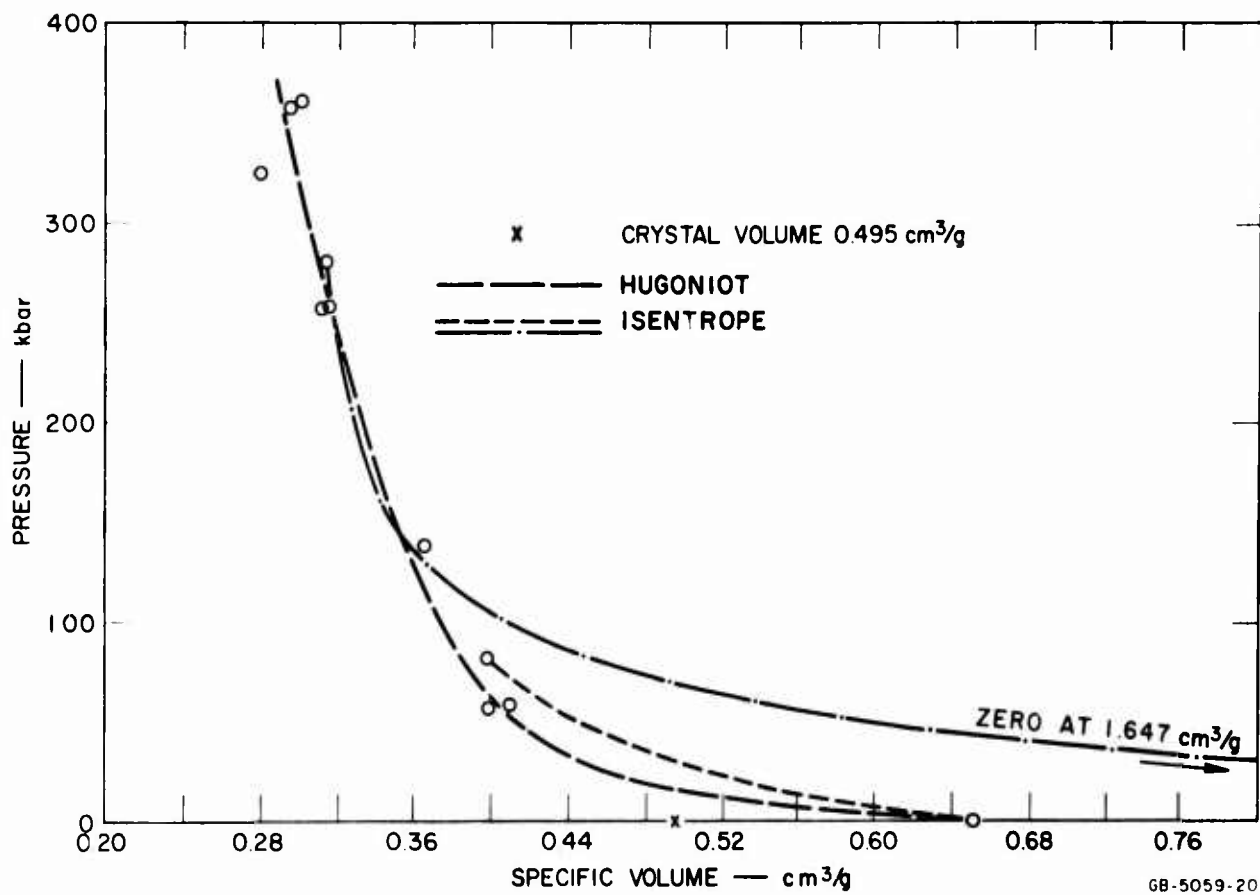


FIG. 3-9 HUGONIOT AND RELEASE ISENTROPES FOR NTS PLAYA
($\rho_0 = 1.55 \text{ g/cm}^3$, moisture content = 18.9 percent)

based upon it are not greatly different from actual measurements. A similar result was reported last year (1) based on Sandia data for dry and saturated sandstone.

(2) Adiabat Experiments

The results of the adiabat measurements are presented in Table 3-VI and Figs. 3-10 and 3-11. The table is again divided into two categories according to whether the wave was initiated in the driver by a flying plate or by explosive in contact. Release isentropes are measured for only two of the five initial playa states which were examined during the Hugoniot experiments. It is felt that the other initial states would not yield significantly different results and hence did not warrant the additional effort. The two states examined are both of density 1.55 g/cm^3 , one dry, the other of moisture content 19 percent. The tolerances on the soil sample parameters are as quoted in the previous section on Hugoniot experiments.

Table 3-VI

RELEASE ISENTROPE DATA FOR NTS PLAYA

$$\rho_0 = 1.55 \pm 0.01 \text{ g/cm}^3$$

SHOT NO.	DRIVER DATA		ADIABAT DATA					
	Explosive System	2024 Aluminum Driver Pressure (kbar)	Material	Initial Density (g/cm ³)	Shock Velocity (mm μ sec)	Free-Surface Velocity (mm μ sec)	Particle Velocity (mm μ sec)	Pressure [†] (kbar)
11,447	Aluminum flyer* plate P-80 + 4" HMX	512	Playa M.C. = 0%	1.55	--	5.65	3.11	262
			Ethyl Ether	0.708	6.54	--	3.29	152
			H ₂ O	0.997	6.65	--	3.20	212
11,456	1" Comp B + 2" Baratol	264	Playa M.C. = 0%	1.55	--	3.37	1.99	116
			H ₂ O	0.997	5.01	--	1.93	96
			H ₂ O	0.997	4.94	--	1.88	92
11,458	4" HMX	517	Playa M.C. = 19.3%	1.55	--	7.41	3.07	281
			Ethyl Ether	0.708	6.85	--	3.52	171
			H ₂ O	0.997	6.86	--	3.36	230
11,459	1" Comp B + 2" Baratol	265	Playa M.C. = 19.3%	1.55	--	4.65	1.93	130
			Ethyl Ether	0.708	4.91	--	2.30	80
			H ₂ O	0.997	5.03	--	1.95	98
	Direct contact P-80 +							
11,457	1" Comp B + 2" Baratol	181	Playa M.C. = 19.3%	1.55	--	2.80	1.44	80.5
			Ethyl Ether	0.708	4.19	--	1.80	53
			H ₂ O	0.997	4.36	--	1.53	66.5
11,446	1" Comp B + 2" Baratol	183	Playa M.C. = 0%	1.55	--	2.36	1.52	71.5
			Ethyl Ether	0.708	4.08	--	1.74	50
			H ₂ O	0.997	4.30	--	1.51	65.0

* 1/16" lucite buffer, 1/4" Al flyer and 1/8" Al driver.

† Playa pressures and particle velocities are inferred from measurement of Al driver free-surface velocity and known playa Hugoniot.

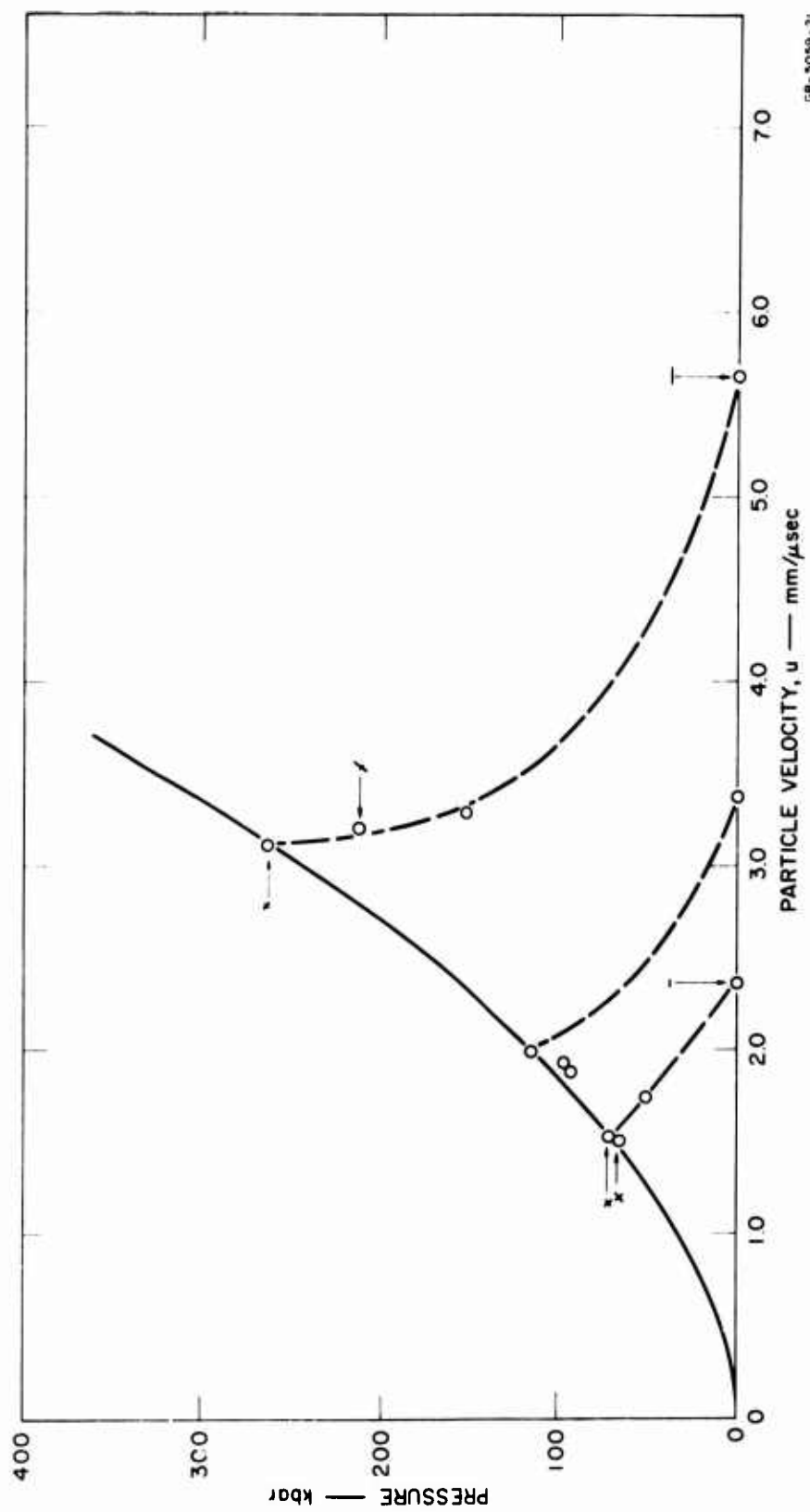


FIG. 3-10 RELEASE ISENTROPES FOR NTS PLAYA ($\rho_0 = 1.55 \text{ g/cm}^3$, moisture content = 0 percent)
Crosses Denote Error Estimates

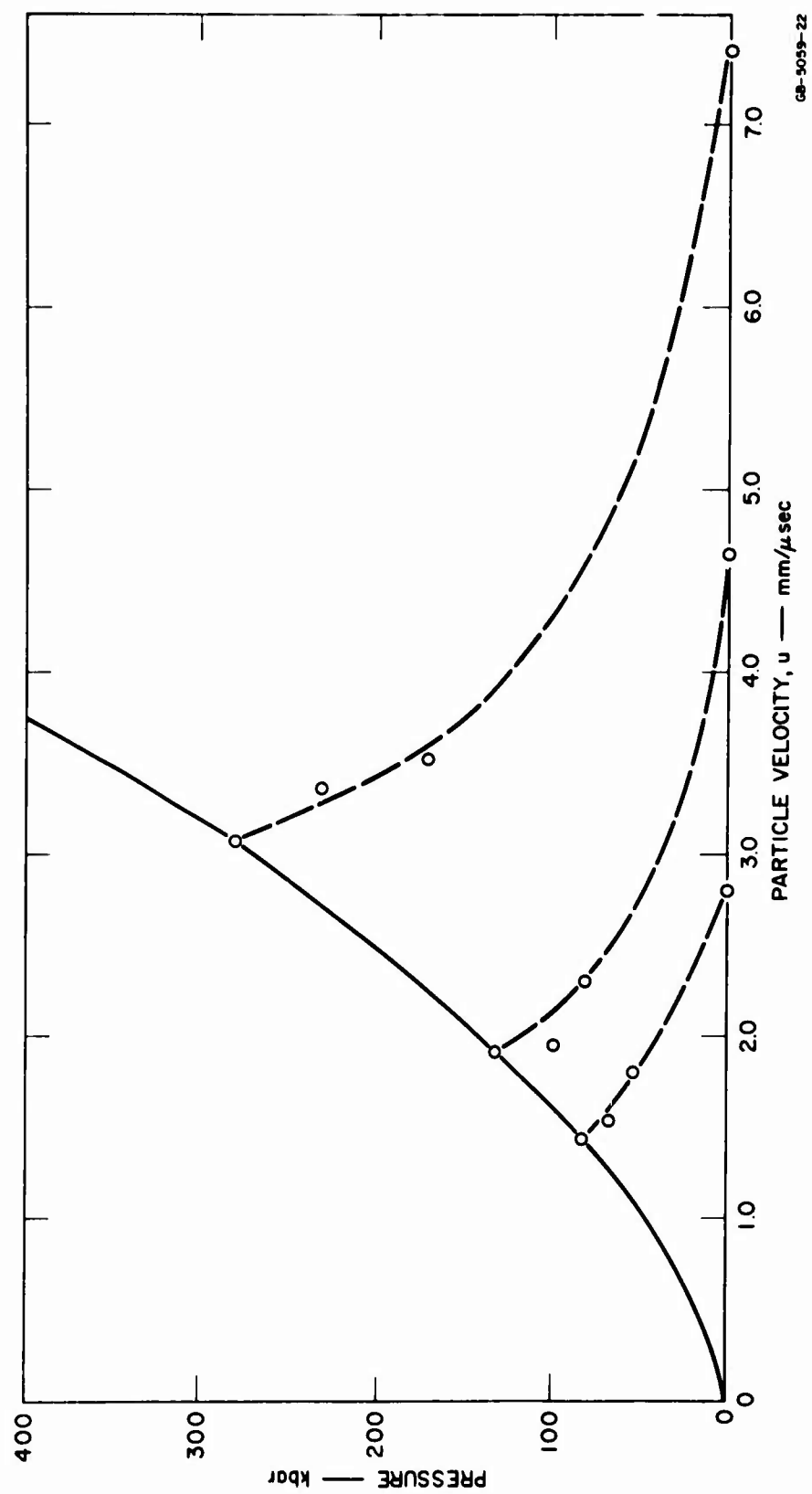


FIG. 3-11 RELEASE ISENTROPES FOR NTS PLAYA ($\rho_0 = 1.55 \text{ g/cm}^3$, moisture content = 18.9 percent)

Each shot yields four points defining one release isentrope as described in an earlier section. In the release isentrope experiments, the Hugoniot state from which the release occurs is not directly measured. Since the Hugoniot in the pressure, particle-velocity plane is quite well defined from all previous data, in the present experiments it is inferred from a measurement of the state in the aluminum driver. The three release states are determined by measurement of the shock velocity through the liquid reflectors and the free-surface velocity of the playa. Typical tolerances are shown in Fig. 3-10 for points on the high and low release isentrope. These tolerances are calculated by a similar method to that used in the Hugoniot program. Rectangular tolerance bars are not used since in this case one wants to know the variation possible in a curve centered on the Hugoniot rather than at the origin, and the projection of rectangular bars in that direction does not cover the entire error region. The tolerances shown for the free-surface velocities are the deviations from the average of the two values measured on each shot.

It should be noted that the intermediate pressure release isentropes for both moist and dry playa contain fewer points than the other isentropes. For the dry playa both liquid cells were filled with water as the seal between them was ruptured after the leak testing procedure. Hence there were three water cells fired with the intermediate pressure driver system. All of these cells recorded the same shock velocity within experimental error. This shock velocity is anomalously low in the sense that the resulting release isentrope points are not credible on physical grounds. On a pressure-particle velocity plot the isentrope points fall at lower pressure and lower particle velocity than the Hugoniot points from which they originate. This phenomenon could be explained by postulating that there exists a double wave in water, and that the velocity which is being measured is that associated with the first wave. In support of this explanation it should be noted that the Russians⁴ have reported a phase transition in water with the velocity of the first wave being within 10 percent of the velocity we have observed. These three points are recorded on the graph but are not taken into account in sketching the shapes of the

release isentropes. As four points are not sufficient to determine the structure, if any, of the isentropes, they are assumed to be smooth curves.

An interesting difference exists between the free-surface velocities for the two moisture content playas. For dry playa the free-surface velocity is always less than twice the particle velocity behind the initial shock. For moist playa of the same density the free-surface velocity is greater than twice the particle velocity except for the lowest pressure in which case it is almost exactly twice the particle velocity. Free-surface velocity data for the moist playa may indicate either an expansion to a volume considerably greater than the initial volume or, upon release, the water may be vaporized and thus produce a free-surface velocity much greater than that of dry playa. Some of the early shots using inclined mirrors to record free-surface velocities, indicated that the mirror was sustaining two impulses such as could be delivered by the moist playa if water vapor and then playa struck it successively. As the scope of the project did not permit further examination of this hypothesis, it should be borne in mind that the free-surface velocities recorded here refer to the first material to arrive at the recording mirror. The velocity is characteristic of moist playa and is reproducible to the accuracy shown by the tolerance bars on the graph.

Since the impedance match technique, making use of the continuity of pressure, and particle velocity across an interface between two media, is used to measure both release adiabats and Hugoniot, the data are naturally obtained in the form of pressure, particle-velocity states. The conversion of a Hugoniot pressure-particle velocity state to a pressure-volume state is quite readily achieved through the application of the Rankine-Hugoniot jump conditions. Pressure-particle velocity adiabat points cannot be as readily converted to pressure-volume points. This is because the transition from the initial Hugoniot state to a state of lower pressure and higher particle velocity and volume is achieved by a continuous process through a rarefaction wave rather than an essentially discontinuous jump as in a shock. Consequently, the jump conditions relating the two states in the case of a shock must be replaced by an integration between the two states which involves all intermediate states.

Applying the equations for isentropic flow the volume at some state in a rarefaction wave relieving the material from a shocked state is given by

$$V = V_1 - \int_{u_1}^u \frac{du}{(dP/du)_s}$$

where V_1 and u_1 are the volume and particle velocity state behind the initial shock. If the isentropic pressure, particle-velocity curves are known, the derivative $(dP/du)_s$ can be calculated and the integral evaluated.

Smooth curves have been drawn through the experimental adiabats in the P-u plane in order to map them into the P-V plane. If slightly different curves were drawn through the data different P-V adiabats would result so that the curves shown in Figs. 3-8 and 3-9 are somewhat arbitrary. However, some quantitative conclusions can be drawn from the general shapes of the curves. The adiabats coming from the higher pressure Hugoniot points indicate the adiabat is quite steep in the P-u plane compared to the Hugoniot. This behavior is also apparent in the P-V plane. Such a phenomenon has been observed also in tuff.⁵ This small increase in volume or particle velocity with decreasing pressure upon release can be explained by assuming a polymorphic phase change occurring at the higher pressures. As approximately 50 percent of the playa is silica it is reasonable to suspect a transition to stishovite. The adiabats releasing the material from the lower pressure states behave in a more normal manner. The calculated adiabat for the moist playa ($\rho_0 = 1.55$, moisture 18.9 percent by weight) releasing from the highest pressure point indicates an extremely large specific volume, $1.65 \text{ cm}^3/\text{g}$, upon release to zero pressure. This value of the volume is again dependent upon the assumed curve in the pressure, particle-velocity phase for the isentrope. However, the high free-surface velocities observed for this moist material at high pressures imply a zero pressure volume larger than the initial specific

volume. The effect of moisture in the soil appears significant in releasing from the higher pressures. This behavior may be due to vaporization of the water as the pressure is released.

Values of Γ , Grüneisen's ratio, have been estimated from the slopes of the Hugoniot and isentropes of dry playa at their point of intersection. The value for the lower pressure isentrope is $\Gamma = 1.3$. At the higher pressure point $\Gamma = -16$. This anomalous value results from the possible phase change.

E. LOW PRESSURE SHOCK WAVE EXPERIMENTS

The extremely low stress levels, less than 1 kbar, may well be the most important stress region for study from the point of view of application. In the case of a blast occurring in or near the earth the majority of the medium affected by the ensuing wave motion will be subjected to stresses in this regime. Some preliminary dynamic data on the behavior of dry playa of initial density 1.55 g/cm^3 were obtained. Since the techniques of inducing very low amplitude waves into soil samples and recording the amplitudes and velocities were unlike any techniques used in other phases of this program, the largest part of the effort went into technique development. The low amplitude waves were induced by a low velocity gas gun projectile and the stress-time recording was done with a quartz pressure transducer.

(1) The Gas Gun

The gun consists of a smooth bore 2-1/2-inch-inside-diameter barrel which is evacuated ahead of the projectile. The projectile is accelerated down the barrel by gas introduced from a high pressure reservoir. Carefully spaced electrical pins measure the projectile velocity near the target assembly as shown in Fig. 3-12. The mass and length of the 2-1/2-inch-diameter projectile are variable and may be chosen to accommodate each experiment. At the present time the maximum projectile velocity is approximately $0.7 \text{ mm}/\mu\text{sec}$. In the present study a low velocity of about $0.3 \text{ mm}/\mu\text{sec}$ or 100 ft/sec is necessary. The main problems encountered using slow projectiles are velocity control and tilt. The tilt, a measure of the deviation from parallel

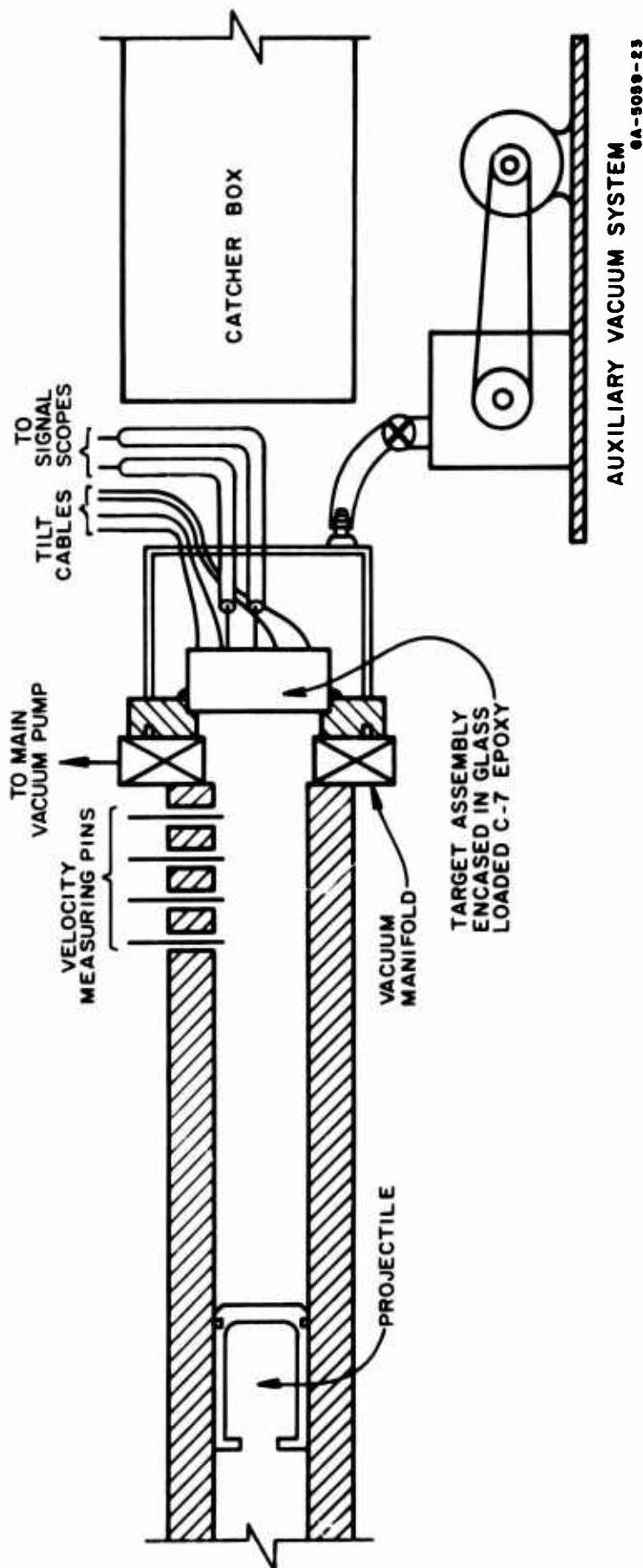


FIG. 3-12 GUN AND TARGET ASSEMBLY

of the target and projectile surfaces at impact, is measured by four arrival pins in the target assembly. These pins are shorted, giving rise to electrical pulses, by the projectile as it strikes the target. The pulses, which are binary coded to assure later identification, are displayed in sequence on an oscilloscope. The time interval between the first and last closure measures the total tilt.

(2) The Quartz Pressure Transducer

The quartz gage consists of an x-cut quartz disk which has a conducting layer evaporated on both flat surfaces. A circular groove, which is concentric with the disk and is called the guard ring, is machined into one face and divides the disk electrically into two regions. Only the portion of the quartz gage within the guard ring is used for recording. The outer portion is to minimize edge effects and maintain a uniform electric field in the recording area.

When a pressure pulse traverses the quartz, a voltage proportional to the difference in stresses at the two faces is generated. The gage is calibrated to a pressure of 25 kbar and records for a time interval equal to the transit time of a wave through the crystal. The sensitivity of the gage is about 0.8 volts/kbar. A more comprehensive treatment of the behavior of the quartz gage is given by Graham et al.⁶

(3) Shot Assembly and Data

Dry playa samples of initial density 1.55 g/cm^3 prepared in the manner described earlier were used in the low pressure studies. The samples were 2-1/2 inches in diameter and approximately 1/8 inch thick. The shot assembly which is mounted over the end of the gun barrel is shown in Fig. 3-13. The projectile strikes an aluminum driver plate inducing a pressure pulse into it. The driver plate transmits the pulse to the sample. Upon reaching the soil-

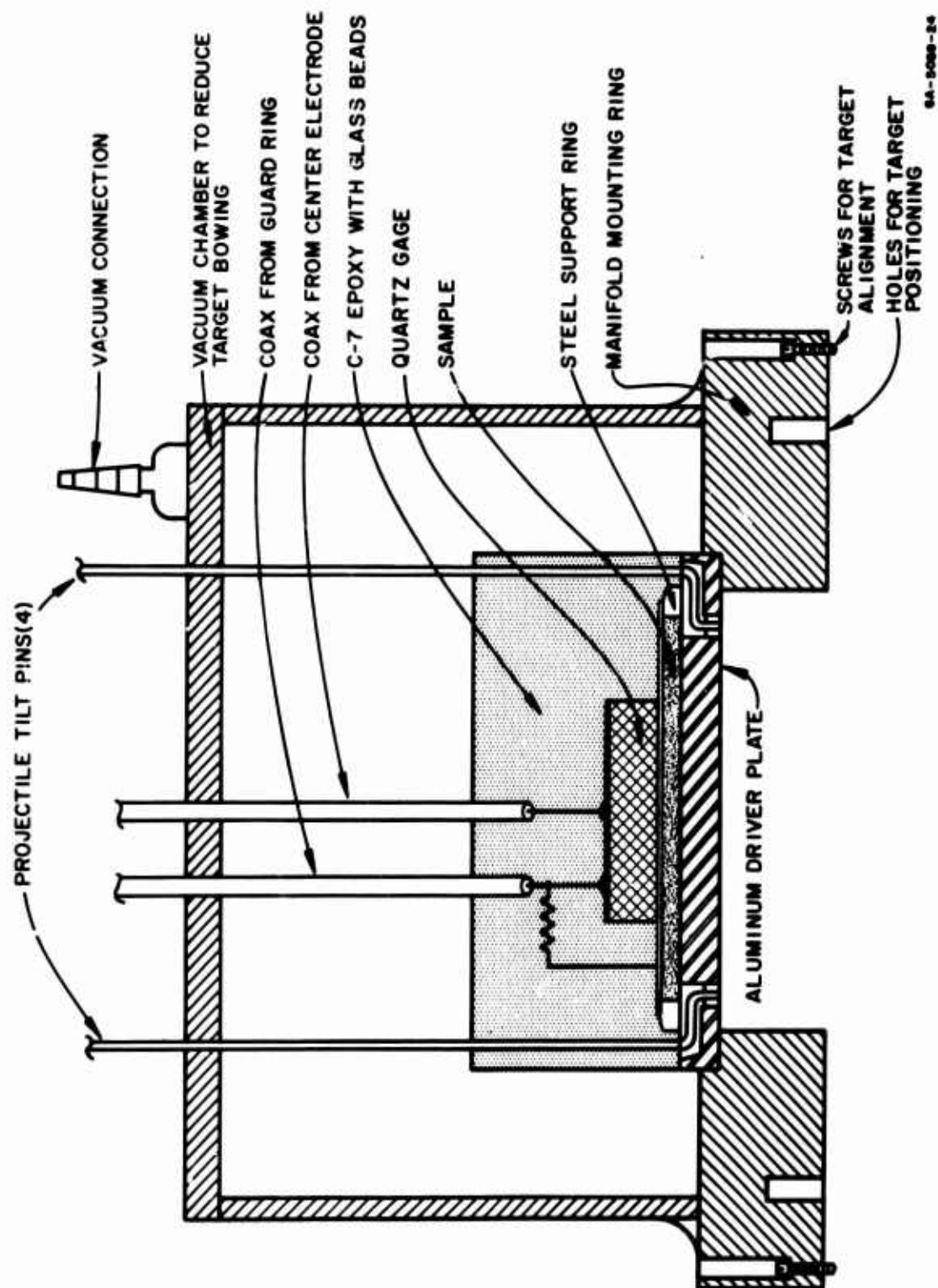


FIG. 3-13 DETAILS OF SHOT ASSEMBLY SHOWING SAMPLE AND GAGE

quartz interface the pressure pulse is reflected back into the soil and transmitted to the quartz. During the time of passage of the initial pulse through the quartz, the pressure at the quartz-soil interface is recorded by the transducer.

An aluminum driver plate was used rather than impacting the projectile directly into the sample. Since the gun barrel is evacuated this arrangement is much simpler experimentally. Very low projectile velocities were used so as not to exceed the Hugoniot elastic limit of the driver plate. If a double wave system emerges from the aluminum the interpretation of the gage record becomes more confused in looking for a double wave system in the soil. The aluminum driver is equipped with pins to measure projectile tilt upon impact. A layer of aluminum foil is placed on top of the soil to provide an electrical connection to ground for the gage. The gage is placed on the soil sample and the entire assembly is potted in C-7 epoxy which has been doped with glass beads 50 - 150 μ in diameter. This potting is done to more closely match the impedance of the surroundings to that of the soil and gage, thereby minimizing edge effects. An appropriate resistor is added from the guard ring to ground to equalize the electric field in the quartz between the guard ring and center electrode.

Working at low projectile velocities introduces experimental problems which are not serious at high velocities. The most serious of these problems is tilt. Since the projectile velocity is much lower than the induced pressure pulse velocity, large refraction effects in the wave front arise due to the nonsimultaneity of impact. The low velocities also require extreme precision in flatness of the colliding surfaces. An effort was made to maintain all impacting surfaces flat and parallel within ± 0.0001 inches. It was found that bowing of the target assembly due to the pressure difference when the gun barrel is evacuated produces a nonplanarity much larger than the tolerance specified above. To eliminate this effect an auxiliary vacuum system was added to the back of the target. The other difficulty in working at low projectile velocity is the reproducibility of the velocity itself. Frictional forces between the barrel and projectile become quite important and lead to wide scatter in velocity for the same initial accelerating gas pressure in the reservoir. A

series of thirteen shots with no targets was fired to study this problem. It was found that using a massive projectile and argon rather than helium as an accelerating gas considerably increased the reproducibility.

The pressure-time profiles recorded by the quartz gages for two shots (11,467 and 11,468) are shown in Fig. 3-14. Time is increasing to the right. Both records were subject to considerable tilt despite the precautions taken to minimize it. These two shots were exploratory and were the only experiments of this type performed. Consequently, in the absence of any other data for direct comparison, these results must be regarded as tentative. The oscilloscope record for Shot 11,467 shows no definite double wave structure.* The abrupt change in slope in the rise of this pulse corresponds to a pressure of about 0.09 kbar in the quartz. The peak is at about 0.45 kbar in the quartz. If an elastic precursor in the soil is present, but obscured by the slow rise time due to tilt, it would have an amplitude of 0.04 to 0.09 kbar. The record from Shot 11,468, given by the upper trace, clearly shows a rise, followed by a plateau and then a second rise. The signal on the lower trace is from the guard ring. The first and second amplitudes from this record correspond to pressures of 0.12 and 0.42 kbar in quartz, respectively. Interpreting the record as indicating a double wave structure in the soil, the first wave amplitude would be 0.06 to 0.12 kbar.

Estimates of the wave velocities may be obtained from the time interval between impact of the projectile on the driver and the arrival of the wave at the soil-quartz interface as indicated on the gage record. The transit time of the input wave through the aluminum driver must be subtracted out. This transit time can be computed from the known Hugoniot of aluminum. The pressure behind the second wave can then be estimated, ignoring the initial wave which is small, from the wave velocity and the fact that the pressure, particle-velocity state behind the second wave must lie on a relief cross curve of aluminum. The pressures and particle velocities behind the main wave in the soil calculated in this manner are presented in Table 3-VII. The pressures obtained from the quartz gages for the main wave, which must be the pressure behind the reflected shock in the soil at the quartz interface, are lower than would be expected. As the impedance of x-cut quartz and aluminum are quite close at these low pressures it would seem that the pressure in the quartz

*The amplitude of the first wave was taken as half of the initial pressure rise.

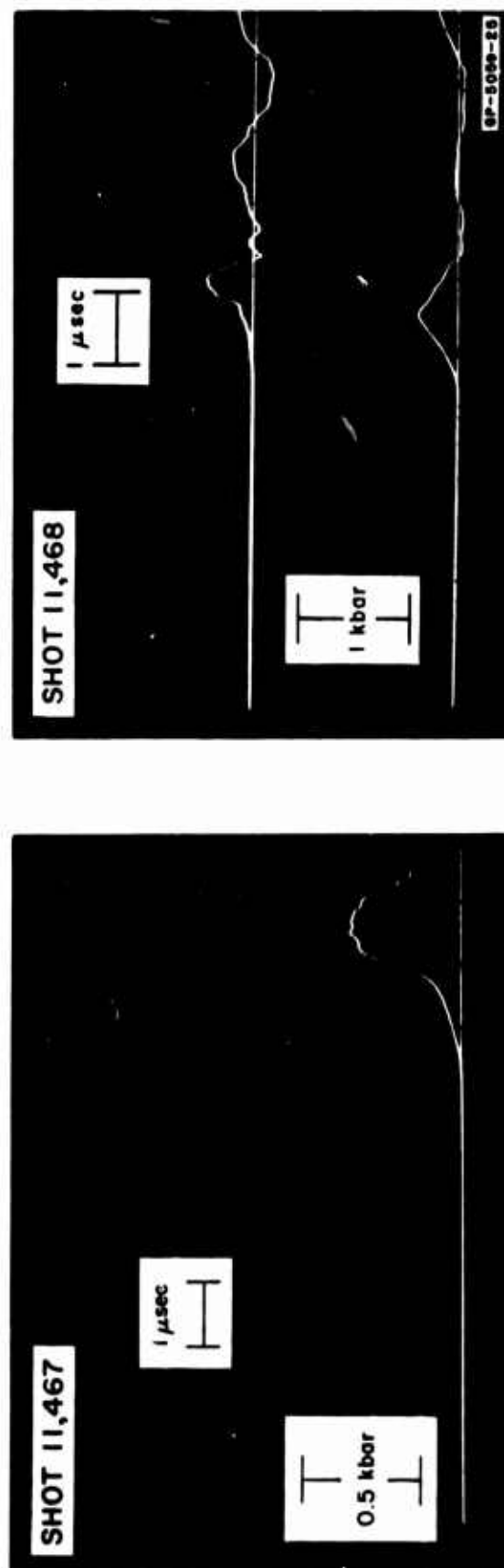


FIG. 3-14 OSCILLOSCOPE RECORDS SHOWING THE PRESSURE-TIME PROFILE FOR QUARTZ GAGE SHOTS.
(Lower trace of shot 11,468 shows guard ring signal).

would be at least double the initial pressure in the soil if the soil impedance remained the same behind the shock. If the main wave crushed or compacted the soil, one would expect the impedance to increase and the pressure to more than double upon reflection from quartz. The results from the quartz gage indicate a pressure less than twice the estimated initial pressure, implying that the reflected shock Hugoniot of the soil is of smaller slope than the initial Hugoniot in the pressure, particle-velocity plane. These results do not conform to any other data and since they are preliminary they must be regarded as quite tentative pending further investigation.

Table 3-VII
LOW PRESSURE DATA FOR DRY NTS PLAYA

SHOT NO.	SAMPLE DENSITY (g cm ³)	PROJECTILE VELOCITY (ft/sec)	PROJECTILE TILT (μsec)	WAVE VELOCITIES (mm/μsec)		APPROXIMATE PRESSURE IN SOIL (kbar)		APPROXIMATE PARTICLE VELOCITY BEHIND SECOND WAVE (mm/μsec)
				First	Second	First	Second	
11,467	1.54	163	2.6	0.57 ± 0.04	0.54 ± 0.04	0.04-0.09	0.39	0.047
11,468	1.55	143	3.1	0.42 ± 0.04	0.39 ± 0.04	0.06-0.12	0.25	0.041

This page intentionally left blank.

4-THEORY

Christian Peltzer

A. INTRODUCTION

When attempting to obtain equations of state for porous earth media one faces several problems in addition to those encountered with simple solids, namely:

- a. Already in its initial state, the medium is generally a three-component system consisting of a solid phase, a gas phase (air) and a liquid phase (water).
- b. The solid phase itself is an essentially isotropic mixture of many different compounds and/or mineralogic species.
- c. The individual constituents of the solid phase are often complex compounds rather than simple monatomic crystallites.

It is customary to treat the three phases as noninteracting systems so that all thermodynamic extensive variables are obtained additively from those of each phase and also to assume that pressure equilibrium is attained behind the shock front and maintained during pressure release. A unique specification of the thermodynamic state of the system requires of course further assumptions, either that of complete thermodynamic equilibrium or specific assumptions on the behavior of each phase under the shock transition and during pressure release.

Similarly, the solid phase is often treated as a mixture of independent phases and its thermodynamic state functions are then calculated additively from those of the simpler individual constituents, usually under the assumption of complete thermodynamic equilibrium.

Note: See List of Symbols at end of section, page 69.

A meaningful evaluation of the validity of such assumptions would require a better understanding of the structure of a shock front in dense mixtures and little can be added presently to the elementary discussion given in the previous report.¹

Hugoniot for wet playas obtained as described there from the Hugoniot of solid quartz and water are in reasonable agreement with the experimental wet playa data. Also an estimate of the effect of a decreased Hugoniot temperature in wet playa (as compared to dry playa) can be gained by taking successively for the solid phase Hugoniot the experimental data of solid quartz and of dry porous playa.

Calculated Hugoniot of solid mixtures are relatively insensitive to the averaging procedure used⁷ to obtain them from the individual constituent Hugoniot and in the absence of a better understanding of the physical mechanisms underlying the propagation of shock waves in solid mixtures, there are little real grounds for selecting any one of the several averaging schemes proposed (per weight fraction, per molar fraction, ----) in preference to the others, the difference between the resulting Hugoniot being of the order of the experimental uncertainty. The lack of sufficient adiabatic release data precludes at the present any analysis of the same problem there.

A further complicating factor in analyzing playa data is the existence of polymorphic phase transitions for SiO_2 , in particular that to stishovite. In view of the particularly large volume change and the change in coordination number associated with this transition, the absence of conclusive experimental evidence for or against its occurrence in dynamic compression of playa makes any comparison of the experimental data with postulated equations of state rather academic for the time being.

Nevertheless, one may conclude from a comparison of the experimental data on playas and quartz and from the limited parameter variations performed with the equation of state used here, that porous silica is a satisfactory tentative model for the description of the thermodynamic behavior of the Nevada playas considered in this program.

The effects of small variations in the chemical and mineralogical composition appear of little significance in view of the other uncertainties affecting both the experimental and theoretical situations, although such variations could conceivably be of more importance in the (little studied) low pressure region (< 20 kbars) and in the dynamics of eventual phase transitions.

For these reasons, the theoretical work has been based on SiO_2 data only, considered as a single thermodynamic system (see reference 1).

B. DERIVATION OF EQUATIONS OF STATE (EOS)

Presently, a direct first principles derivation of a complete EOS for sufficiently realistic models for most physical systems is an almost impossible task and if one requires an EOS to be valid over a relatively wide range of the thermodynamic variables it is still necessary to resort to semiempirical formulations. Most equations of state proposed so far can be grouped into four types.

- a. Purely empirical EOS: these are obtained simply by fitting largely arbitrary analytical expressions to some experimental data such as a Hugoniot; if such EOS may be of interest in some calculations, they are but an economical way of presenting specific experimental data; they are totally inadequate for any extrapolation and prediction purposes and generally of no theoretical value or particular significance.
- b. Semiempirical EOS: these are in principle obtained by choosing a thermodynamically consistent functional form for some EOS and by determining its parameters from experimental data and/or theoretical predictions (see c.)
- c. Theoretical EOS: These are obtained from first principles according to the laws of statistical mechanics; they are presently limited to a few simple systems (classical and quantum) such as a free electron gas, a harmonic lattice solid, etc., and are exact within the well defined limits of the model and its underlying physical laws.

- d. Semitheoretical EOS: In this disparate group, one can include many EOS which although partly derived from first principles, can only be obtained by additional assumptions of an heuristic nature whose degree of validity is difficult to assess; e. g. , Thomas-Fermi, (TF) Thomas-Fermi-Dirac (TFD), etc.

In view of the many loose statements implying the contrary, it may not be superfluous to repeat that semitheoretical EOS such as the T-F, T-F-D, etc. , are in no way exact EOS of a well defined model and that at the present there exists no true estimate, in a proper mathematical sense, of their degree of validity in any particular range of the thermodynamic variables, but only more or less optimistic guesses as to their applicability (see later).

We shall limit ourselves here to a consideration of some semiempirical EOS and we shall also discuss a few questions concerning the use of the T-F, T-F-D EOS and the nature of certain corrections proposed by various authors (see also Appendix.)

C. SOME THERMODYNAMICS OF EOS[†]

For the reasons given earlier (see also Ref. 1), we consider here only single thermodynamical systems (homogeneous, isotropic) describable in terms of two independent variables, taken mostly to be V and T or E^* and T , where E^* is the thermal energy.

(1) The General Mie-Grüneisen EOS

The general Mie-Grüneisen EOS is defined by the relation

$$\Gamma = \Gamma(V, T) \quad (4-1)$$

Γ being the Mie-Grüneisen ratio defined as

$$\Gamma = V \frac{\left(\frac{\partial P}{\partial T}\right)_V}{\left(\frac{\partial E}{\partial T}\right)_V} = V \left(\frac{\partial P}{\partial E}\right)_V \quad (4-2)$$

[†] For notation see reference 1.

This EOS was discussed in reference 1 and we only recall its main features:

- (i) it is an incomplete EOS that leaves the cold energy $E_c(V)$ unspecified
- (ii) it uniquely determines all other adiabats of the system in the V - T plane, these are the characteristics of the partial differential equations,

$$T\Gamma(V, T)\left(\frac{\partial S}{\partial T}\right)_V - V\left(\frac{\partial S}{\partial V}\right)_T = 0 \quad (4-3)$$

$$S(V, 0) = \text{constant} (= 0) \quad (4-3a)$$

and so are given by

$$z = \phi\Gamma(V, T) = \text{constant} \quad (4-4)$$

where $\phi\Gamma(V, T)$ is a function of V, T uniquely determined by $\Gamma(V, T)$

- (iii) The entropy is a function of z only, arbitrary up to general thermodynamic restrictions on admissible $S(V, T)$'s (positive definite, etc.)

$$S = \sigma(z) \quad (4-4')$$

- (iv) A complete specification of the system requires besides $\Gamma(V, T)$ the knowledge of $E_c(V)$ and that of $\sigma(z)$ or its equivalent, e.g., one isobar $V_{P_0} = V_{P_0}(T)$ or one isotherm $P_{T_0} = P_{T_0}(V)$ ($T_0 \neq 0$) or a specific heat $C_{V_0} = C_{V_0}(T)$, etc.

Two useful equivalent forms of the general Mie-Grüneisen EOS are:

$$P - P_c(V) = \frac{\Gamma(V, T)}{V} T \left(\frac{\partial E^*}{\partial T} \right)_V - \left(\frac{\partial E^*}{\partial V} \right)_T \quad (4-5)$$

$$P_c = - \frac{dE_c}{dV} \quad E_c = E_c(V, 0) \quad (4-5a)$$

and

$$P(V, T) = \frac{\Gamma(V, T)}{V} E(V, T) + R(V, T) \quad (4-6)$$

$$R_c(V) = - \frac{dE_c}{dV} - \frac{\Gamma_c(V)}{V} \left(\frac{\partial R}{\partial T} \right)_V = - \frac{E}{V} \left(\frac{\partial \Gamma}{\partial T} \right)_V \quad (4-6a)$$

It is important to note that R is a function of V alone if and only if Γ does not depend explicitly on T .

(2) Special Cases of the General Mie-Grüneisen EOS

Two special cases of the general Mie-Grüneisen EOS have been frequently used, namely

(i) The usual Mie-Grüneisen EOS

$$\Gamma = \Gamma(V) \quad (4-7)$$

usually written in one of the two equivalent forms:

$$P - P_c(V) = \frac{\Gamma(V)}{V} [E - E_c(V)] \quad (4-8)$$

$$P_c = - \frac{dE_c}{dV} \quad E_c = E_c(V) \quad (4-8a)$$

or

$$P = \frac{\Gamma(V)}{V} E + R(V) \quad (4-9)$$

$$-\frac{dE_c}{dV} = \frac{\Gamma(V)}{V} E_c + R(V) \quad (4-9a)$$

The explicit form of the principal thermodynamic state functions for this case were given in reference 1, as well as further details on its use for Hugoniot and adiabat calculations.

(ii) The Hildebrandt EOS

In any domain $(T_0 \neq 0, T)^\dagger$ where E^* is a function of T only, the general Mie-Grüneisen EOS can be put in the form

$$P - P_c(V) = \frac{\Gamma(V, T)}{V} T \frac{dE^*}{dT} \quad T \neq 0 \quad (4-10)$$

$$P_c = \frac{dE_c}{dV} \quad E_c = E_c(V) \quad E^* = E^*(T)$$

or equivalently

$$PV + \frac{dE_c(V)}{d \ln V} = \frac{V\alpha}{\kappa} T \quad T \neq 0 \quad (4-10')$$

$$E^* = E^*(T)$$

These two special cases are not mutually exclusive and it can be shown that:

The usual Mie-Grüneisen EOS and the Hildebrandt one are equivalent in a domain $(T_0 \neq 0, T)$ if and only if $C_V = \text{const}$ and E^* is of the form $E^* = C_V T + \text{const}$, Γ being then necessarily a function of V alone, given by

$$\Gamma = \frac{VS'_{T_0}(V)}{C'_V} \quad (4-11)$$

where $S_{T_0}(V)$ is the entropy along the T_0 - isotherm.

[†]Since this special case is incompatible with the 3^d law, T_0 must be > 0 .

In particular, one can note that a perfect gas and a Dulong-Petit solid both satisfy this equivalence criterion.

- (iii) More generally, if $\Gamma(V, T)$ is of the form $\Gamma_c(V) \Gamma_t(T)$, explicit forms for all thermodynamic state functions can be obtained just as for a usual Mie-Grüneisen system $\Gamma = \Gamma(V)$. For other forms of Γ , the characteristic equation of (4-3) cannot, in general, be integrated in closed form and particular attention should be given to the consistency of separate assumptions on the forms of $\Gamma(V, T)$ and other thermal entities such as E^* or C_V .

(3) Modified Mie-Grüneisen EOS

Several other related EOS's have been considered in the literature, in particular the following ones.

- a. As already remarked, an EOS of the form

$$P(V, T) = \frac{\tilde{\Gamma}(V, T)}{V} E(V, T) + X(V) \quad (4-12)$$

cannot be a Mie-Grüneisen EOS, i.e., the function $\tilde{\Gamma}(V, T)$ cannot--if it depends explicitly on T --be identical to the Mie-Grüneisen ratio Γ defined by (4-2). The two functions $\Gamma(V, T)$ and $\tilde{\Gamma}(V, T)$ are actually related by:

$$\left| \Gamma - \tilde{\Gamma} \right| \left(\frac{\partial E}{\partial T} \right)_V = \frac{E}{V} \left(\frac{\partial \tilde{\Gamma}}{\partial T} \right)_V \quad (4-13)$$

It is possible to choose $\tilde{\Gamma}$ such that $\Gamma_0(V) \equiv \tilde{\Gamma}(V)$ but then one must also have

$$R_c(V) = X(V) = P_c(V) - \frac{\Gamma_c(V) E_c(V)}{V} \quad (4-14)$$

i.e., only two of the three functions $X(V)$ (or $R_c(V)$), $E_c(V)$ and $P_c(V)$ (or $\Gamma_c(V)$) can be chosen arbitrarily, the third one being given by Eq. (4-14)

A detailed study of this modified Mie-Grüneisen EOS, (4-12), can easily be carried out, but will be omitted here since this form does not appear to offer any particular advantages over the general Mie-Grüneisen EOS.

b. Some authors have made use of the following EOS:⁸

$$P(V, E) = \frac{\tilde{G}(V, E)}{V} E + X(V) \quad (4-15)$$

The function $\tilde{G}(V, E)$ is also distinct from the Mie-Grüneisen ratio Γ if it depends explicitly on E , the two being related by

$$\Gamma - \tilde{G} = E \left(\frac{\partial \tilde{G}}{\partial E} \right)_V \quad (4-16)$$

If (4-15) is to hold along the cold isotherm, one obtains the equation

$$- \frac{dE_c}{dV} = \frac{G(V, E_c(V))}{V} E_c(V) + X(V) \quad (4-17)$$

relating $G(V, E)$, $E_c(V)$, and $X(V)$.

If the forms of $G(V, E)$ and $X(V)$ have been chosen a priori⁸ (with adjustable parameters determined empirically), Eq. (4-17) must be used to obtain the cold energy $E_c(V)$. Such a procedure is perfectly legitimate for semi-empirical EOS purposes, although it may be preferable to choose first the forms of $E_c(V)$ and $\tilde{G}(V, E)$ and then use Eq. (4-17) to determine $X(V)$. $E_c(V)$ is a relatively accessible quantity both theoretically and experimentally and this procedure would make easier a comparison with other formulations and a verification of the necessary stability requirements for $E_c(V)$. The more serious drawback of this formulation is that the dependence of \tilde{G} on E_c and E^* (and so on T) is the same and already determined by the relation (4-17) along the cold isotherm. This rather artificial feature renders any interpretation of the thermal dependence of \tilde{G} difficult and precludes any

nonpurely numerical comparison of this EOS with other formulation and models.

c. For these reasons, the following EOS appears preferable:

$$P(V, E^*) - P_c(V) = \frac{G(V, E^*)}{V} E^* \quad (4-18)$$

$$P_c = - \frac{dE_c}{dV} \quad E_c = E_c(V)$$

The ratio $G(V, E^*)$ is again identical to the Mie-Grüneisen ratio Γ if and only if it does not depend explicitly on E^* , in which case Eq. (4-18) reduces to the usual Mie-Grüneisen EOS.

In contrast to Eq. (4-15), it does not impose any a priori coupling between the cold and thermal components of the thermodynamic state functions and although it does not appear to offer any advantages theoretically over the general Mie-Grüneisen EOS, it can be of interest in semiempirical EOS work and shock calculations.

The use of so many similar but distinct EOS (and a host of other semi-empirical and semitheoretical ones) is unfortunate inasmuch as it makes a comparison of various authors' results a tedious and difficult process while contributing very little but added confusion in understanding and solving the many remaining problems in this area. The general Mie-Grüneisen EOS (or eventually the modified Mie-Grüneisen EOS (4-18)) could provide a sufficiently general formulation for the present needs. A systematic, unified presentation of the existing experimental and theoretical data for the many systems investigated up to now would provide one with a much better picture of the present situation and help considerably in identifying those areas where further work is most needed.

D. DERIVATION OF A SEMIEMPIRICAL EOS

When seeking a semi-empirical EOS for a specific system, it appears best to proceed in successive steps as follows:

- a. First choose a suitable form for the cold energy $E_c(V)$
- b. Select then an appropriate thermodynamic type of EOS, e.g., the general Mie-Grüneisen EOS
- c. Starting from the simplest ones, make further consistent assumptions on the specific form of the thermodynamic state functions determining the thermal components of the system, e.g., $\Gamma(V, T)$ and $C_V(T)$.

With guidance from both experimental data (static compression, Hugoniot, etc.) and theoretical considerations, considerable progress can be achieved in an orderly and systematic way towards the understanding and semiempirical representation of the principal factors determining the EOS of many materials over a fairly wide range of the variables. This is well illustrated, e.g., by the work of the Russian school (Kormer, Al'tshuler et al.) on metals (solid and porous), recently extended to the alkali halides, which, if still unsatisfactory in several aspects, appears nevertheless to have led to the most successful EOS for those materials presently available.

Most purely theoretical results are limited so far to a few very simple systems which provide in this context mainly very high density and or very high temperature asymptotic models. The cold isotherms corresponding to these models are reviewed in the appendix and although a similar study of the corresponding temperature dependent ones would be of interest, its need is diminished by the recent appearance of a comprehensive survey of the thermodynamic properties of matter at high pressures and temperatures by S. G. Brush.⁹ Extensions of the theory to more complex systems is the object of considerable activity but we cannot go here into these recent developments of the many-body theory.

There also exists many more or less successful theories and calculations of the ground state energy and first excited states of crystals near normal densities, but little use has been made of these results in semiempirical EOS work, this region being generally treated empirically.

On the other hand, considerable use is made of the semi-classical statistical theories[†] (T-F, T-F-D, etc.) in bridging the gap between the experimentally accessible region and the simpler asymptotic models. But

"Although the T-F method is known to be approximate, the necessary analysis of the applicability of these results has not been carried out. In the literature there are only qualitative considerations of the non-applicability of the method for small compressions (in the region of low temperatures) and on the improvement of its applicability with increase in temperature. However, the quantitative problems of the limits of the regions of density and temperature in which the method is applicable with a given accuracy, and on the size of the corrections to the quasi-classical equations of state, remain essentially unresolved."^{††}

This paper and several others by the same author as well as similar investigations by S. Golden, N. L. Balazs, Alfred, etc.,¹⁰ present attempts at a solution of this problem. In view of the formal nature of the developments used, the conclusions reached are still tentative and the proper limits of applicability of the statistical models remain unknown. The main result reached in these studies is that inclusion of exchange effects exactly within the framework of the semiclassical model (T-F-D) is inconsistent and that it would be more valid to keep exchange corrections to the lowest order since higher order times are of the same order as neglected quantum corrections. If this is the case, it is questionable whether these statistical models have greater range of validity than their leading terms in an asymptotic expansion in inverse powers of the volume, which can be obtained directly from an electron gas model in a suitable background. It should also be pointed out that calculations on solvable models along the statistical approach with quantum corrections (harmonic oscillator, etc.) have been notably unsuccessful. Furthermore the conclusions reached in the studies mentioned above are basically for isolated atoms or at most for simple monatomic crystals and even less is known about the applicability of the statistical models to polyatomic structures.

Finally, many of the semiempirical EOS for solids are not single phase EOS but rather those of a two-component system: a lattice part and an

[†]Extensive reviews of this approach are available (see appendix and reference 9).
^{††}D.A. Kirzhnits, Soviet, Physic 8, 1081 (1959).

electronic component, the total thermodynamic state functions being obtained additively under the assumption of complete thermodynamic equilibrium. Such a separation corresponds to the usual adiabatic (or the static) approximation in quantum mechanics; in semiempirical EOS work, the two components are generally taken to be noninteracting, although the Kormer et al. EOS with variable lattice specific heat¹¹ does couple them empirically. One should note that in the high density asymptotic models, the separation is that into a system of bare nuclei and one containing all the electrons while near normal densities it is usually one into ionic cores--(nuclei and tightly bound electrons) and a system of conduction electrons. At the present it is still an open question whether a smooth transition between these two regions is possible or whether electronic phase transitions (with or without polymorphic lattice ones) must necessarily occur.

E. SEMIEMPIRICAL EOS FOR SiO_2 .

(1) In the previous report (reference 1), semiempirical EOS for quartz and stishovite were given which agree reasonably well with the experimental Hugoniot data obtained in this program and elsewhere for quartz and dry playas, if the quartz one is used in the low pressure region and the stishovite one in the high pressure region. Detailed calculations for the probable mixed phase region were not made in view of the too great uncertainties affecting the quartz-stishovite transition (see section 3)

The procedure adopted was the one described in reference 1:

(a) The cold isotherm $E_c(V)$ was obtained in the form of a single analytical expression for the whole range of V , the interpolation terms being chosen to be compatible with the functional form of the cold energy as given by the standard T-F asymptotic model. The use of an approximate analytical expression for this asymptotic (T-F) $E_c(V)$ entails a negligible error as compared to the other uncertainties of the model; the largest one of these results[†] from the necessity of introducing an effective monatomic model* for

[†]See reference 1 and the appendix.

*The averaging procedure adopted here differs from that used by L. Knopoff and G. MacDonald (Geophys. Journ. 1, 284, 1958).

the SiO_2 complex if use is to be made of the existing T-F calculations. (Direct T-F calculations for molecules are difficult and few are available).

(b) The usual Mie-Grüneisen EOS with constant Γ was adopted as a thermal description of the system. If no phase transition occurred, a value of $\Gamma = 2/3$ can be taken as giving a crude behavior of SiO_2 over the whole V-T range since $\Gamma = 0.65$ at the reference state and $= 2/3$ in the very high density and/or very high temperature asymptotic models. A higher value of $\Gamma = 1.4$ for stishovite gives closer agreement with high pressure data for quartz although any value from $2/3$ to 1.6 leads to calculated Hugoniot within the experimental error at these pressures (~ 500 kbar).

The effect of a variable chemical composition (exclusive of water content) expressed as a variation in effective Z and V_0 is less than that of a change in the form of the interpolation terms and of no significance in view of the overall limitations of the model. The low pressure cold isotherm is of course sensitive to the bulk modulus at the reference state but playas cannot easily be compacted to solid density and no conclusive experimental data is available on the effect of small changes in the chemical and mineralogic composition on the bulk modulus of the solid phase.

(2) Other possible semiempirical EOS.

The form of $E_c(V)$ used here appears adequate for the present and requires only three parameters determined from the initial density, initial compressibility and sublimation energy of the solid (in addition to its chemical composition) while converging to the high density models* at high pressure.

A simpler form could be derived in the same way by replacing the E_c T-F term by the cold energy expression of an electron gas in a positive lattice background.^{13, 14} This procedure would avoid the use of an effective monatomic model and allow a distinction between polymorphs. The correlation pressure term of this model is known for a few lattices, but the probably more important inhomogeneity correction is still in doubt.¹¹ Further development of such a high density model for polyatomic substances would be worthwhile. The use of

*Nonrelativistic ones.

a simple constant Γ Mie-Grüneisen EOS is of course only a crude first approximation. Several more complex EOS can be used with the same cold isotherm.

(a) An EOS of the form (4-18), in preference to (4-15) for the reasons given in §III with, e.g.,[†]

$$G(V, E^*) = a + \frac{b}{cE^*\rho^{-2}+1}$$

where $\rho = V/V_0$ and a, b, c are adjustable parameters. The parameters would be determined as follows:

$$a + b = \Gamma_0 (\Gamma \text{ at } V = V_0, T = 0, P = 0)$$

"a" chosen a priori to be either 2/3 (perfect gas asymptotic limit) or determined with c by a least square fit to experimental data and temperature dependent T-F calculations corresponding to the parameters of the effective monatomic SiO_2 model. This empirical form would serve mainly to bring the semiempirical EOS thermal components closer to the T-F values at high temperatures. If there is no particular problem using it for stishovite with $\Gamma_0 \approx 1.4$, it may be troublesome for α -quartz in view of the low initial Γ value (0.65) resulting from the loose structure of this crystalline form of SiO_2 . This procedure would require a small computer program and in view of the relative insensitivity of the experimental Hugoniot to Γ , it should be based on a minimum of release adiabat points if a greater range of pressures and/or porosity than those examined are beyond the experimental possibilities.

(b) A Hildebrandt EOS of the form (4-10)

Assuming a purely temperature dependent E^* and C_V from room temperature up, one could make use of an EOS of the form (4-10). $C_V(T)$ would be taken from experimental data at the lower temperature, and extrapolated with the eventual addition of a purely temperature dependent electronic component. Such a model could not reasonably be used over a very extended

[†] Similar to Tillotson's formulation based on (4-15).

range of compression if only because of the volume dependence of the electronic energy band gap and electron effective mass, but may be of limited interest for Hugoniot up to a few megabars.

(c) Two components EOS of the general form

$$E_c = E_c(V) \quad P_c = - \frac{dE_c}{dV}$$

$$E^*(V, T) = E_{\text{latt}}^* + E_{\text{el}}^* \quad P^*(V, T) = P_{\text{latt}}^* + P_{\text{el}}^*$$

offer more flexibility in handling the thermal components in semi-empirical EOS work. The cold isotherm can be handled as previously and separate assumptions can be made on the lattice and the electronic thermal components of the state functions.

The lattice part can be treated in any of the ways described earlier (usual Mie-Grüneisen, Hildebrandt EOS, etc.). In particular one can use the simple Dulong-Petit solid model (constant specific heat $C_V = 3R$) from some non-zero reference temperature T_0 on [†]i.e.,

$$E^*(T) = C_V T + \text{const}$$

$$= 3R \left(T - T_0 + \frac{E_{\text{latt}}^*(T_0)}{3R} \right) = 3R (T - \hat{T}_0)$$

$$P^*(V, T) = \frac{\Gamma(V)}{V} 3R (T - \hat{T}_0) = g_{\text{latt}}(V) T + \text{const}$$

For materials with a relatively high Debye temperature, such a model is rather unsatisfactory at lower temperature and it would be preferable to use a temperature dependent $C_V(T)$, determined from static experimental data

[†]As done by Altshuler, et al for metals ref. 12, 9.

and a better theoretical model (Debye solid, Debye-Einstein solid, etc.). The Hildebrandt EOS is well adapted for not too low temperatures, giving, if T_0 is the reference state (room temperature e.g.)

$$P(V, T) = \frac{VS'_{T_0}(V)}{C_V(T)} = \frac{g_{T_0}(V)}{C_V(T)}$$

$$E_{\text{latt}}^*(T) = \int_{T_0}^T C_V(T) dt + \text{const}$$

$$D_{\text{latt}}^*(T) = \frac{g_{T_0}(V)}{V} T + \text{const}$$

The form of $C_V(T)$ can be chosen to decrease at high temperatures from the $3R$ Dulong-Petit value to the $3R/2$ perfect liquid lattice value*. Since such a model is not extendable to $T_0 = 0$, it is in our opinion best to avoid the use of Slater or McDugall type of relations and treat $g_{T_0}(V)$ empirically.

The electronic thermal component can similarly be treated in several ways, although the quasi-free electron gas model as used by Altschuler, et.al., for metals is of course not applicable directly to the semi-conductors or insulators which constitute the playas. Up to a few ev, one can use the various E_{el}^* , P_{el}^* expressions developed for semi-conductors e.g., as Kormer et al,¹¹ or at higher temperatures the approximate analytical expressions resulting from a fit to the T-F temperature calculations of Latter and others, or combine both. The degree of validity of such assumptions is considerably more difficult to assess than the still unsolved one of the cold models, but there is little doubt, in view in particular of the extensive Russian work on porous metals and ionic crystals, that reasonable EOS must include an electronic component along the above lines already at medium pressures (a few megabars), specially for porous media.

*See e.g., Kormer et al, ref. 11.

If a wide range of porosity and pressure exceeds the present experimental possibilities, it is necessary to include in any semiempirical determination of the thermal components of the EOS a minimum of release adiabat points, because the Hugoniot itself for a solid or a low porosity medium is relatively too insensitive to, e.g., the Γ chosen (such data were not available in time to be included in the theoretical work of this program).

F. CONCLUSIONS AND RECOMMENDATIONS

1. Almost any semiempirical EOS formulation can be used to represent the Hugoniot data in the experimentally accessible region and such Hugoniot points can be reasonably well predicted in the absence of phase changes, from a limited number of parameters determined at the reference state.

2. Such low and medium pressure EOS can be extended in a compatible way to high and very high pressures by introducing various asymptotic models. But, at the present there is no immediate way of asserting the degree of validity of the resulting EOS in any given range of the parameters (outside the experimental region) and this prevents one from selecting on sound grounds a particular EOS as superior to others and of making more than qualitative estimates (guesses) on their respective validity.

3. Although many so-called "corrections" have been introduced with an aim at refining the original semiclassical statistical T-F model, these are often inconsistent and have not increased the degree of reliability of the resulting modified statistical models.

4. Recent developments in many-body quantum (and classical) statistical mechanics give hope that significant progress could be achieved now in obtaining, through bona-fide estimates, quantitative reliability and unambiguous predictions at least for the high density models. Such theoretical work, in conjunction with a more systematic use of existing, near normal density theories and experimental work could allow significant progress to be made in resolving some of the many existing problems in EOS work.

Before any quantitative reliability can be given to proposed EOS of playas, it is definitively necessary to conduct a considerably more intensive investigation of the eventual phase transformations of SiO_2 and other constituent minerals

in dynamic compression and upon pressure release. In particular, any electronic thermal component of the thermodynamic state functions can in no way be extrapolated across such phase transitions from reference state data on the basis of present knowledge.

LIST OF SYMBOLS

Γ	Grüneisen ratio
V	Volume
T	Temperature
P	Pressure
E	Internal energy
S	Entropy
C_v	Specific Heat at constant volume
$P_c(V)$	0°K isotherm
$E_c(V)$	0°K compressional energy
E^*	Thermal component of energy
ρ	Density
$\Gamma_c(V)$	Temperature dependent Grüneisen ratio at 0°K

This page intentionally left blank.

5-EFFECTS OF A PHASE TRANSITION ON THE PROPAGATION OF FINITE AMPLITUDE WAVES

G. E. Duvall and Y. Horie*

A. INTRODUCTION

Many materials have been found to undergo a phase transition on compression. Under some conditions the transition has important effects on the structure and propagation history of a finite amplitude stress wave. One such effect is to produce an instability in the compressive shock wave; another is to introduce the possibility of rarefaction shocks. In Section B below the theory of shock wave stability is reviewed and extended to a form appropriate for discussion of effects due to phase transitions. In Sections C and D polymorphic transitions in which the density increases upon the increase of compression are classified, their phase boundaries are described, and some adiabats and R-H curves in the coexistence region are calculated. The theory is used to discuss transitions in iron, bismuth and quartz, all of which have been studied experimentally.

Notation

P	=	pressure
V	=	specific volume
T	=	temperature in degrees Kelvin
S	=	specific entropy
E	=	specific internal energy
G	=	specific Gibbs energy
H	=	specific enthalpy
ρ	=	mass density = $1/V$
Γ	=	Grüneisen constant
U	=	shock propagation velocity
u	=	particle velocity

*Dept. of Physics, Washington State University

The locus of states in the P-V plane which can be reached by a single shock from a given initial state is called the Hugoniot or R-H curve for that initial state.

The jump conditions for a single shock running into material in the state $P_0, V_0, E_0, u_0 = 0$ and compressing it to the state P_1, V_1, E_1, u_1 are

$$\rho_0 U_1 = \rho_1 (U_1 - u_1) \quad (5-1)$$

$$P_1 - P_0 = \rho_0 U_1 u_1 \quad (5-2)$$

$$E_1 - E_0 = \frac{1}{2}(P_1 + P_0)(V_0 - V_1) \quad (5-3)$$

A number in parentheses in the text indicates one of the numbered references at the end of the report.

B. STABILITY OF SHOCK WAVES

(1) Thermodynamic Criteria

The stability of a single shock transition was first discussed by Rayleigh Ref. (15), who concluded that only compressive shock waves were stable in gases. This conclusion resulted from an analysis which showed entropy change to be positive for a compression shock and negative for one of rarefaction. A negative entropy change violates the second law, so he concluded that only compression shocks are stable. Bethe Ref. (16) investigated the stability condition for a more general equation of state and found the entropy condition to be satisfied if the curvature of the adiabat is everywhere positive, i. e.

$$\left(\frac{\partial^2 P}{\partial V^2} \right)_S > 0 \quad (5-4)$$

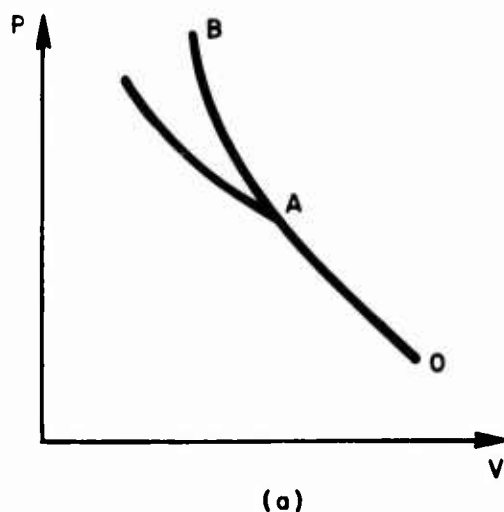
He concluded that if this condition were violated at any point, that point would be one of instability for break-up of the compression shock into multiple

waves. He also demonstrated that Condition (5-4) can be violated at a phase boundary, which then emerges as a point of instability.

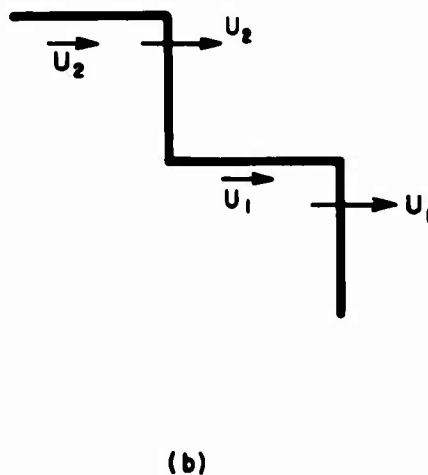
Minshall (17) reported the observation of multiple compression shocks in iron in 1954, and attributed them to plastic yielding and to a polymorphic phase transition. Drummond (18) showed that violation of Condition (5-4) leads to the existence of rarefaction shocks and made calculations in iron.

Rice, McQueen and Walsh (19) suggested a stability criterion which differ from Cond. (5-4). Suppose OAB in Fig. 5-1 is an R-H curve--derived, perhaps, from experimental data--and we wish to test whether or not a single compression shock from O to B is stable against breakup into two shocks: one from O to A and a second from A to B. In order to do this we suppose the single shock to be unstable, having a compression profile like that shown in Fig. 5-1(b). Then the velocity of the first shock with respect to the material following is

$$U_1 - u_1 = V_1 \left(\frac{P_A - P_O}{V_O - V_A} \right)^{1/2} \quad (5-5)$$



ASSUMED R-H CURVE



COMPRESSION PROFILE FOR ASSUMED INSTABILITY AT A

GA-5059-42

FIG. 5-1

The velocity of the second shock with respect to the material ahead of it is

$$U_2 - u_1 = V_1 \left(\frac{P_B - P_A}{V_A - V_B} \right)^{1/2} \quad (5-6)$$

Then if $U_2 - u_1 > U_1 - u_1$, the assumption of instability at A is untenable, since the second shock must overtake the first, in violation of the assumption. Repetition of this test for every point A leads to the following statement: if, for every $P_0 < P_A < P_B$,

$$\frac{P_B - P_A}{V_A - V_B} > \frac{P_A - P_0}{V_0 - V_A} \quad (5-7)$$

then a single shock from O to B is stable. Cond. (5-7) does not appear to be particularly useful. It is not particularly appropriate for a priori construction of a Hugoniot from the equation of state; and in normal practice it is not required for testing of experimental data, since the conditions of the experiment reveal multiple shock structures. If double shock data were reduced by single shock theory, Cond. (5-7) would be useful in principle. In practice a point of possible instability would be revealed by inspection of the P-V or $U_S - u_p$ data.

(2) Hydrodynamic Criterion

In Reference (20) it is shown that if

$$\left| \partial(u + a)/\partial P \right|_S > 0 \quad (5-8)$$

at any point on the path of an accelerating piston, then that point may produce a shock discontinuity in the flow. Moreover this condition is found to be equivalent to Cond. (5-4) at each point on the adiabat of the material.

Except in very simple cases the construction of a Hugoniot requires numerical computations. This suggests the combined procedure for constructing the R-H curve and testing for instability to be described in the next two sections.

(3) Differential Equation of the R-H Curve

We assume all required equation of state information to be known and we seek a procedure whereby the R-H curve can be constructed step-by-step, starting at the initial pressure and proceeding to higher values, testing at each step to determine whether or not a single shock from the initial state to the next higher pressure will be stable. The procedure for constructing the R-H curve in this way is available if we have its differential equation and a suitable test. The differential equation can be obtained as follows:

Suppose the R-H curve is known up to a pressure P_1 and that a single shock from (P_0, V_0) to (P_1, V_1) is stable. Then the internal energy at (P_1, V_1) is given by the R-H equation:

$$E_1 - E_0 = \frac{1}{2}(P_1 + P_0)(V_0 - V_1) \quad (5-9)$$

If a single shock to the higher pressure $P_1 + \delta P_1$ is stable, the change in internal energy will be, to first order in small quantities,

$$\delta E_1 = \frac{1}{2}\delta P_1(V_0 - V_1) - \frac{1}{2}(P_1 + P_0)\delta V_1 \quad (5-10)$$

A thermodynamic path can be found which connects $(P_1 + \delta P_1, V_1 + \delta V_1)$ and (P_1, V_1) . This will require the addition of heat and work. The First and Second laws of Thermodynamics are to be satisfied, so that

$$dE_1 = T_1 dS^e - P_1 dV_1, \quad (5-11)$$

where any entropy change due to irreversible internal processes is included in $P_1 dV_1$. Equating Eqs. (5-10) and (5-11) yields a relation for the rate of increase of entropy along the R-H curve, relative to that which exists in the adiabat:

$$dS^e/dV = (V_0 - V_1)(dP/dV)_{R-H}/2T_1 + (P_1 - P_0)/2T_1 \quad (5-12)$$

if we suppose pressure to be a function of volume and entropy, we can express the rate of change of pressure with respect to volume in any direction in terms of its partial derivatives. In particular, for the R-H curve,

$$\left(\frac{dP}{dV}\right)_{R-H} = \left(\frac{\partial P}{\partial V}\right)_{\text{adiab.}} + \left(\frac{\partial P}{\partial S^e}\right)_V \left(\frac{dS^e}{dV}\right)_{R-H} \quad (5-13)$$

Eliminating dS^e/dV between Eqs. (5-12) and (5-13) yields the differential equation of the R-H curve:

$$\left(\frac{dP}{dV}\right)_{R-H} = \left[\left(\frac{\partial P}{\partial V}\right)_{\text{ad}} + \frac{\Gamma}{2V_1} (P_1 - P_0) \right] \left[1 - \frac{\Gamma}{2V_1} (V_0 - V_1) \right]^{-1} \quad (5-14)$$

In obtaining Eq. (5-14), the following identities have been used:

$$\left(\frac{\partial P}{\partial S}\right)_V = \left(\frac{\partial P}{\partial T}\right)_V \left(\frac{\partial T}{\partial S}\right)_V = \frac{\Gamma T}{V} \quad (5-15)$$

For a material in which compression is reversible, $(\partial P/\partial V)_{\text{ad}} = (\partial P/\partial V)_S$ and S^e is the total entropy.

Integration of Eq. (5-14) yields the R-H curve, provided a single shock is stable everywhere.

(4) Point Stability Criterion

We wish now to answer the following question: if a single shock is stable at the pressure P_1 , will a single shock be stable to $P_1 + \delta P_1$? The Rayleigh line connecting (P_0, V_0) and (P_1, V_1) intersects the R-H curve only at these two points (6); accordingly

$$-\left(\frac{dP}{dV}\right)_{RH, P_1} \geq \frac{P_1 - P_0}{V_0 - V_1}. \quad (5-16)$$

If P_1 is a point of discontinuity in $(dP/dV)_{RH}$, the value on the lower side of P_1 is to be taken. If the point $P_1 + \delta P_1$ is also to be attained through a single shock, Cond. (5-16) must hold above P_1 ; i.e.

$$-\left(\frac{dP}{dV}\right)_{RH, P_1 + \delta P_1} \geq \frac{P_1 - P_0}{V_0 - V_1} \quad (5-17)$$

Substitution of Eq. (5-14) into this inequality yields the condition for stability:

$$\left[\frac{\frac{a^2}{(U_1 - u_1)^2} - \frac{\Gamma(V_0 - V_1)}{2V_1}}{1 - \frac{\Gamma}{2V_1}(V_0 - V_1)} \right]_{P = P_1 + \delta P_1} \geq 1 \quad (5-18)$$

If

$$\Gamma(V_0 - V_1)2V_1 < 1, \quad (5-19)$$

then Cond. (5-18) reduces to a simpler one: P_1, V_1 is a stable point if

$$\lim_{\delta P_1 \rightarrow 0} \left[\frac{a^2}{(U_1 - u_1)^2} \right]_{P_1 + \delta P_1} \geq 1 \quad (5-20)$$

Since Cond. (5-19) is normally satisfied, Cond. (5-20) is a useful one which corresponds to the hydrodynamic Condition that the flow be subsonic behind the shock. *

A situation in which P_1 is a state of instability is illustrated in Fig. 5-2.

C. THERMODYNAMIC FUNCTIONS IN THE COEXISTENCE REGION

We are concerned here with instabilities which may arise when the Hugoniot curve intersects a phase boundary and the compressed material is forced into the coexistence region or on into a second phase. Bethe (16) has shown that such a point may be a point of shock instability.

We restrict consideration to materials which transform isothermally to a higher density form when pressure is applied. Transitions will be classified according to the sign of dP/dT in the coexistence or mixed phase region and the sign of dS/dT on the phase boundary; procedures for constructing

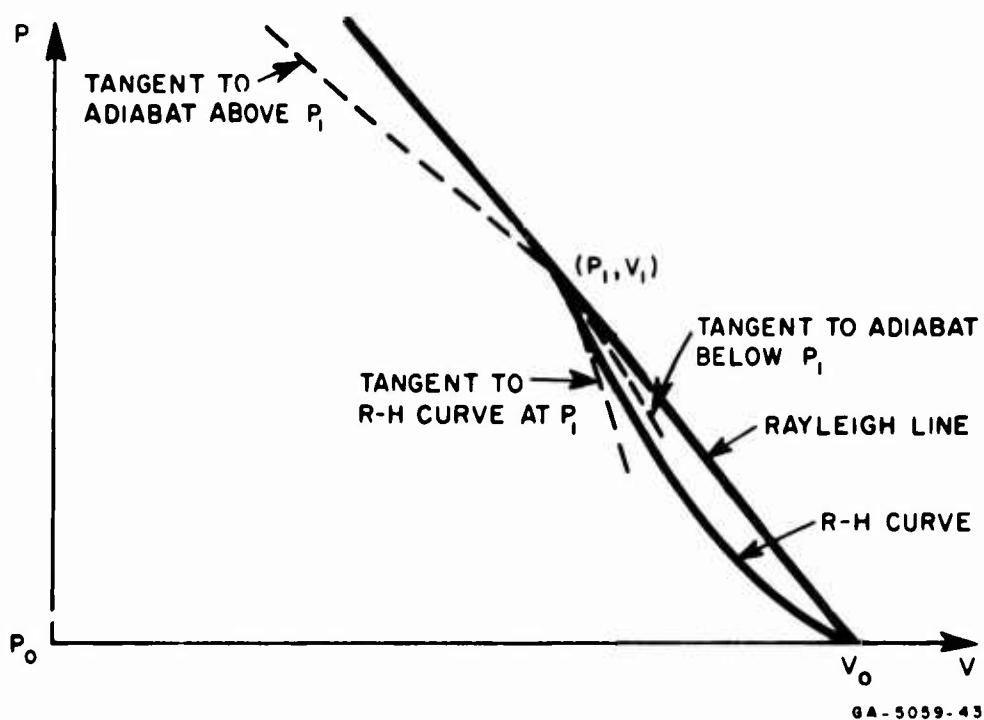


FIG. 5-2 COMPARISON OF SLOPES AT A POINT OF INSTABILITY

*When Cond. (5-19) is satisfied, Cond. (5-18) implies Cond. (5-20) and vice-versa. When Cond. (5-19) is violated, a more detailed investigation based on hydrodynamics will be required to establish the proper criteria for stability.

adiabats and R-H curves in the mixed-phase region are described, some general properties are derived, and some examples are treated.

Although interest here is centered primarily in polymorphic transitions of solids, there is no difference thermodynamically between these and the transformations of melting and vaporization; all are governed by the Clausius - Clapeyron equation in the coexistence region. This will henceforth be designated "C-region" or "C-R", and thermodynamic quantities in the C-region will be denoted by a subscript "M". It is also assumed that isothermal changes satisfy the Gibbs condition at constant P and T .

In Section 5-1, a classification of transitions is made according to the sign of dP/dT and dS_1/dT , where the subscript "1" denotes changes along the boundary between the less dense phase, denoted as phase one or ϕ_1 , and the C-region; and relations between the phase boundary, the adiabat in ϕ_1 and the isotherm in ϕ_1 are derived. In Section 5-2 the slopes of adiabat and Hugoniot in the C-region are derived and some relations at the boundary are established. The slopes of adiabats and R-H curves are compared and the curvature of the adiabat is discussed.

For simplicity we assume the region of interest to be far from a triple-point.

(1) Phase Boundaries

The basis for conventional thermodynamic treatment of phase transitions is the assumption that extensive thermodynamic properties are mass-weighted averages of properties of the two components, i.e., phases. Examples of such are entropy, specific volume, and Gibbs free energy, all of which depend on amount of material, and so vary throughout the C-region. Pressure and temperature can be simultaneously constant during a phase change because they are intensive variables; their values do not depend on the amount of material present.

The mass-weighted relation for extensive variables comes directly from the condition that P and T are constant in the C-region and that surface energies can be neglected. Since $dP = dT = 0$, then $dG = 0 = g_1 dM_1 + g_2 dM_2$, where dM_1 is the fraction of unit mass which goes into phase 1 and

dM_2 is the fraction which goes into phase 2 in the contemplated change. But $-dM_1 = dM_2 = dX$, so $g_1 = g_2$. Here X denotes the fraction of mass that has transformed from phase 1 to phase 2 (Fig. 5-3): $X \equiv (V - V_1)/(V_2 - V_1)$.

With this definition of X , the specific volume at point Q of Fig. 5-3 is

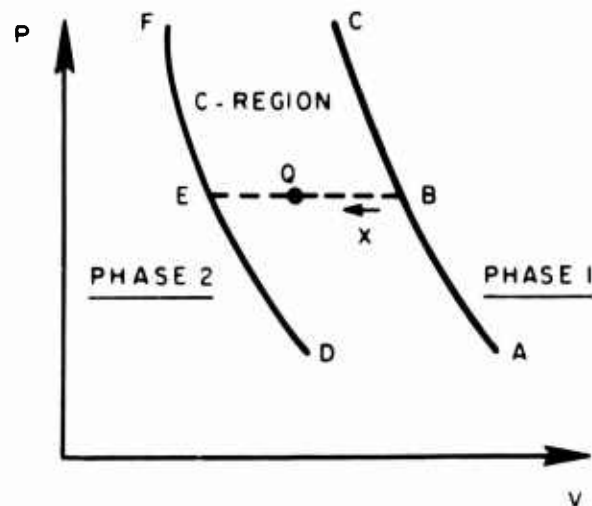
$$\begin{aligned} V &= XV_2 + (1 - X)V_1 \\ &= V_1 + X\Delta V, \quad 0 \leq X \leq 1 \end{aligned} \quad (5-21)$$

where V_1 is specific volume at point B of Fig. 5-3, V_2 is its value at point E , and

$$\Delta V = V_2 - V_1 < 0 \quad (5-22)$$

Then for constant T we have

$$dV = \Delta V dX; dT = 0 \quad (5-23)$$



GA-5059-44

FIG. 5-3 DEFINITION OF THE TRANSITION PARAMETER X

Other extensive variables such as H , S , E , are given by similar expressions:

$$H = H_1 + X \Delta H \quad (5-24)$$

$$S = S_1 + X \Delta S \quad (5-25)$$

$$E = E_1 + X \Delta E \quad (5-26)$$

Temperature on the phase boundary ABC of Fig. (5-3) will be found from the Clausius-Clapeyron equation:

$$dP/dT = \Delta H/T\Delta V = \Delta S/\Delta V \quad (5-27)$$

$$T = T_1 = \int (\Delta V/\Delta S) dP = \int (dT/dP) dP \quad (5-28)$$

Phase changes are commonly studied under static or quasi-static conditions in which either P or T is held nominally constant and the other quantity is slowly varied through the phase transition. The results of such studies are complete when a curve $P(T)$ representing the phase transition is obtained, along with $\Delta V(T)$. Dynamic processes are usually other than isothermal, and this fact leads to the necessity for investigating the geometry of phase boundaries, coexistence regions, adiabats and R - H curves in the S - T and P - V planes if the relations between phase transitions and wave propagation are to be understood.

We first consider phase boundaries in the S - T plane and restrict discussion explicitly to those materials for which

$$\Delta V < 0 \quad (5-29)$$

$$(\partial V/\partial T)_{P_1} > 0 \quad (5-30)$$

Here the subscript " P_1 " denotes a coefficient at constant pressure in ϕ_1 evaluated at the boundary between ϕ_1 and the C-region. A derivative written with a block "d", having subscript "1" on the variable in the numerator, denotes a derivative along the phase boundary between ϕ_1 and C-R. Subscripts "2" have analogous meanings for ϕ_2 and its boundary with the C-region.

The rate of change of entropy along the phase boundary can be expressed as

$$\frac{dS_1}{dT} = \left(\frac{\partial S}{\partial T} \right)_{P_1} + \left(\frac{\partial S}{\partial P} \right)_{T_1} \frac{dP}{dT} \quad (5-31)$$

$$= \frac{C_{P_1}}{T} - \left(\frac{\partial V}{\partial T} \right)_{P_1} \frac{dP}{dT} \quad (5-32)$$

The transformation from Eq. (5-31) to (5-32) is made using a Maxwell relation and the definition of specific heat at constant pressure. We assume that

$$C_{P_1} > 0 ; \quad (5-33)$$

then, with Cond. (5-30) we see that, if $dP/dT < 0$, then $dS_1/dT > 0$. We label this a transition of Type 1. If $dP/dT > 0$, then dS_1/dT may be either positive or negative, depending on the magnitude of dP/dT . We label these transitions Type 2 and Type 3, respectively. These classifications and their properties are summarized in Table 5-I.

Table 5-I
CLASSIFICATION OF POLYMORPHIC TRANSITIONS

$$\Delta V < 0, (\partial V / \partial T)_{P1} > 0, C_{P1} > 0$$

TYPE OF TRANSITION	dP/dT	ΔS	dS ₁ /dT
1	< 0	> 0	> 0
2	> 0	< 0	> 0
3	> 0	< 0	< 0

The slope of the second phase boundary comes from the identity

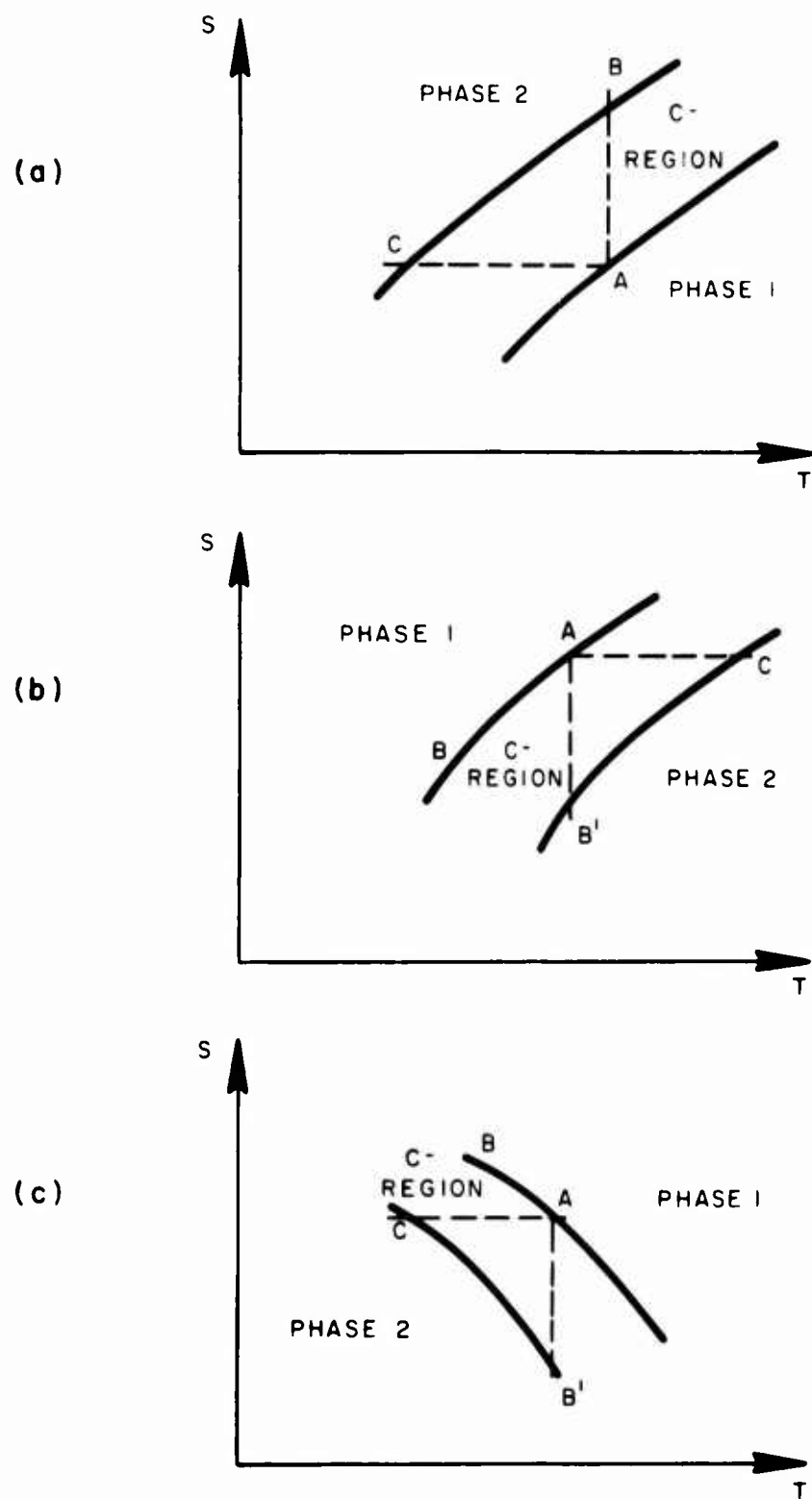
$$\frac{dS_2}{dT} = \frac{dS_1}{dT} + \frac{d}{dT} (\Delta H/T) .$$

if $\Delta H/T$ increases with T , then $dS_2/dT > dS_1/dT$ and vice-versa. It is unfortunate that knowledge of most phase transitions does not include the sign and magnitude of this derivative. It will be neglected in most of what follows.

From Table 5-I it is possible to construct schematic representations of the geometry of the phase boundaries in the S-T plane. These are shown in Fig. 5-4. For Type 1, Fig. 5-4(a) ϕ_2 lies above and to the left of ϕ_1 since $\Delta S > 0$; consequently temperature decreases along an adiabat AC traversed from ϕ_1 to ϕ_2 . Type 2, shown in Fig. 5-4(b) has the relative locations of ϕ_1 and ϕ_2 interchanged, $\Delta S < 0$ and T increases from ϕ_1 to ϕ_2 along an adiabat. Type 3, Fig. 5-4(c) has phase boundaries of negative slope, ϕ_1 is above and to the right of ϕ_2 , and T decreases from ϕ_1 to ϕ_2 along an adiabat.

Bridgman (21) has noted that dP/dT for polymorphic transitions is commonly the order of 50 bars per degree Centigrade; i. e. transitions of Types 2 and 3 are more common than those of Type 1. Slater (22) points out that this is to be expected since increases in entropy are normally associated with increases in volume. He goes farther to show that, if $\Delta S/\Delta V$ is identified with $(\partial S/\partial V)_T$ for a single phase, we have

$$(\partial S/\partial V)_T = \Gamma C_{V/V} \quad (5-34)$$



GA-5059-45

FIG. 5-4 RELATIVE POSITIONS OF PHASE BOUNDARIES IN S-T PLANE; $\Delta V < 0$

(a) Type 1: $dP/dT < 0$, $\Delta S > 0$, $dS/dT > 0$

(b) Type 2: $dP/dT > 0$, $\Delta S < 0$, $dS/dT > 0$

(c) Type 3: $dP/dT > 0$, $\Delta S < 0$, $dS/dT < 0$

where Γ is the Grüneisen constant and C_V is specific heat at constant volume. For $C_V = 3R$ per mol, $\Gamma = 2$ and $V = 10$ cc/mol,

$$\Delta S/\Delta V = (\partial S/\partial V)_T \simeq 50 \text{ bars/}^\circ\text{C} \quad (5-35)$$

Using Eq. (5-34) in Eq. (5-32) and equating C_P to C_V , we arrive at the expression

$$\frac{dS_1}{dT} \simeq \frac{C_P}{T} \left[1 - \frac{\Gamma T}{V} \left(\frac{\partial V}{\partial T} \right)_P \right]. \quad (5-36)$$

Taking $\Gamma = 2$ and $(1/V)(\partial V/\partial T)_P \lesssim 3 \times 10^{-4}$, we conclude that

$$dS_1/dT \gtrsim (C_p/T) \left[1 - 0.6 \times 10^{-3} T \right] \quad (5-37)$$

for most solids. Thus, except for very high temperature transitions, we will normally expect Type 2 to prevail. In fact no transition of Type 3 is known to the authors.

Incidentally, the above classification suggests a fourth Type in which dS/dT is negative with ϕ_2 above ϕ_1 ; this corresponds to $\Delta V > 0$, which is a case of no interest at present.

A procedure for determining the relative dispositions of the pure phase regions and their boundaries in the P - V plane is suggested by a calculation in Reference (16). Considering specific volume to be a function of P and T , we have

$$\left(\frac{\partial V}{\partial P} \right)_{S1} = \left(\frac{\partial V}{\partial P} \right)_{T1} + \left(\frac{\partial V}{\partial T} \right)_{P1} \left(\frac{\partial T}{\partial P} \right)_{S1} \quad (5-38)$$

$$\frac{dV_1}{dP} = \left(\frac{\partial V}{\partial P} \right)_{T_1} + \left(\frac{\partial V}{\partial T} \right)_{P_1} \frac{dT}{dP} \quad (5-39)$$

For $(\partial T/\partial P)_{S_1}$,

$$\left(\frac{\partial T}{\partial P} \right)_{S_1} = - \frac{\left(\frac{\partial S}{\partial P} \right)_{T_1}}{\left(\frac{\partial S}{\partial T} \right)_{P_1}} = \frac{T}{C_{P_1}} \left(\frac{\partial V}{\partial T} \right)_{P_1} > 0 \quad (5-40)$$

The inequality follows from Conds. (5-30) and (5-33) and implies that

$$(\partial V/\partial P)_{S_1} > (\partial V/\partial P)_{T_1} \quad (5-41)$$

Conversely, this inequality implies that of Eq. (5-40). Eqs. (5-38), (5-39) and (5-40) then imply the following relations among dV_1/dP , $(\partial V/\partial P)_{S_1}$, and $(\partial V/\partial P)_{T_1}$ for the three types of phase transitions described in Table 5-I;

Type 1

$$\frac{dP}{dT} < 0, \quad \frac{dV_1}{dP} < \left(\frac{\partial V}{\partial P} \right)_{T_1} < \left(\frac{\partial V}{\partial P} \right)_{S_1}. \quad (5-42)$$

Type 2

$$\frac{dP}{dT} > 0, \quad \frac{dS_1}{dT} > 0, \quad \frac{C_{P_1}}{T} > \left(\frac{\partial V}{\partial T} \right)_{P_1} \frac{dP}{dT}$$

$$\therefore dT/dP > (\partial T/\partial P)_{S_1} \text{ and} \quad (5-43)$$

$$\frac{dV_1}{dP} > \left(\frac{\partial V}{\partial P} \right)_{S_1} > \left(\frac{\partial V}{\partial P} \right)_{T_1}.$$

Type 3

$$\begin{aligned} \frac{dP}{dT} > 0, \frac{dS_1}{dT} < 0, \frac{C_{P1}}{T} < \left(\frac{\partial V}{\partial T} \right)_{P1} \frac{dP}{dT} \\ \therefore \frac{dT}{dP} < \left(\frac{\partial T}{\partial P} \right)_{S1} \text{ and} \\ \left(\frac{\partial V}{\partial P} \right)_{S1} > \frac{dV_1}{dP} > \left(\frac{\partial V}{\partial P} \right)_{T1}. \end{aligned} \quad (5-44)$$

These relations are described in Fig. 5-5. For Type 2, dV_1/dP may be positive; for the others it must be negative if $(\partial V/\partial P)_S$ and $(\partial V/\partial P)_T$ are both negative.

The slope of the second phase boundary is obtained from the definition $V_2 - V_1 = \Delta V = f(P) < 0$. Then

$$dV_2/dP = dV_1/dP + d(\Delta V)/dP$$

or

$$\frac{dP_2}{dV} = \frac{dP_1/dV}{1 + \frac{dP_1}{dV} \frac{d(\Delta V)}{dP}} \quad (5-45)$$

if $d(\Delta V)/dP > 0$ and $(dP_1/dV) \left| d(\Delta V)/dP \right| > -1$, then $dP_2/dV < 0$ and $|dP_2/dV| > |dP_1/dV|$. This follows from the previous result that $dP_1/dV < 0$ when $dP/dT < 0$. However, if $(dP_1/dV) \left| d(\Delta V)/dP \right| < -1$, then the denominator of Eq. (5-45) is negative and $dP_2/dV > 0$. This behavior would be expected near a critical point where $\Delta V \rightarrow 0$ as $P \rightarrow P_C$.

For purposes of illustration we consider a region where $dP_2/dV = dP_1/dV$. Then, for example, for Type 1 there may be a situation like that shown in Fig. 5-6. Here part of the region contained between the two phase boundaries is triply mapped: first by the isotherm GB of phase 1, then by

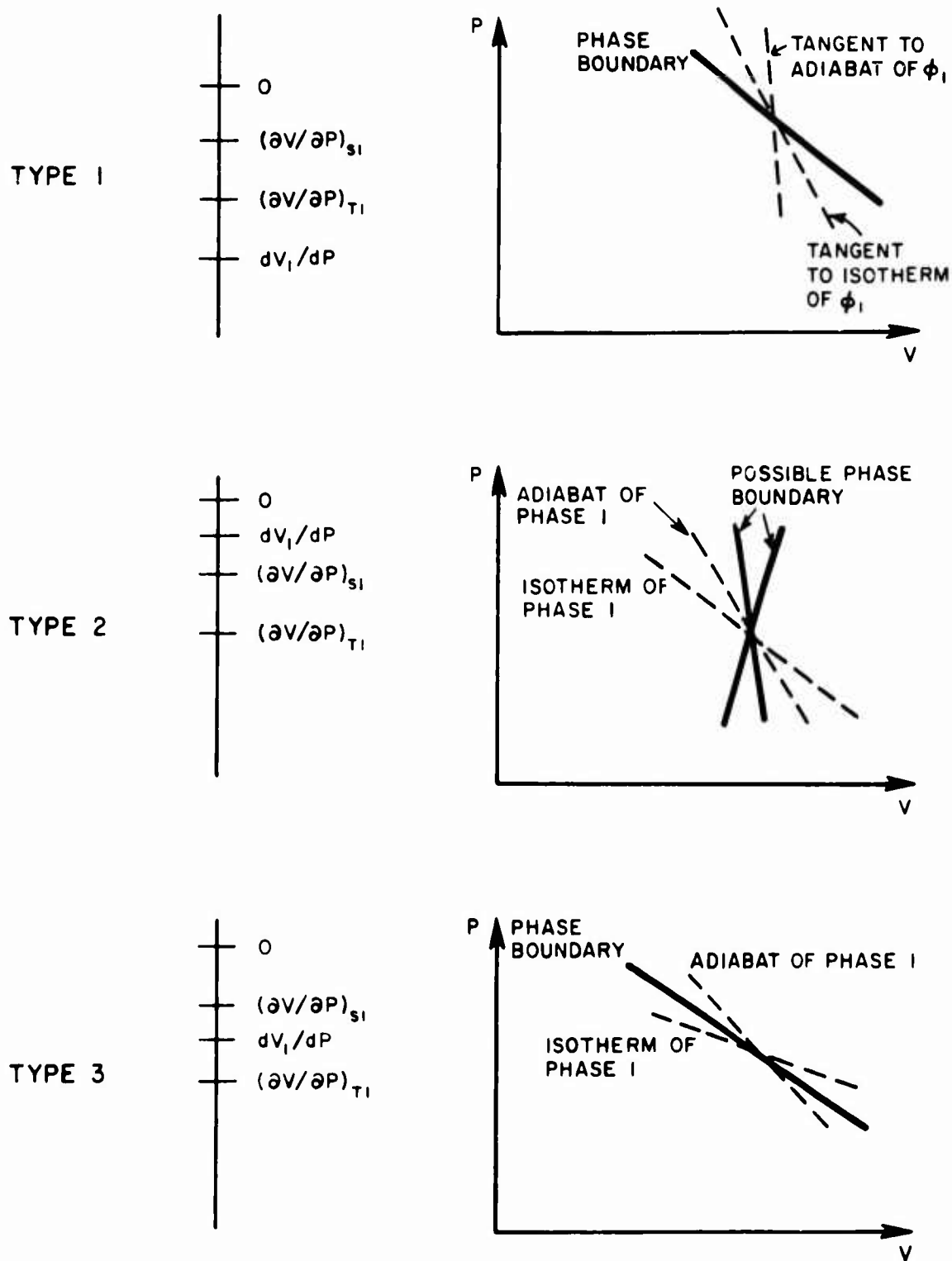


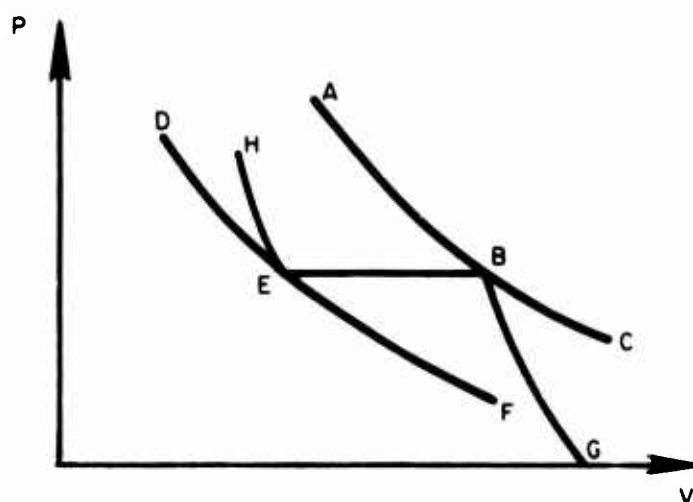
FIG. 5-5 RELATIVE SLOPES OF ISOTHERM, PHASE BOUNDARY AND ADIABAT IN P-V PLANE

the isotherms BE of the mixed phase, and lastly by the isotherms EH of Phase 2. EH must lie above DEF if $(\partial V/\partial T)_{P_2} > 0$ and $C_{P_2} > 0$ by virtue of the equation corresponding to Eq. (5-39) for the second phase boundary when $dP/dT < 0$.

Any apparent anomaly in such a multiple mapping of the P-V plane is immediately resolved by recalling that

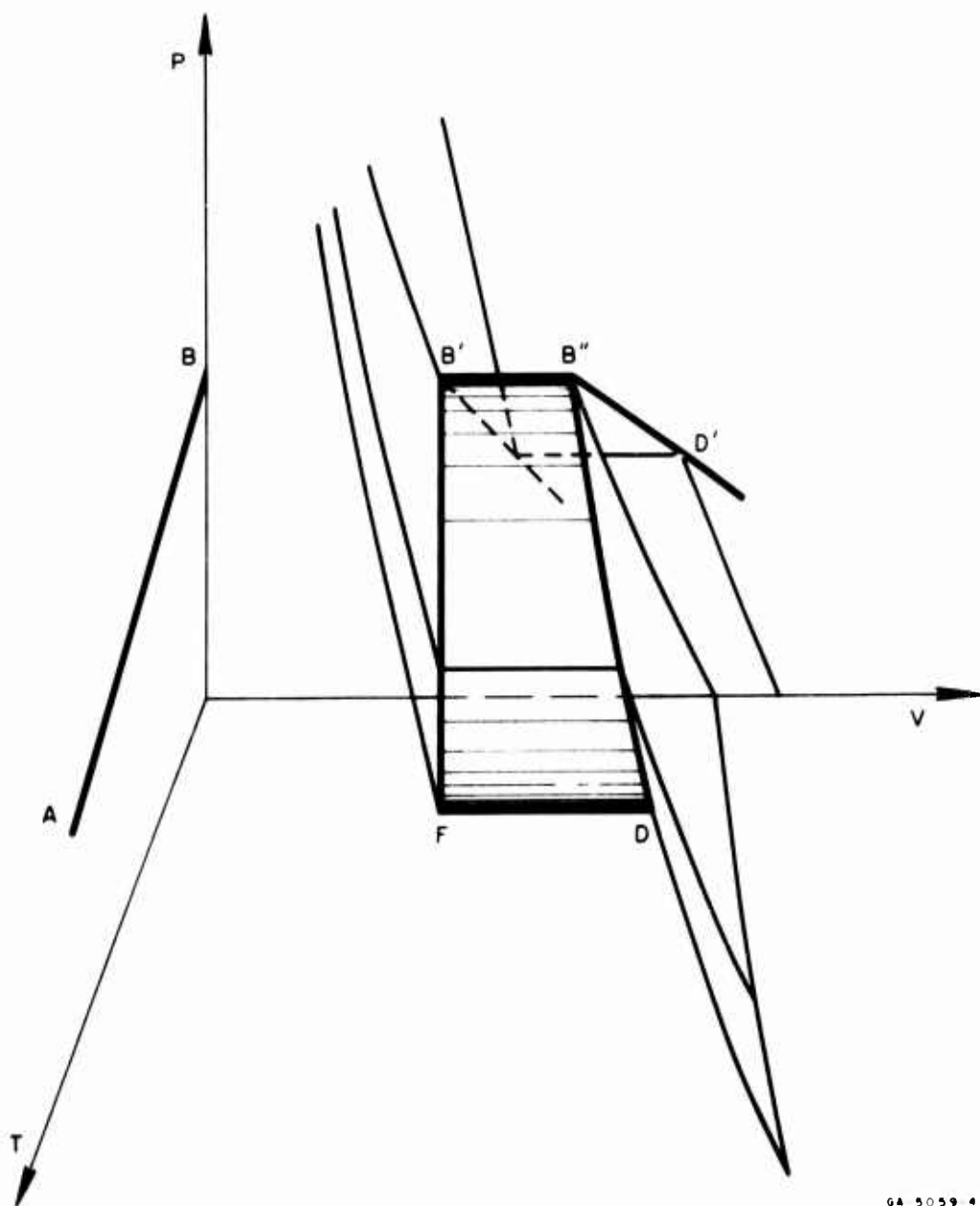
behavior in the P-V plane simply reflects a projection of relations on the P-V-T surface. Fig. 5-7 represents a P-V-T surface for a material with a phase change of Type 1. AB is the phase line in the P-T plane, $dP/dT < 0$; it is the projection of the cylindrical surface of the coexistence region, DFB'B'', onto the P-T plane, B''D' is the projection of B''D onto the P-V plane, etc.

The three types are summarized graphically in the P-V and S-T planes in Fig. 5-8.



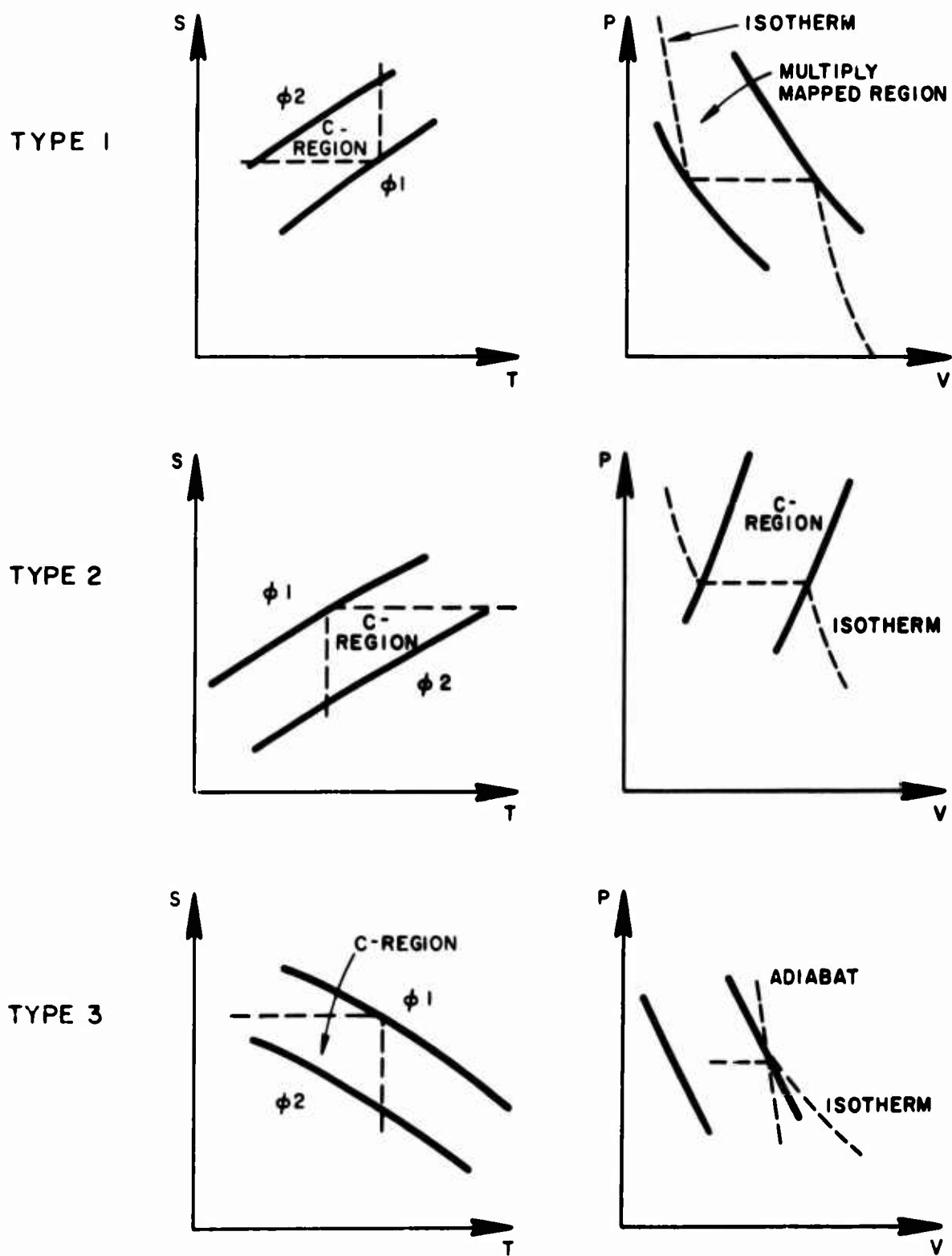
GA-5059-4'

FIG. 5-6 TRIPLY-MAPPED REGION IN THE P-V PLANE FOR TYPE 1



GA 5059 48

FIG. 5-7 EQUATION OF STATE SURFACE IN P-V-T SPACE



GA-5089-49

FIG. 5-8 PHASE BOUNDARIES IN S-T AND P-V PLANES

(2) Adiabats and R-H Curve

(2.1) Adiabat. We first obtain an expression for the adiabat traversing the coexistence region in the P - V plane. Referring to Fig. 5-9, we wish to calculate the volume at point C , pressure P , which has the same entropy as point A on the phase boundary. In order to do this we compute the entropy at C by integrating along ABC and setting $S_C - S_A = 0$. The resulting equation can be differentiated and solved for the adiabatic slope at C ; i.e.

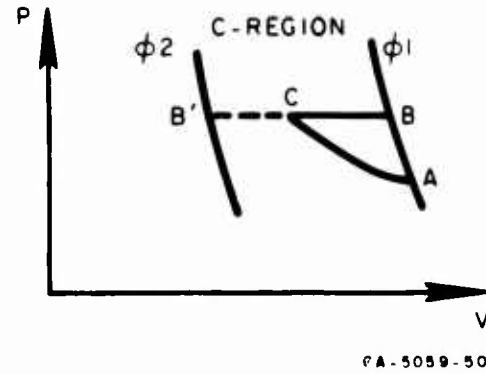


FIG. 5-9 ADIABAT IN THE COEXISTENCE REGION

$$S_C - S_A = 0 = \int_A^B (dS_1/dP)dP + X\Delta S \quad (5-46)$$

where $\Delta S = S_2 - S_1$ evaluated at $P = P_B$. Henceforth the quantities at B and B' are denoted by subscripts "1" and "2"; quantities at the boundary point A will be denoted by subscript "A".

From Eq. (5-21)

$$X = X(P) = (V - V_1)/(V_2 - V_1) \quad (5-47)$$

Combining Eqs. (5-46) and (5-47):

$$\int_A^B (dS_1/dP)dP + (\Delta S/\Delta V)(V - V_1) = 0 \quad (5-48)$$

Differentiate this to obtain

$$\frac{dS_1}{dP} + \frac{\Delta S}{\Delta V} \left[\left(\frac{\partial V}{\partial P} \right)_{SM} - \frac{dV}{dP} \right] + (V - V_1) \frac{d}{dP} \left(\frac{\Delta S}{\Delta V} \right) = 0. \quad (5-49)$$

Here, as before, total derivatives refer to variations along the phase boundary adjacent to phase 1. All quantities are functions of the pressure P , and the subscript SM means entropy is constant and the quantity is evaluated in the mixed phase region. Recall that $\Delta S/\Delta V = dP/dT$ and solve for the adiabatic derivative:

$$\left(\frac{\partial V}{\partial P}\right)_{SM} = \frac{dV_1}{dP} - \frac{dS_1}{dP} \frac{dT}{dP} - (V - V_1) \frac{d}{dP} \left(\ln \frac{dP}{dT}\right). \quad (5-50)$$

This is the required adiabatic slope. The derivatives dV_1/dP and dS_1/dP are given by Eqs. (5-39) and (5-51) following:

$$\frac{dS_1}{dP} = \left(\frac{\partial S}{\partial P}\right)_{T1} + \left(\frac{\partial S}{\partial T}\right)_{P1} \frac{dT}{dP} \quad (5-51)$$

$$= -\left(\frac{\partial V}{\partial T}\right)_{P1} + \frac{C_{P1}}{T} \frac{dT}{dP}. \quad (5-52)$$

Substitution of Eqs. (5-39) and (5-52) into Eq. (5-50) yields

$$\left(\frac{\partial V}{\partial P}\right)_{SM} = \left(\frac{\partial V}{\partial P}\right)_{T1} + 2\left(\frac{\partial V}{\partial T}\right)_{P1} \frac{dT}{dP} - \frac{C_{P1}}{T} \left(\frac{dT}{dP}\right)^2 - (V - V_1) \frac{d}{dP} \left(\ln \frac{dP}{dT}\right). \quad (5-53)$$

Eq. (5-53) applies to an arbitrary point in the coexistence region. At the boundary of phase 1, $V = V_1$, and it is seen that a discontinuity in the adiabatic slope exists, as shown by Bethe (16); i. e., at the phase boundary

$$\left(\frac{\partial V}{\partial P}\right)_{SM1} = \left(\frac{\partial V}{\partial P}\right)_{T1} + 2\left(\frac{\partial V}{\partial T}\right)_{P1} \frac{dT}{dP} - \frac{C_{P1}}{T} \left(\frac{dT}{dP}\right)^2 \quad (5-54)$$

$$\left(\frac{\partial V}{\partial P}\right)_{S1} = \left(\frac{\partial V}{\partial P}\right)_{T1} + \left(\frac{\partial V}{\partial T}\right)_{P1} \left(\frac{\partial T}{\partial P}\right)_{S1} = \left(\frac{\partial V}{\partial P}\right)_{T1} + \frac{T}{C_{P1}} \left(\frac{\partial V}{\partial T}\right)_{P1}^2, \quad (5-55)$$

where the subscript SM1 refers to the mixed phase side at the phase boundary. Subtracting the first of these from the second yields

$$\begin{aligned} \left(\frac{\partial V}{\partial P}\right)_{S1} - \left(\frac{\partial V}{\partial P}\right)_{SM1} &= \frac{T}{C_{P1}} \left(\frac{\partial V}{\partial T}\right)_{P1}^2 - 2 \left(\frac{\partial V}{\partial T}\right)_{P1} \frac{dT}{dP} + \frac{C_{P1}}{T} \left(\frac{dT}{dP}\right)^2 \\ &= \left[\sqrt{\frac{T}{C_{P1}}} \left(\frac{\partial V}{\partial T}\right)_{P1} - \sqrt{\frac{C_{P1}}{T}} \frac{dT}{dP} \right]^2 > 0. \end{aligned} \quad (5-56)$$

Consequently there is always a discontinuity in the adiabatic slope at the phase boundary, except when $(\partial T/\partial P)_{S1} = dT/dP$; and the slope of the adiabat in the pure phase is always steeper than that in the mixed phase, i. e.

$$|\partial P/\partial V|_{S1} > |\partial P/\partial V|_{SM1} \quad (5-57)$$

The relation of $(\partial V/\partial P)_{SM1}$ to other slopes at the phase boundary can be determined for the three Types of transition as follows:

Type 1

According to Eqs. (5-39) and (5-54),

$$\left(\frac{\partial V}{\partial P}\right)_{SM1} - \frac{dV}{dP} = \left(\frac{\partial V}{\partial T}\right)_{P1} \frac{dT}{dP} - \frac{C_{P1}}{T} \left(\frac{dT}{dP}\right)^2 < 0. \quad (5-58)$$

Type 2

Eq. (5-54) can be written

$$\left(\frac{\partial V}{\partial P}\right)_{SM1} - \left(\frac{\partial V}{\partial P}\right)_{T1} = - \left(\frac{dT}{dP}\right)^2 \left[2 \frac{dS_1}{dT} - \frac{C_{P1}}{T} \right]. \quad (5-59)$$

By the argument leading to Eq. (5-37), we may expect that the right hand side of Eq. (5-59) is normally negative, though it may have either sign.

Type 3

$$\left(\frac{\partial V}{\partial P}\right)_{SM1} - \frac{dV_1}{dP} > 0. \quad (5-60)$$

The relations between various slopes at the phase boundary are displayed in Fig. 5-10.

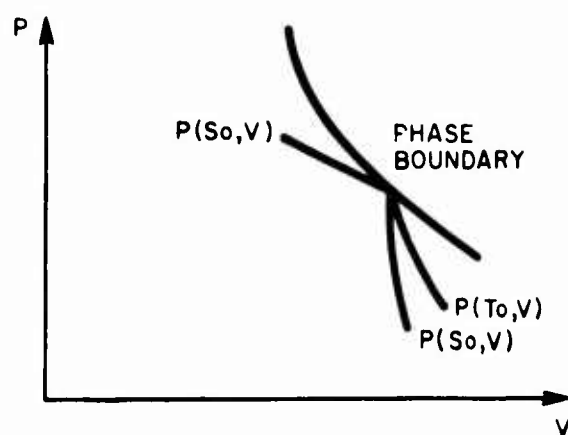
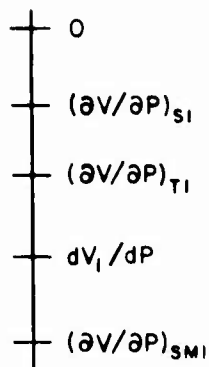
The curvature of the adiabat can be obtained by differentiating Eq. (5-50) directly:

$$\begin{aligned} \left(\frac{\partial^2 V}{\partial P^2}\right)_{SM} &= \frac{d}{dP} \left[\frac{dV_1}{dP} - \frac{dS_1}{dP} \frac{dT}{dP} \right] - \left[\left(\frac{\partial V}{\partial P}\right)_{SM} - \frac{dV_1}{dP} \right] \\ &\quad \cdot \frac{d}{dP} \left(\ln \frac{dP}{dT} \right) - (V - V_1) \frac{d^2}{dP^2} \left(\ln \frac{dP}{dT} \right). \end{aligned} \quad (5-60.1)$$

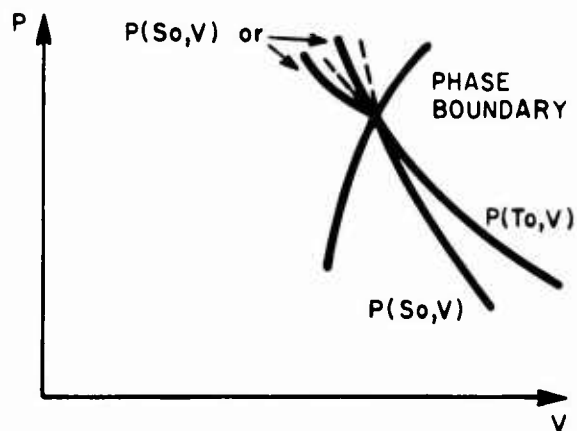
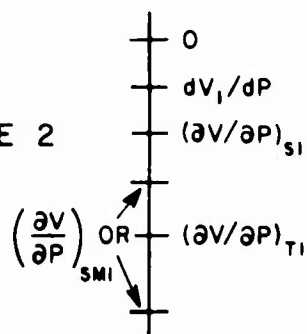
At the phase boundary where $V = V_1$, this reduces to

$$\left(\frac{\partial^2 V}{\partial P^2}\right)_{SM1} = \frac{d}{dP} \left[\frac{dV_1}{dP} - \frac{dS_1}{dP} \frac{dT}{dP} \right] - \left[\left(\frac{\partial V}{\partial P}\right)_{SM1} - \frac{dV_1}{dP} \right] \frac{d}{dP} \left(\ln \frac{dP}{dT} \right). \quad (5-60.2)$$

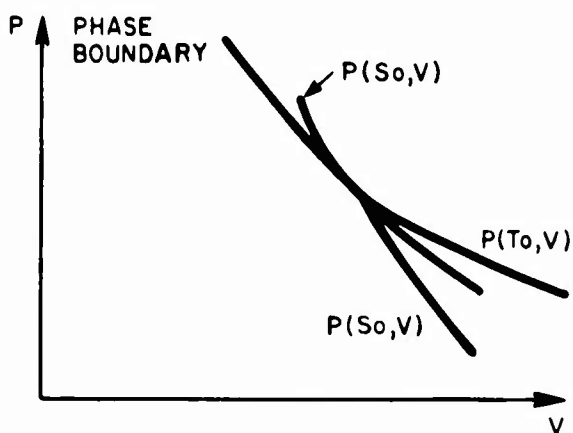
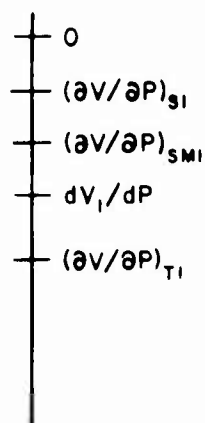
TYPE 1



TYPE 2



TYPE 3



GA-5059-51

FIG. 5-10 RELATIVE SLOPES AT THE PHASE BOUNDARY

(2.2) R-H Curve. The R-H curve and adiabat in a normal material of single phase have a second-order contact at the origin of the Hugoniot (9); the entropy difference between Hugoniot and adiabat is then third order in the compression. If the intersection of phase boundary and Hugoniot is a point of instability for a single shock with final amplitude in the C-region or phase 2, then this intersection, A in Fig. 5-11, may be expected to serve as initial state for a second shock following the first (\mathcal{S}_2 in Fig. 5-11). Accordingly the relation between that portion of the Hugoniot originating at point A and the adiabat in the C-region originating at A may be expected to be the same as that existing between adiabat and Hugoniot in a single phase. A careful review of the premises on which the single-phase result is based reveals no reason for doubting that it holds for the C-region, and a direct calculation, based on the following analysis, verifies it.

In order to determine the locus of the R-H curve in the C-region, consider the situation depicted in Fig. 5-12. Point B represents the final state of a second shock originating at point A on the phase boundary. The enthalpies at A and B are connected by the R-H equation; they can also be calculated by an integration along the path ADB. Equating the two yields the equation of the

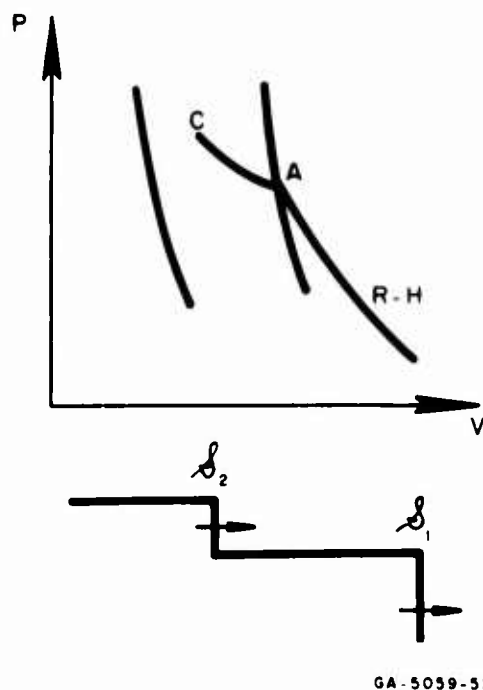


FIG. 5-11 SECOND SHOCK ORIGINATING AT A PHASE BOUNDARY

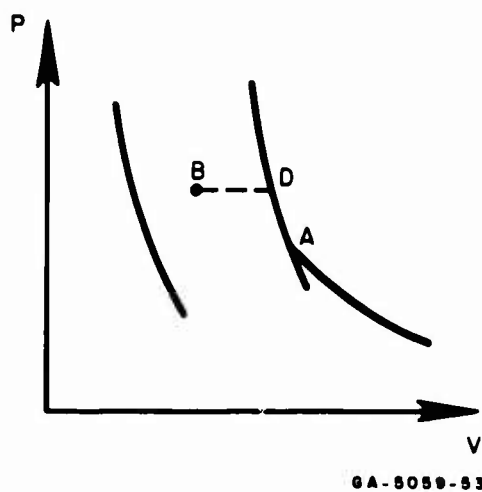


FIG. 5-12 CALCULATION OF HUGONIOT IN C-REGION

R-H curve in the C-region:

$$H_B - H_A = \frac{1}{2} (P - P_A) (V + V_A) = \int_{P_A}^P (dH_1/dP) dP + X\Delta H. \quad (5-61)$$

where $H_1(P)$ is enthalpy on the phase boundary and

$$X\Delta H = \frac{V - V_1}{V_2 - V_1} \Delta H = T (V - V_1) \frac{dP}{dT}. \quad (5-62)$$

The right hand side of Eq. (5-62) is a function of P alone. Substituting Eq. (5-62) into Eq. (5-61) and differentiating with respect to P yields an equation for the slope of the Hugoniot in the C-region.

$$\begin{aligned} \left(\frac{dV}{dP} \right)_{RH} \left[T \frac{dP}{dT} - \frac{1}{2} (P - P_A) \right] &= T \frac{dP}{dT} \frac{dV_1}{dP} - \frac{dH_1}{dP} \\ &- T (V - V_1) \frac{d}{dP} \left(\frac{dP}{dT} \right) + \frac{1}{2} (V_A - V) + V_1. \end{aligned} \quad (5-63)$$

Divide Eq. (5-63) by $T dP/dT$ and substitute into it the identity

$$dH_1/dP = V_1 + T dS_1/dP \quad (5-64)$$

to obtain

$$\begin{aligned} \left(\frac{dV}{dP} \right)_{RH} - \frac{1}{2T} \frac{dT}{dP} (P - P_A) \left(\frac{dV}{dP} \right)_{RH} &= \frac{dV_1}{dP} - \frac{dS_1}{dP} \frac{dT}{dP} \\ &- (V - V_1) \frac{d}{dP} \left(\ln \frac{dP}{dT} \right) + \frac{V_A - V}{2T} \frac{dT}{dP}. \end{aligned} \quad (5-65)$$

The slope at the phase boundary, $(dV/dP)_{RH1}$, is given by Eq. (5-54) or by setting $V = V_1 = V_A$ in Eq. (5-65); the curvature at the phase boundary is given by Eq. (5-60.2).

(2.3) Relative Slopes of Adiabats and R-H Curve. For material in a single phase, the slope of the Hugoniot and the slope of an adiabat crossing the Hugoniot are related by Eq. (5-14), which can be cast in the following form:

$$\frac{c^2 - a^2}{c^2} = \frac{\Gamma}{2V} (V_0 - V) \left[1 - \frac{(U - U_0)^2}{c^2} \right], \quad (5-66)$$

Here

$$c^2 = -V^2 (dP/dV)_{RH}$$

$$a^2 = -V^2 (\partial P / \partial V)_S$$

$$\Gamma = (V/C_V)(\partial P / \partial T)_V.$$

A relation identical in form can be derived for the C-region. Eq. (5-65) can be written:

$$\left(\frac{dP}{dV} \right)_{RHM} = \left(\frac{\partial P}{\partial V} \right)_{SM} \frac{1 - \frac{1}{2T} \frac{dT}{dP} (P - P_A)}{1 + \frac{V_A - V}{2T} \frac{dT}{dP} \left(\frac{\partial P}{\partial V} \right)_{SM}}, \quad (5-67)$$

where (P_A, V_A) represents the intersection of the ϕ_1 phase boundary and the Hugoniot.

Define c^2 and a^2 as in Eq. (5-66), then Eq. (5-67) becomes

$$\frac{c^2 - a^2}{c^2} = \frac{\Gamma_M}{2V} (V_A - V) \left[1 - \frac{\frac{P - P_A}{V_A - V}}{-\left(\frac{dP}{dV}\right)_{RHM}} \right], \quad (5-68)$$

where

$$\Gamma_M = \frac{V}{C_{VM}} \frac{dP}{dT} = - \frac{V}{T} \left(\frac{\partial P}{\partial V} \right)_{SM} \frac{dT}{dP} C_{VM} = T \left(\frac{\partial S}{\partial T} \right)_{VM} \quad (5-69)$$

$$\left(\frac{\partial P}{\partial T} \right)_{VM} \equiv \left(\frac{\partial P}{\partial T} \right)_{SM} \equiv \frac{dP}{dT}.$$

The specific heat in the C-region can also be expressed in the form:

$$C_{VM} = T \frac{dS_1}{dT} + T(V - V_1) \frac{d^2 P}{dT^2} - T \frac{dV_1}{dP} \left(\frac{dP}{dT} \right)^2. \quad (5-70)$$

This is obtained by differentiating Eq. (5-46).

In order to determine the sign of $c^2 - a^2$ in Eq. (5-68), note that the sign of the bracket is positive if the slope of the R-H curve at P is greater than that of the Rayleigh line from P_A . This is certainly true if $(d^2 P / dV^2)_{RHM} > 0$; this condition is unnecessarily restrictive, but we shall use it for simplicity. Similarly if $(d^2 P / dV^2)_{RHM} < 0$ everywhere between P_A and P , the bracket is negative. In order to determine the sign of $-(\partial V / \partial P)_{SM}$, refer to Eq. (5-50); it can be written

$$\left(\frac{\partial V}{\partial P} \right)_{SM} = \left(\frac{\partial V}{\partial P} \right)_{SM1} - (V - V_1) \frac{d}{dP} \left(\ln \frac{dP}{dT} \right). \quad (5-71)$$

Here $(\partial V/\partial P)_{SM1}$ is evaluated at $V_1(P)$; it is not the slope of the adiabat of Eq. (5-71) where it intersects the phase boundary. Then if $(\partial V/\partial P)_{S1} < 0$ at all points of the phase boundary, so is $(\partial V/\partial P)_{SM1}$ according to Fig. 5-10. Then if the second term on the right-hand side of Eq. (5-71) does not override the first, $(\partial V/\partial P)_{SM} < 0$; $V_A - V$ is positive, so that

$$\text{sgn } (c^2 - a^2) = \text{sgn } (dT/dP) \text{sgn } (d^2P/dV^2)_{RHM}, \quad (5-72)$$

where

$$\text{sgn } x = + 1 \text{ if } x > 0$$

$$\text{sgn } x = - 1 \text{ if } x < 0.$$

For $(d^2P/dV^2)_{RHM} > 0$:

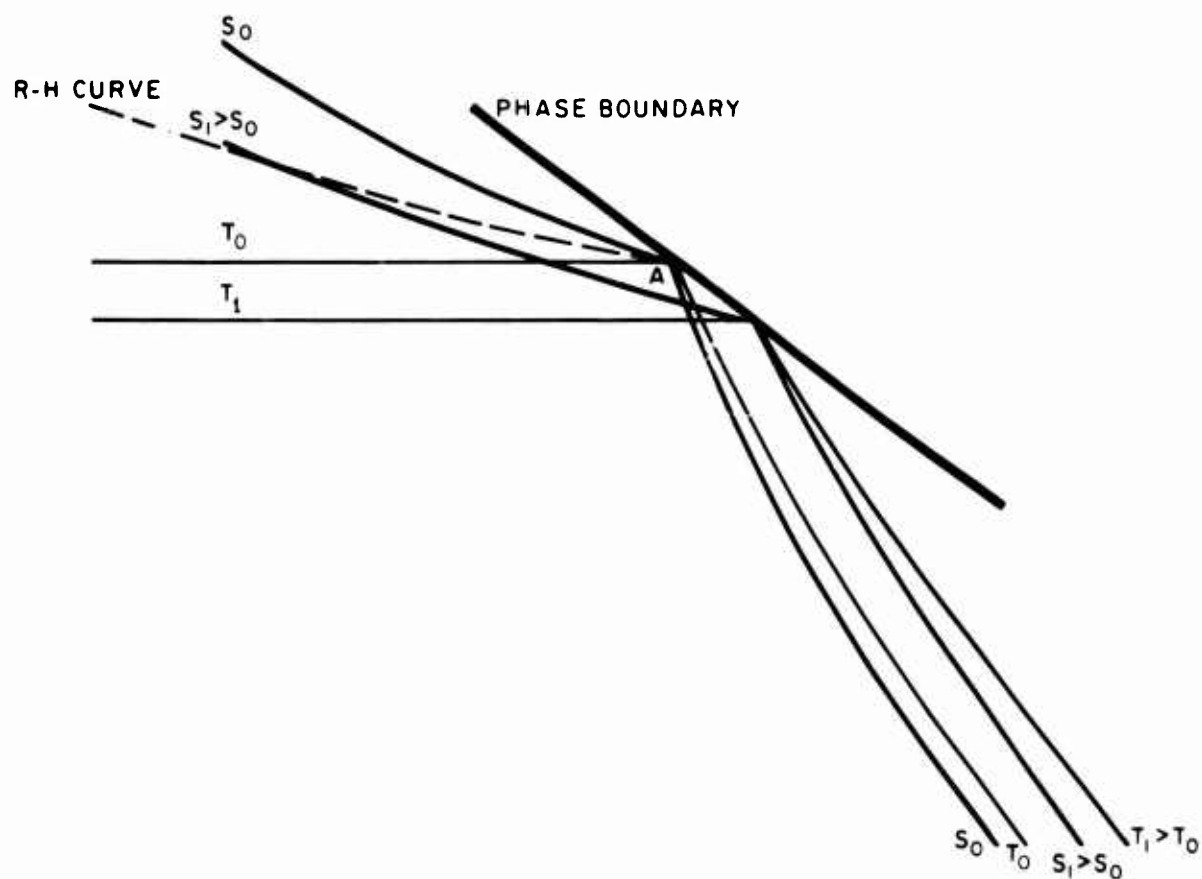
Type 1,

$$c^2 - a^2 < 0$$

Types 2 and 3,

$$c^2 - a^2 > 0$$

The relation between c^2 and a^2 is normal for Types 2 and 3, i.e. the same as for a single phase with $(\partial^2P/\partial V^2)_S > 0$. Type 1 is abnormal, but corresponds to the inversion of the order of adiabats in the C-Region. This is illustrated in Fig. 5-13. A single shock from point A into the C-region is stable. Type 2 exhibits the same structure as a normal single phase material. Type 3 is interesting because the phase boundary splits the isotherms and adiabats (Cf. Fig. 5-10). However, the geometric structure is not violated by the assumption of positive curvature and Cond. (5-72). This is illustrated in Fig. 5-14.



GA-5059-54

FIG. 5-13 ANOMALOUS R-H CURVE FOR TYPE 1 TRANSITION

The assumption that $(d^2P/dV^2)_{RHM} < 0$ reverses the sign of $c^2 - a^2$ in Cond. (5-72); this leads to instability in the shock for all Types.

This calculation can be verified in the neighborhood of the boundary by expanding $V(S, P)$ in a series about the boundary point A:

$$\begin{aligned}
 V(S, P) = & V_0 + \left(\frac{\partial V}{\partial P}\right)_S (P - P_A) + \left(\frac{\partial^2 V}{\partial P^2}\right)_S \frac{(P - P_A)^2}{2!} + \left(\frac{\partial^3 V}{\partial P^3}\right)_S \frac{(P - P_A)^3}{3!} \\
 & \dots + \left(\frac{\partial V}{\partial S}\right)_P (S - S_A) + \dots = V_{Ad} + \left(\frac{\partial V}{\partial S}\right)_P (S - S_A) + \dots
 \end{aligned}
 \tag{5-73}$$

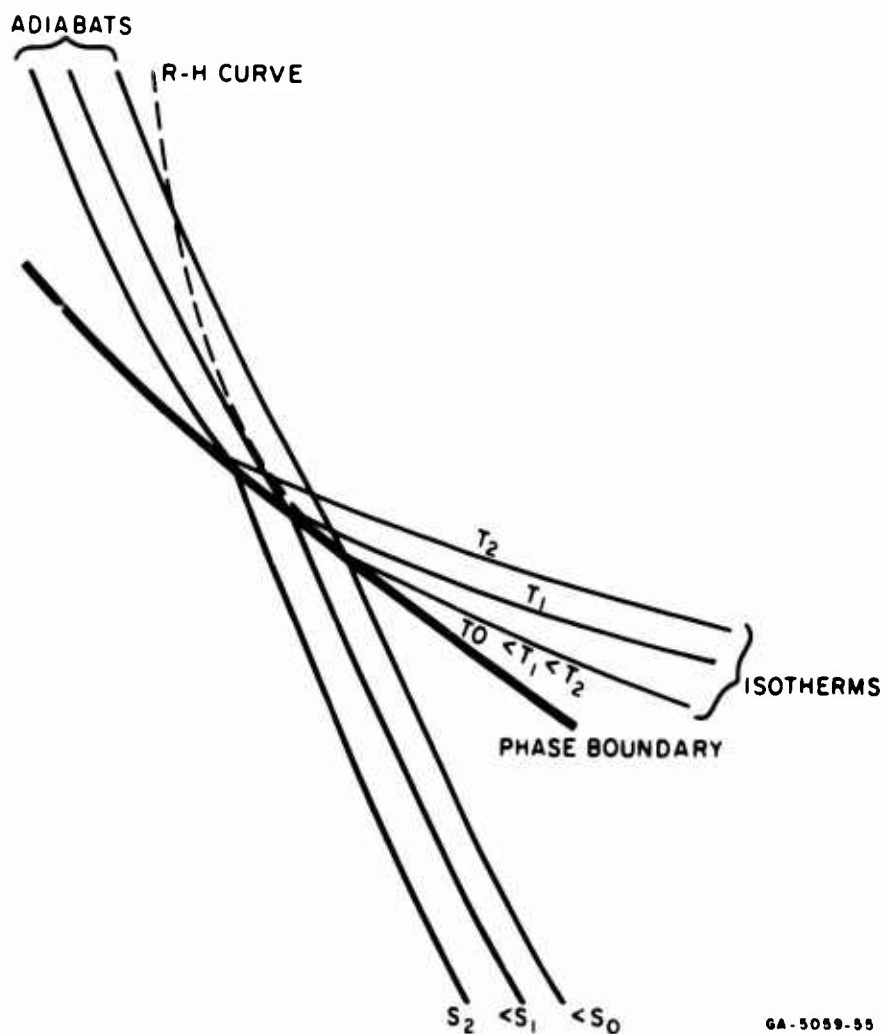


FIG. 5-14 ADIABATS AND HUGONIOT FOR TYPE 3 TRANSITION

$S - S_A$ can be expanded in powers of $(P - P_A)$ along the Hugoniot in the manner described by Courant - Friedrichs (23) with the result:

$$S - S_A = \frac{1}{12T_A} \frac{d^2V}{dP^2} (P - P_A)^3 + \dots \quad (5-74)$$

Entropy increases along this segment of the Hugoniot as P increases, for $d^2V/dP^2 > 0$.

From Maxwell's relations,

$$(\partial V / \partial S)_P = (\partial T / \partial P)_S = dT/dP \quad (5-75)$$

in the C-region. Consequently Eq. (5-73) becomes

$$V_{RH} - V_{Ad} = \frac{1}{12T_A} \left(\frac{dT}{dP} \frac{d^2V}{dP^2} \right)_A (P - P_A)^3 + 0 \left[(P - P_A)^4 \right]. \quad (5-76)$$

Differentiating Eq. (5-76) yields

$$\left(\frac{dV}{dP} \right)_{RHM} - \left(\frac{\partial V}{\partial P} \right)_{SM} = \frac{1}{4T_A} \left(\frac{dT}{dP} \frac{d^2V}{dP^2} \right)_A (P - P_A)^2 + \dots \quad (5-77)$$

For $(d^2V/dP^2)_A > 0$, the right hand side of Eq. (5-77) has the sign of dT/dP . This is in accord with Cond. (5-72) since $(dV/dP)_{RHM} - (\partial V/\partial P)_{SM}$ has the same sign as $c^2 - a^2$.

(2.4) Curvature of Adiabats. The curvature of the adiabat in the C-region depends upon second order thermodynamic coefficients, and it is, accordingly, difficult to make any general statements about its sign. Eq. (5-56) can be written

$$\left(\frac{\partial V}{\partial P} \right)_{SM1} = \left(\frac{\partial V}{\partial P} \right)_{S1} - \frac{T}{C_{P1}} \left(\frac{dS_1}{dP} \right)^2; \quad (5-78)$$

so we can say that if $(\partial V/\partial P)_{S1}$ increases with increasing pressure along the phase boundary, and if $T(dS_1/dP)^2/C_{P1}$ does not increase more rapidly than $(\partial V/\partial P)_{S1}$, then $(\partial V/\partial P)_{SM1}$ increases with P so $(\partial^2 V/\partial P^2)_{SM1} > 0$. Eq. (5-60.1) provides an explicit statement of the curvature. It is of little help, however, for the same reason that affects Eq. (5-78): d^2S_1/dP^2 is not normally known. An expression for the curvature in terms of more directly

observable quantities can be written as follows:

$$\begin{aligned}
 \left(\frac{\partial^2 V}{\partial P^2} \right)_{SM} &= \frac{d^2 V_1}{dP^2} + \left(\frac{\partial^2 V}{\partial T^2} \right)_{P_1} \left(\frac{dT}{dP} \right)^2 + \left(\frac{\partial^2 V}{\partial T \partial P} \right)_1 \frac{dT}{dP} \\
 &+ \left(\frac{\partial V}{\partial T} \right)_{P_1} \frac{d^2 T}{dP^2} - \left(\frac{dT}{dP} \right)^2 \frac{d}{dP} \left(\frac{P_{P_1}}{T} \right) \\
 &- 2 \frac{C_{P_1}}{T} \frac{dT}{dP} \frac{d^2 T}{dP^2} - \left(\frac{\partial V}{\partial P} \right)_{SM} \frac{d}{dP} \left(\ln \frac{dP}{dT} \right) \\
 &+ \frac{dV_1}{d} \frac{d}{dP} \left(\ln \frac{dP}{dT} \right) - (V - V_1) \frac{d^2}{dP^2} \left(\ln \frac{dP}{dT} \right).
 \end{aligned}
 \tag{5-79}$$

This equation, too, contains too many undetermined coefficients, although they are in principle known. Bethe (16) has examined the separate terms of Eq. (5-79) for some known phase transitions, and he speculates that the curvature is always positive. However, no such firm conclusion is justified without more exhaustive study.

D. EXAMPLES

Some data pertaining to phase transitions in bismuth (BiI→BiII), iron ($\alpha \rightarrow$ h.c.p.) and quartz ($\alpha \rightarrow$ stishovite) are given in Table 5-II. Subscript "A" refers to the intersection of the phase boundary and the Hugoniot with origin at room temperature and atmospheric pressure. Values of specific heat and thermal expansion coefficient are taken at atmospheric pressure. Values of dV_1/dP are determined from Eq. (5-39); values of $(dP/dT)_{calc}$ are obtained from measured values of the R-H curve above the phase boundary in the manner described by Duff and Minshall.²⁴ The procedure is to extrapolate the R-H data to the phase boundary and from this determine $(\partial V/\partial P)_{SM}^1 = (dV/dP)_{RH}^1$. Substitution of this into Eq. (5-54) along with the other thermodynamic data makes it possible to calculate $(dP/dT) \approx (dP/dT)_{calc}$. A

useful form of Eq. (5-54) is that given by Duff and Minshall:

$$\left(\frac{dP}{dT}\right)^2 + \frac{2\alpha_1}{\beta_{RH1} - \beta_1} \frac{dP}{dT} - \frac{C_{P1}}{TV(\beta_{RH1} - \beta_1)} = 0 \quad (5-80)$$

where the following abbreviations have been used:

$$\beta_{RH1} = - \frac{1}{V_1} \left(\frac{dV}{dP}\right)_{RH1}$$

$$\beta_1 = \frac{1}{V_1} \left(\frac{\partial V}{\partial P}\right)_{T1} \quad (5-81)$$

$$\alpha_1 = \frac{1}{V_1} \left(\frac{\partial V}{\partial T}\right)_{P1}$$

By substituting directly measured values of dP/dT into Eq. (5-54) it is possible to calculate $\beta_{ADM1} = (1/V)(\partial V/\partial P)_{SM1}$. If β_{RH1} represents equilibrium, then it should be true that $\beta_{RH1} = \beta_{ADM1}$. The failure of this inequality to hold reflects the difference between dP/dT and $(dP/dT)_{calc}$. These differences may result from nonequilibrium effects in shock compression, from errors in extrapolation of the shock data back to the phase boundary, or from nonhydrostatic stress distribution in shocked material. Construction of the equilibrium R-H curve in the C-region can be accomplished by substituting the appropriate thermodynamic coefficients into Eq. (5-61); an alternative procedure is to examine Eq. (5-65) for deviations from constant slope.

TABLE 5-II
PHYSICAL DATA ON PHASE TRANSITIONS

	<u>Bismuth</u>	<u>Iron</u>	<u>Qtz-Stishovite</u>
V_0 , cc/g	.1020	.128	.3775
C_{P1} , kb cc/g°C	1.21×10^{-3} (10)	4.15×10^{-3}	9.2×10^{-3}
α_1 , °C	40.2×10^{-6} (10)	36.3×10^{-6}	38.4×10^{-6}
β_1 , kb ⁻¹	2.46×10^{-3} (10)	0.51×10^{-3} (11)	0.76×10^{-3}
P_A , kb	25.3*	132 (11)	144 (14)
V_A , cc/g	.0929 (13)	.1197 (11)	.3145 (14)
T_A , °K	315 (10)	310 (11)	476 (14)
dP/dT, kb/°C	-.0500, -.0508	-.075 (12)	+.0177 (15)
ΔV , cc/g	-.0047	-.0041 (11)	
$(-1/V) dV_1/dP$	2.86×10^{-3}	$.99 \times 10^{-3}$	-1.5×10^{-3}
β_{RH1} , kb ⁻¹	13×10^{-3}	2.18×10^{-3}	1.59×10^{-3}
β_{ADM1} , kb ⁻¹	21×10^{-3}	23×10^{-3}	194×10^{-3}
$(dP/dT)_{calc}$, kb/°C	-.067	-.29	+.225

*Adjusted to static value.

Numbers in parentheses indicate references at end of paper.

If no reference is indicated, numbers are from Smithsonian tables or calculated here.

α_1 = isobaric volume expansion coefficient.

β_1 = isothermal compressibility of pure phase.

β_{ADM1} = adiabatic compressibility of mixed phase.

β_{RH1} = $(-1/V)(dV/dP)_{RH1}$

(1) Bismuth

Measurements reported by Duff and Minshall²⁴ were assumed to represent the BiI-BiII transition and were of two kinds. They varied initial temperature of the bismuth specimen and measured the pressure amplitude of the first wave. From their data they inferred a value of $-0.0508 \text{ kbar}/^\circ\text{C}$ for the dP/dT . This compares very favorably with Bridgman's value of -0.0500 . The amplitude of the first wave was about 3.5 kbar greater than the pressure reported by Bridgman for the same temperature. This difference might be due to a rate effect in the transition or to nonhydrostatic stress or to both. A limited attempt revealed no decay of the transition pressure with travel distance, which would indicate the absence of any but slow rate effects.

Second, they measured the amplitude of the second shock for different shots with the same initial temperature and extrapolated the results to obtain β_{RH1} , given in Table 5-II. Extrapolation errors are estimated at 60 percent by Duff and Minshall.

With the data of Table 5-II the change of $(dV/dP)_{RH}$ within the C-region can be estimated. From the given value of β_{ADM1} we find at the boundary of phase 1:

$$\left(\frac{dV}{dP}\right)_{RH1} = - 1.95 \times 10^{-3} \text{ cc/g kb}$$

Assume that $C_{P1} = C_{V1}$, $dP/dT = \text{const.}$, $dV_1/dP = \text{const.}$ and that α_1 , β_1 , C_{P1} are constant. Since $dP/dT = \text{const.}$,

$$(T - T_A) = - 20 (P - P_A) .$$

Integration of Eq. (5-65) with the above assumptions yields the solid curve of Fig. 5-15. The difference between this and the measured R-H curve is notable because of its magnitude and because the curvature of the computed curve is negative. The latter result may well be due to neglect of variations of thermodynamic coefficients. The former is so large that one is almost forced to conclude that kinetic effects are entering into the shock compression, particularly

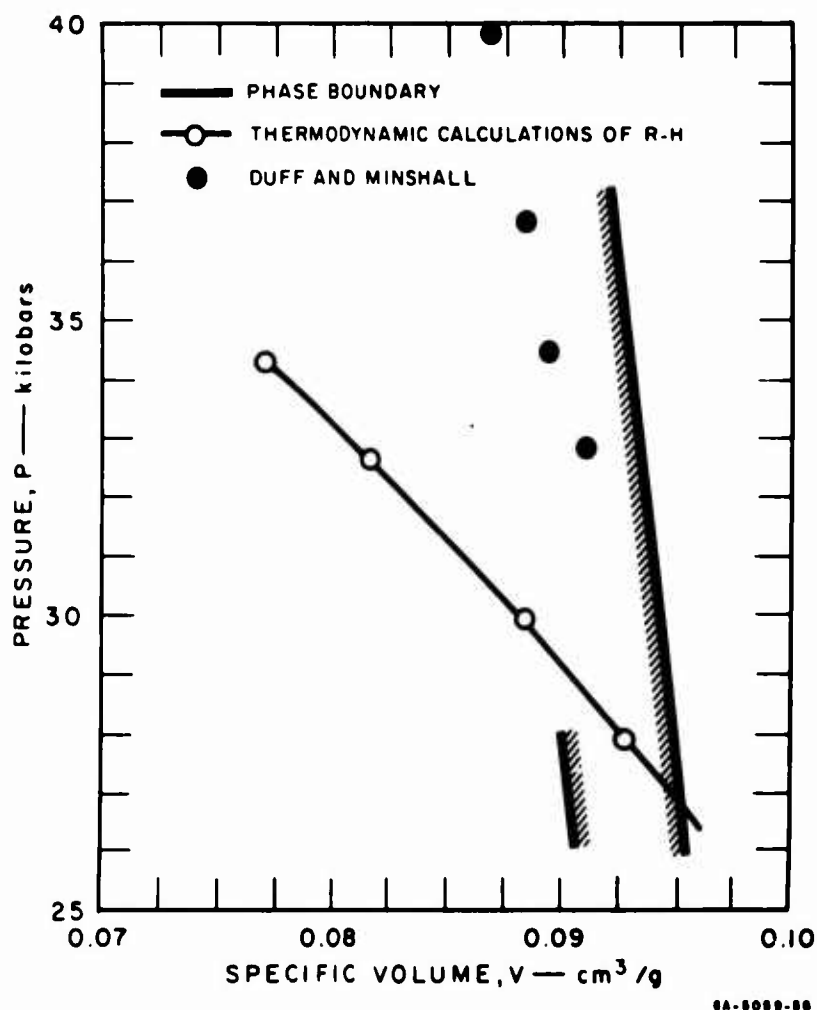


FIG. 5-15 COEXISTENCE REGION FOR BiI-BiII

when it is recalled that the pressure of the phase boundary measured in shock compression exceeds that reported by Bridgman.

A comparison of static and dynamic data near the transition pressure is shown on an expanded scale in Fig. 5-16.

(2) Iron

Minshall described a double shock structure in iron in 1954 (17) and suggested it might be due to a phase transition at 130 kb. These and other measurements were later reported in detail by Bancroft and others (25) and analyzed in more detail. Johnson, Stein, and Davis reported an extensive set of measurements in 1961 (26) in which initial temperature was varied from liquid nitrogen to nearly the $\alpha - \gamma$ temperature. They suggested on this basis that the 130-kb transition was a transition to a new phase, and this has since been verified by x-ray diffraction

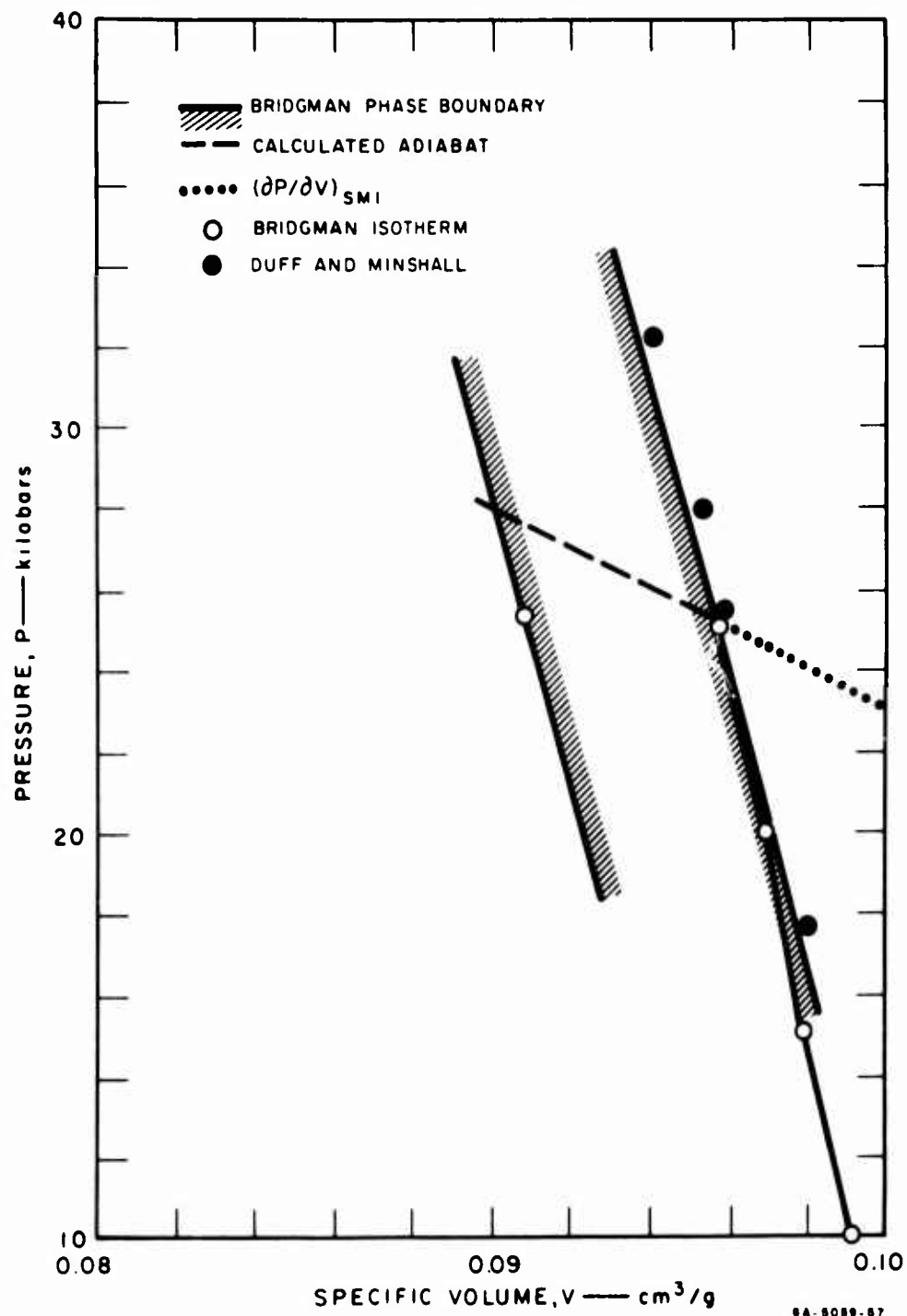


FIG. 5-16 PHASE DIAGRAM FOR BISMUTH

measurements at static high pressure and the new phase is found to be h. c. p. From their data, $dP/dT = -0.075 \text{ kb}/^\circ\text{C}$. Substitution of this value into Eq. (5-80) gives β_{ADM1} shown in Table 5-II.

Minshall's data include measurements of the second shock amplitude. These can be extrapolated to obtain β_{RH1} as reported in Table 5-11. This is only 10 percent of β_{ADM1} ; the difference is much greater than was found for Bi. The value of $(dP/dT)_{calc}$ derived from β_{RH1} differs

correspondingly from the directly measured value. Remarkably enough it is the same as dP/dT for the $\alpha - \gamma$ transition as determined by Claussen and others (26). The phase diagram for iron is shown in Fig. 5-17.

It is difficult to attribute such differences to rate effects in shock, since the first-wave amplitudes agree very well with the static values. Moreover there is little evidence for decay of the 130-kb wave, which further indicates the absence of rate effects. The resolution of this puzzle must await additional measurements - preferably near the transition point.

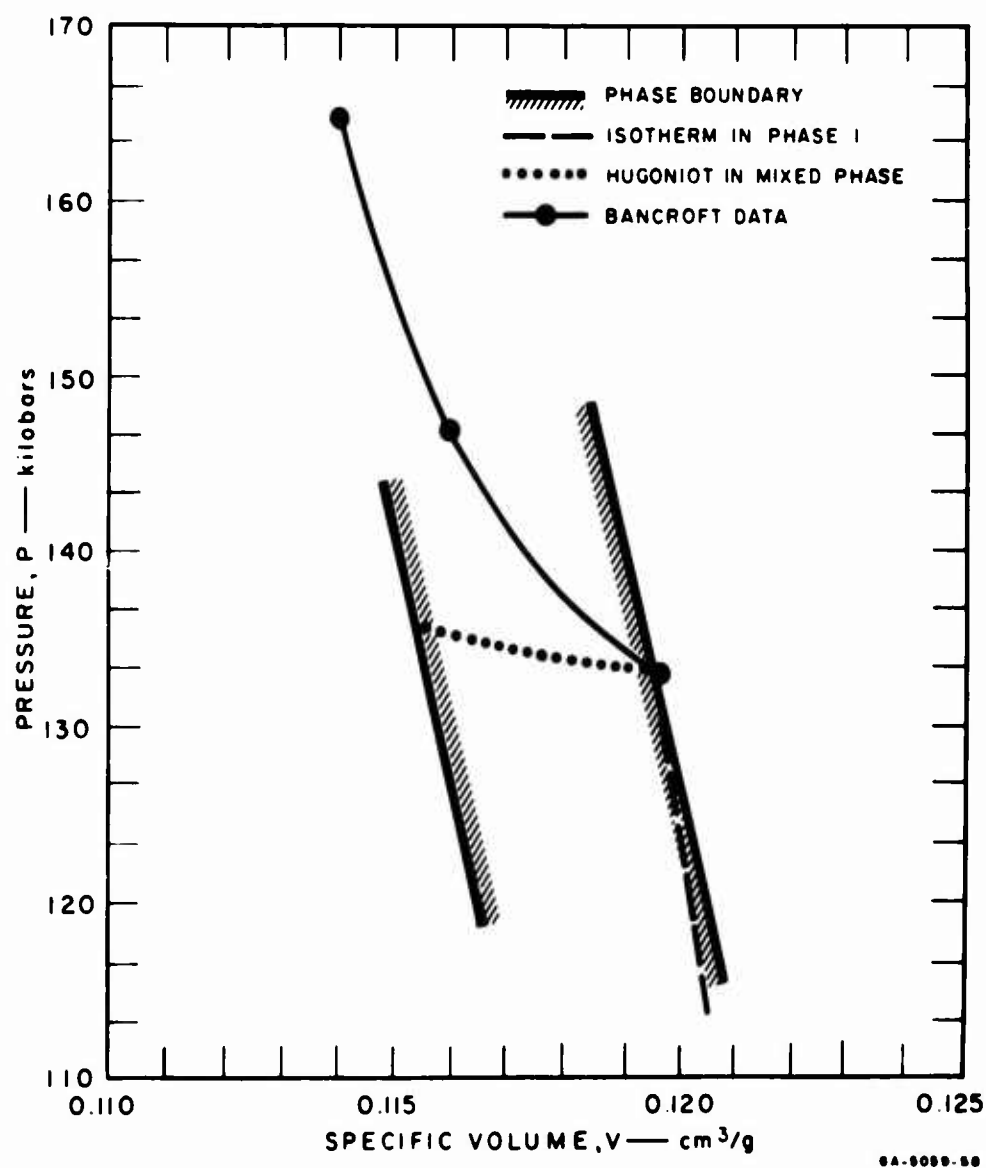


FIG. 5-17 PHASE DIAGRAM FOR IRON ($\alpha \rightarrow \text{hcp}$)

(3) Quartz

The two known high density forms of quartz are coesite and stishovite. The former is produced at relatively low pressures but is a slow transition and is believed to be produced to only a limited extent by shock compression (28). Stishovite is believed to be produced in shock (28,29) under the conditions shown in Table II; this is believed not to be an equilibrium point (30). Nonetheless the Wackerle compression data have been used in Eq. (5-54) to determine $(dP/dT)_{calc}$. The result, shown in the last row and column of Table 5-II is about twelve times greater than the static value quoted by Ahrens (29). This can be regarded as confirmation of the nonequilibrium character of the transition. The work by Ahrens and Gregson suggests that shock recovery experiments can be used to study the kinetics of the transition, but this remains to be done.

E. DISCUSSION

The ordering of slopes in the P-V plane for transitions of Types 1 and 2 appears to be a useful minor tool in the evaluation of shock data. Transitions of Type 3, though curious, are of no importance. Of greater importance is the relation between adiabatic slope in the mixed phase region and dP/dT ; this allows cross-comparisons to be made between different kinds of measurements. The discrepancies found between direct and inferred values of dP/dT are so large that needs for better thermodynamic data at high pressures and for more critical study of shock data and their interpretation are evidently pressing; this clearly points the way for further productive research.

The discrepancies in the iron data are particularly disturbing. The magnitude of the transition pressure agrees reasonably well with the static value. The static transition is reported to be sluggish (31); but, on the basis of experience with stress relaxation effects (32) one would predict that incomplete transition in shock would lead to a first wave amplitude above the static transition pressure and to a decay of the first wave amplitude with time. We might assume that the shock data are equilibrium values and that the specific heat and thermal expansion coefficients are in error by a large amount. Still another possibility is that the Hugoniot points are at equilibrium

and beyond the mixed phase region. The discontinuity at the second phase boundary would then lead to differences in the observed direction between β_{RH1} and β_{ADM1} . Finally it is not inconceivable that the phase line reported by Johnson et al. is seriously in error. It was obtained by a clever but unusual technique which is not thoroughly understood; verification by more conventional measurements would not be out of order. Minshall made a limited effort to determine dP/dT with pin techniques, but not all of his data have been made available and his conclusions and their certainty are not known to the authors. Static measurements would be important if the pressure of transition can be accurately determined.

This page intentionally left blank.

6- FLOW CALCULATIONS

J. O. Erkman and G. R. Fowles

A. INTRODUCTION

The work on this phase of the program is intended to serve as a guide for assessing the sensitivity of predictions of shock propagation from underground explosions to uncertainties in the constitutive relation (equation of state) of the medium. In a previous report on this program¹ comparisons were shown of the pressure and particle velocity profiles predicted assuming various models for the equation of state. For these calculations spherical symmetry was assumed and the energy source was taken to be an adiabatically expanding gas of prescribed mass and energy. Variations of the zero-degree isotherm (computed for quartz and its high-pressure polymorph, stishovite), Grüneisen's ratio and the initial porosity were examined. Perhaps surprisingly, the differences in the shock profiles showed no drastic effects of these fairly pronounced variations in the equation of state. The largest differences observed in the peak pressure at a given radius, due to combinations of parameter variations, amounted to factors of 2 to 3. Evidently, some variations in the equation of state tend to be self-compensating in their effects on shock propagation. Thus, in the case of variable porosity the energy dissipation is known to be highly dependent on porosity, for smaller values of porosity, and one might expect faster decay of peak pressure in more porous material. However, the high energy loss per unit mass in distended material compared with that in initially compact material tends to be offset by the correspondingly smaller total mass between the source and a given radius. Hence, the pressure is comparable. A similar argument applies to variations in the zero-degree isotherm in that higher initial densities are (usually) associated with lower compressibilities; again greater total mass is associated with less energy dissipation per unit mass. To these effects must be added the other obvious normalizing effect, namely geometrical divergence.

Some of the results obtained from the use of the above models are summarized in Figs. 6-10 to 6-13.

In view of the previous results, an extensive and detailed study of the parameters mentioned above was not pursued during the past year. Instead effort was concentrated on an area that has so far received little attention and which could cause peculiarities in experimentally observed pulse shapes and which might significantly influence shock decay. This problem was suggested by the experimental equation of state measurements and is the problem of the effects of a phase transition on shock propagation. See also Sec. 5. Polymorphic phase transitions are common for rocks and minerals because they are generally composed of open silicate structures that are unstable at high pressures. Moreover, some at least are known to be irreversible. The high pressure polymorphs of quartz, coesite and stishovite have both been recovered in the vicinity of underground nuclear explosions and near the Barringer meteor crater.³³ Where a phase change is irreversible, large energy dissipation occurs that could cause appreciable attenuation of the shock pulse. Perhaps more importantly, phase changes can cause the shock to propagate as two distinct fronts of different velocity. The peak pressure can thereby be considerably delayed with respect to the first shock arrival. Failure to recognize the existence of such shock structure could cause erroneous interpretation of experimental field observations, such as may be obtained with short duration peak pressure gages, or simple time-of-arrival gages.

Initial attempts to include the phase transition in the flow calculations led to difficulties in the form of instabilities. These instabilities are thought to arise from discontinuities in slope of the P-V relation, although the precise reasons for the trouble are not understood. Consequently, some effort was devoted to generating functions that would smoothly represent both reversible and irreversible phase changes. The results of flow calculations based on these functions show qualitatively the kinds of pulse shapes that would be expected in the case of a material that undergoes a phase transformation. Even with these smooth functions, however, oscillations in the flow parameters were not entirely eliminated. For the most part, the phase change has been considered to be reversible. This case is of interest because the model implies

that rarefactions in the flow should interact to form a rarefaction shock.^{35,36,37} Such a discontinuity is as difficult to treat with a finite difference method as the more usual compression shock. Hence, for a reversible phase change, it is necessary to use the artificial viscosity, Q , in the flow calculations for rarefactions as well as for shocks.

One of the models described below represents a reversible phase change only. Another model was devised which could be used to represent both irreversible and reversible phase changes. No provision was made for the phase change of only a portion of the material. That is, the material must be shocked to a critical volume before it is allowed to expand as irreversibly. This model reproduces the 0°K isotherm of stishovite at high pressure. Hence, it is reasonable to compare the results of the flow calculation using this model with results reported previously for distended quartz and stishovite.

B. EQUATIONS OF STATE

As noted in the Introduction, several relations have been used for the equations of state in the computation experiments. In all cases, a form of the Mie-Grüneisen equation of state has been used. This equation relates pressure P , volume V , and energy E for one state, say on an adiabat, to a state at the same volume on the 0°K isotherm, so that

$$P - P_k = \Gamma(E - E_k)/V \quad (6-1)$$

where subscript k refers to the 0°K isotherm and Γ is the Grüneisen ratio. In the following, an equation of state consists of a definition of a 0°K isotherm, which is specified by a relation between P_k and V . For porous materials the initial state is not a true thermodynamic state of the solid. For these cases, therefore, P_k is required to be zero for volumes greater than the initial volume V_0 . The value of V_0 for quartz and stishovite are their respective crystal specific volumes, 0.37 and 0.23 cc/g. For dry playa (as reconstituted for the Hugoniot experiments the value of V_0 is 0.513 cc/g.

Because of the phase change in quartz, theoretical isotherms were derived for both quartz and the high pressure material, stishovite, see Fig. 6-1. The phase change is represented by a transition curve connecting the quartz to the stishovite curve at a pressure of about 0.2 Mbar. During the first year's work,¹ a straight line was used for the transition curve. This, and perhaps other causes, led to instabilities in the computed results. This trouble made it desirable to use as simple a relation as possible for the isotherm so that the cause of the instability could be investigated.

1. Single Function Representation of a Phase Change

The function

$$P_k = 0.2 - 609.4(V - 0.27)^3 + 4114(V - 0.27)^4 \quad (6-2)$$

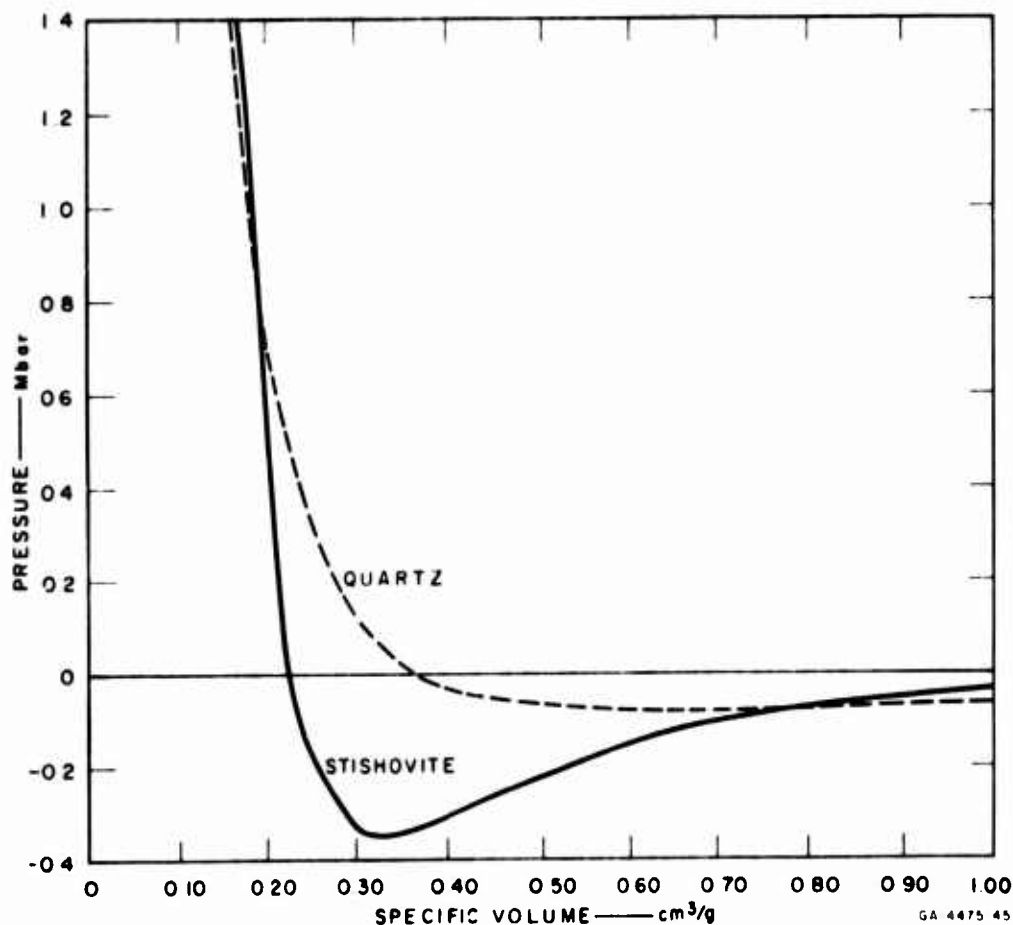


FIG. 6-1 COLD ISOTHERM FOR QUARTZ AND STISHOVITE

is used to relate the pressure, P_k , along the 0°K isotherm to the volume V . Units of P_k are megabars and of volume are cc/g. The interesting feature of this function is shown in Fig. 6-2. The function is flat for $V = 0.27$ cc/g, where the pressure is 0.2 Mbar. The energy for the 0°K isotherm is obtained by evaluating the expression

$$E_k = - \int P_k dV . \quad (6-3)$$

Sound speed is evaluated by use of the expression

$$c = \sqrt{\left(\frac{dP}{d\rho}\right)_s} . \quad (6-4)$$

The initial volume, V_0 , is 0.371 cc/g for this model. Because the same relation is used for compressions as for rarefactions, this model represents a reversible phase change.

2. Multifunction Representation of the Phase Change

A better representation of the theoretical curves for quartz and stishovite can be obtained if three functions are used. This also permits the flow calculations to proceed as if the phase change were either reversible or irreversible. For the interval $0.376 < V \leq M$ where $M = 0.25$, the relation

$$P_k = 0.2 + (V - 0.25)^3 \left[-977.1 + (V - M) [12397.0 - 43129.0(V - M)] \right] \quad (6-5)$$

is used. Equation (6-5) represents the quartz curve fairly well up to about 0.06 Mbar, see Fig. 6-3. Above 0.06 Mbar, the effect of the phase change causes Eq. (6-5) to give results above the quartz curve. At $V = 0.25$, the value of P_k is 0.2 as desired.

For greater pressures the cold isotherm is given by

$$P_k = 0.2 + (V - M)^3 \left[-3483.0 + (V - M) [-21681.0 - 168022.0(V - M)] \right] \quad (6-6)$$

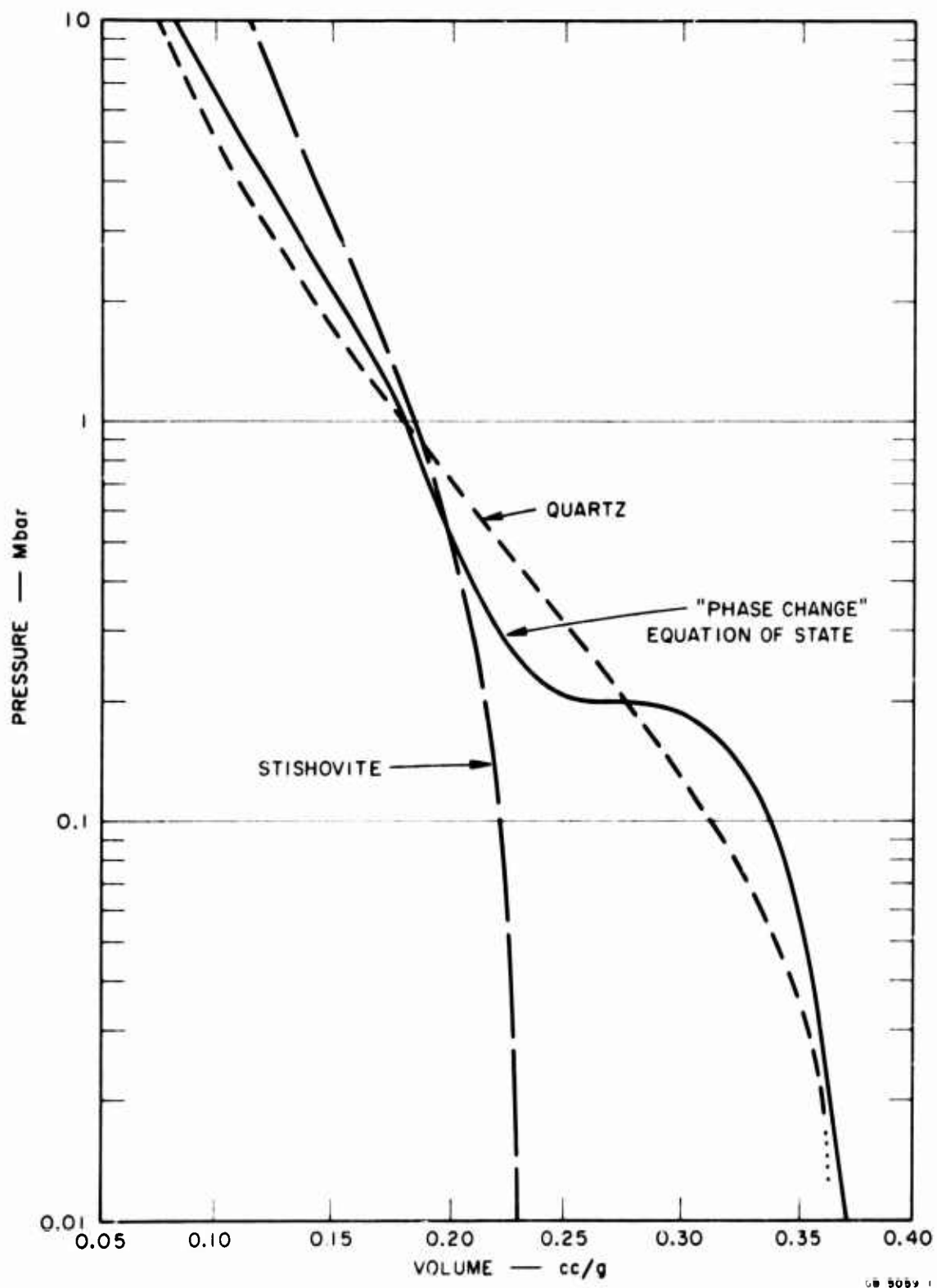


FIG. 6-2 SINGLE FUNCTION REPRESENTATION OF PHASE CHANGE, ZERO-DEGREE ISOTHERM

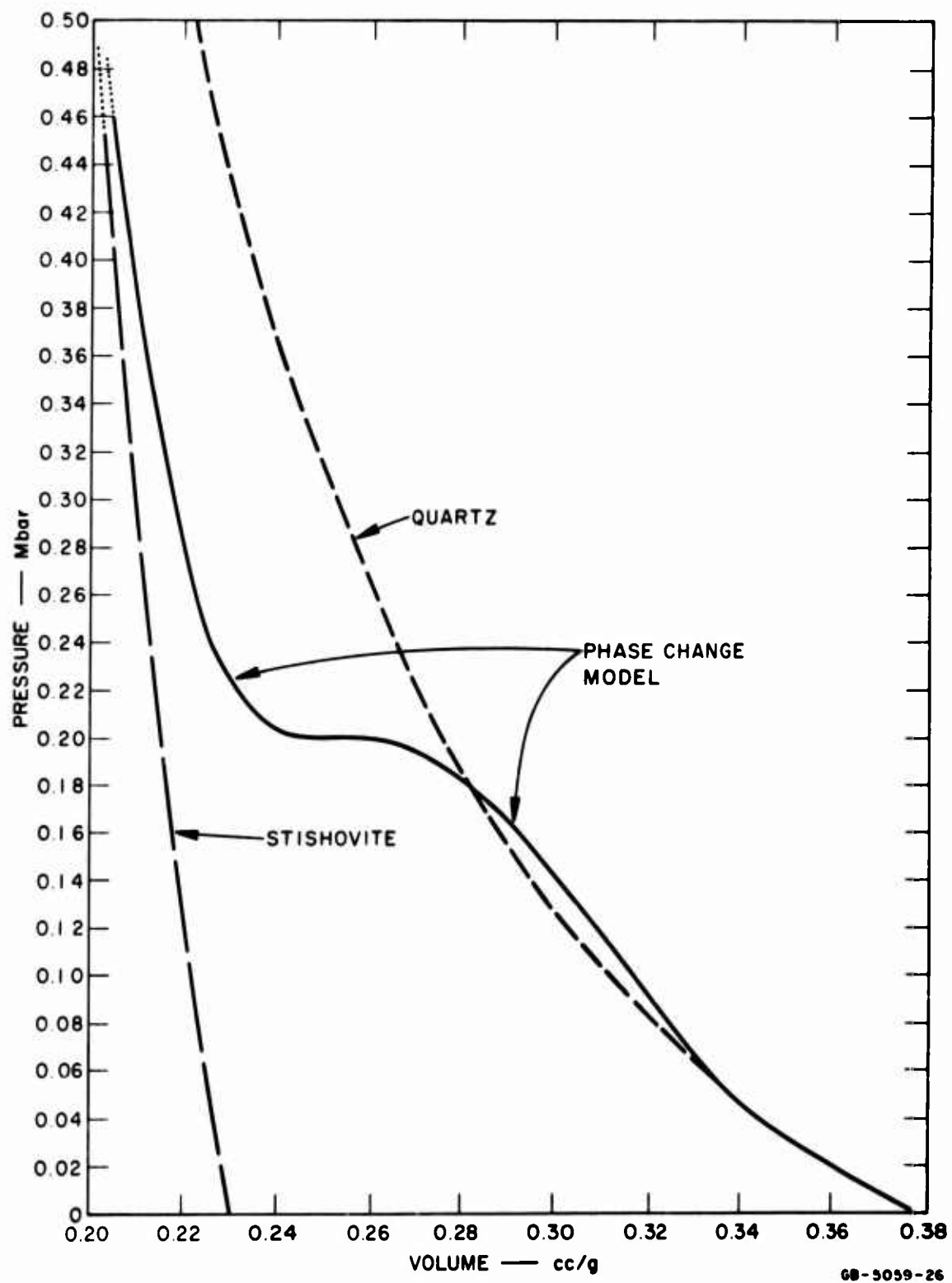


FIG. 6-3 MULTIFUNCTION REPRESENTATION OF PHASE CHANGE, ZERO-DEGREE ISOTHERM

This function joins the stishovite curve rather smoothly at $V = 0.193$, see Fig. 6-3. Finally, for $V < 0.193$, the stishovite curve is represented by

$$P_k = \eta \left[-8.913 + \eta \left[374.23 + \eta \left[5058.0 + 63476 \eta \right] \right] \right] \quad (6-7)$$

where

$$\eta = V - 0.2304.$$

Equation (6-7) gives the same results for pressures up to 10 Mbar as does the more complicated expression used previously for stishovite.

The energy for the cold isotherm is evaluated by the use of Eq. (6-3), using the proper constants of integrations where functions are joined. If the phase change is assumed to be reversible, the path ABCD in Fig. 6-4 is used for the relief process as well as for the compression process. If the phase change is considered to be irreversible, the compression path is still ABCD. For the relief process, however, the path DCE must be followed, so that $E_k = 0$ at $V = V_2$. Hence part of the energy gained by the material in compression is lost in the phase change.

It must be understood that the above scheme is not intended to describe the behavior of any real material. The scheme is intended to be used in flow calculations in order to see what effects a possible phase change has on the computed results. This model makes no provision for a change in phase of a part of the material. In order to expand as stishovite, the material must have been compressed to a volume of 0.193 cc/g or less, for which the corresponding pressure is 0.72 Mbar.

C. SPHERICAL PISTON

The code simulates a situation in which a disturbance in the playa is driven by an event in a cavity 1 meter in radius. Thus the cavity has about the same volume as the cavity for the Rainier event.³⁸ The cavity is assumed to be filled with an ideal gas whose density is 0.14 g/cc and whose energy is 73.5 megabars cc/g (or 73.5×10^{12} ergs/g) so that the pressure is about 6.9 megabars. The adiabatic exponent is assumed to be 5/3. The advantage of using this model is

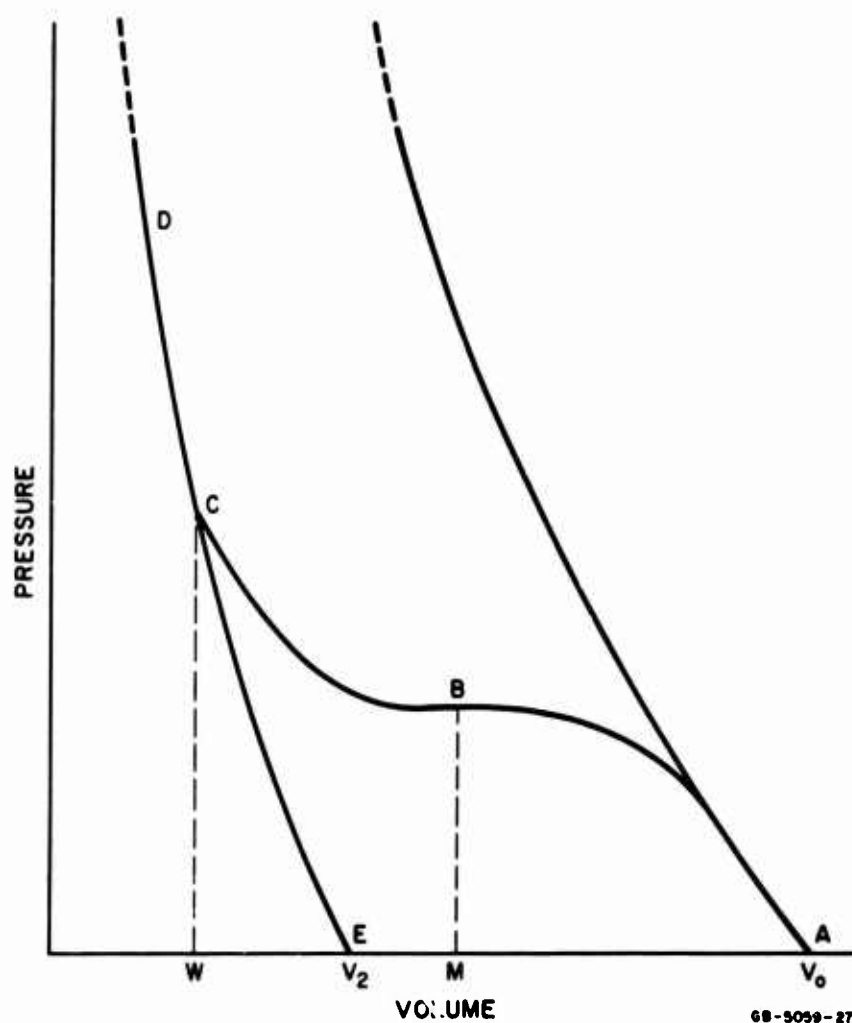


FIG. 6-4 SCHEMATIC OF REVERSIBLE AND IRREVERSIBLE PHASE CHANGE

that the maximum pressure induced in a medium surrounding the cavity depends on the P, V, E relation of the media. In some of the earlier work, an arbitrary relation was assumed between the pressure in the cavity and the time, so that the same maximum pressure was induced in a "soft" material as in a "hard" material.

The assumption that the bomb fills the cavity uniformly with an ideal gas which expands adiabatically precludes the formation and interaction of shock waves in the cavity. In the calculations the cavity is not zoned, and no details of the flow of the gas in the cavity are calculated.

D. RESULTS OF CALCULATIONS

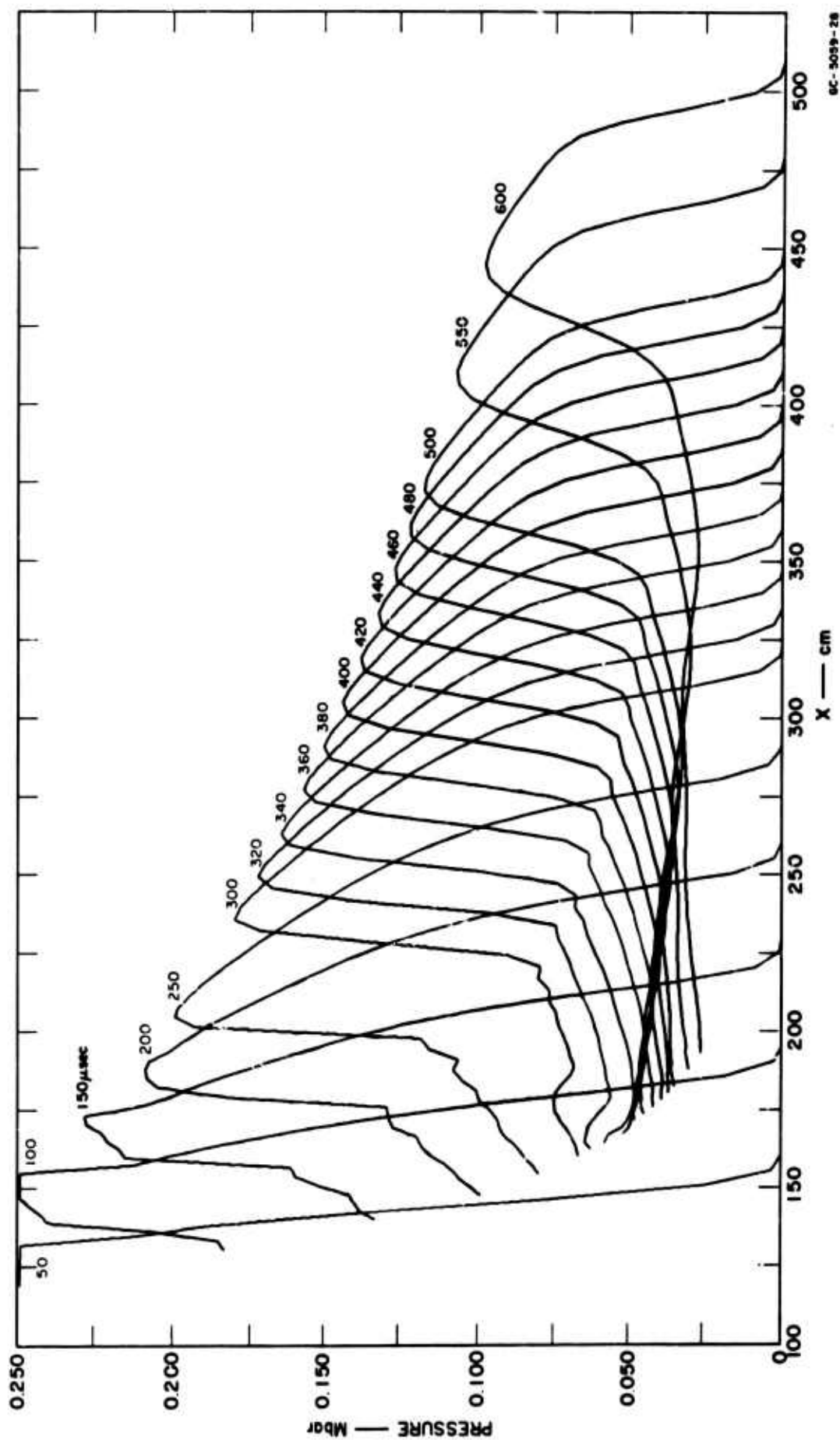
Results of flow calculations will be presented here for each of the equations of states described in Section B. Results are presented graphically, largely by showing the dependence of both the pressure and the particle velocity on distance at fixed times for a particular equation of state. Time of arrival curves and plots of peak pressure vs distance are also used to show some of the results of the changes in the equations of state.

1. Results Using Single Function Representation of a Phase Change

Equation (6-2) is combined with the Mie-Grüneisen equation of state, Eq. (6-1), the value of Γ being $2/3$. Calculations were performed for initial volumes of 0.371 cc/g and for 0.504 cc/g. For these calculations, the bomb energy was reduced from 73.5 to 7.35 Mbar cc/g so that the maximum pressure in the cavity is 0.7 Mbar.

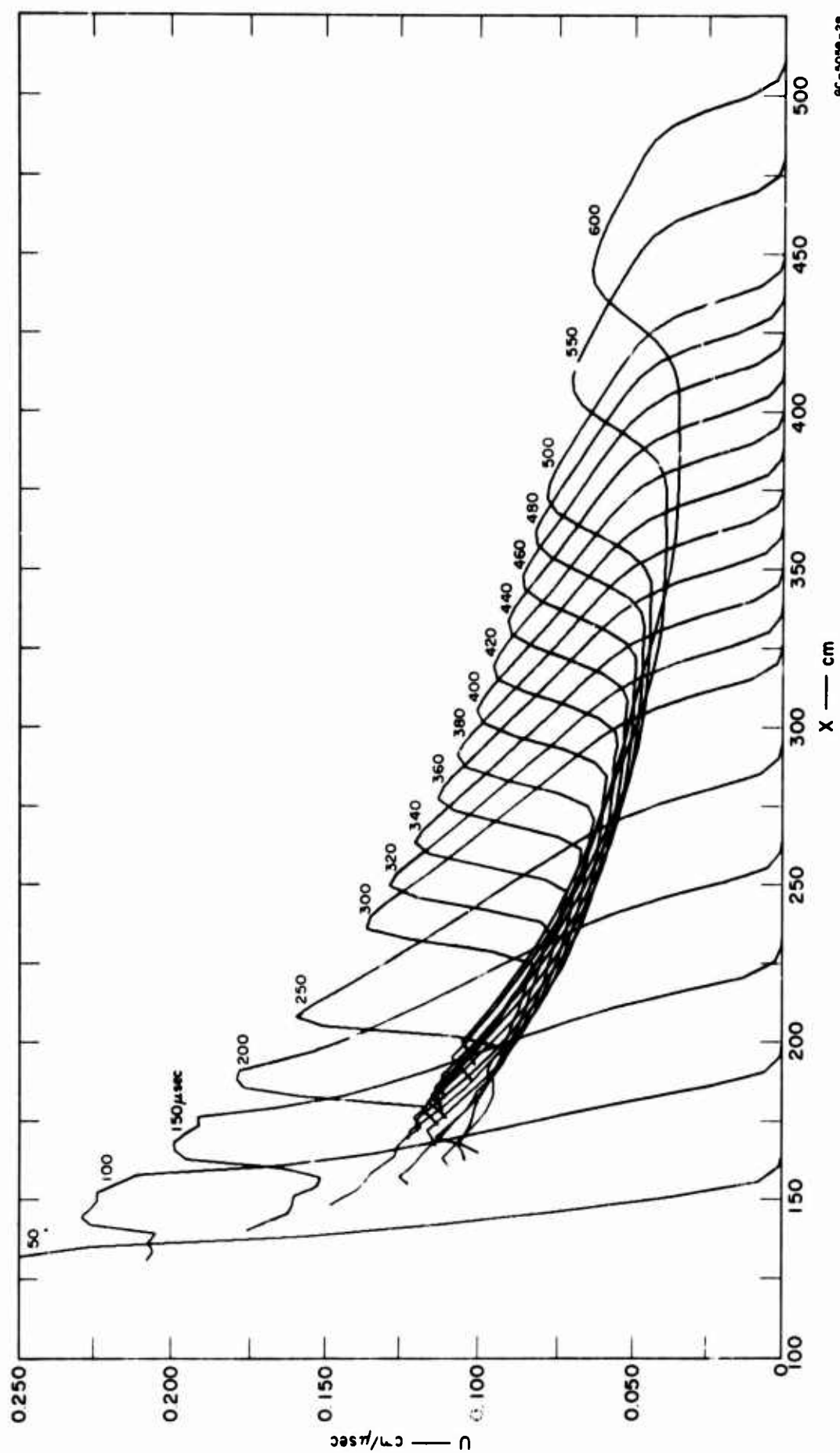
Results obtained from the flow calculations for an initial volume of 0.371 cc/g on are presented in Figs. 6-5(a) and 6-5(b). Figure 6-5(a) shows the pressure as a function of distance from the center of the cavity. The interesting features of the pressure profiles are that the fronts of many of them are no steeper than portions of the back sides of the waves. For these calculations, the artificial viscosity term was employed in both compression and in rarefaction waves. This is consistent with the original formulation of the artificial viscosity method (except that a small linear term has been introduced).³⁴

Further complications result when the material is distended, i.e., the quartz is assumed to be filled with small holes. It is also assumed that when the temperature is 0°K, the material crushes under little or no pressure. Figures 6-6(a) and 6-6(b) represent the results of computations for which the original volume is 0.50 cc/g or about 1.36 times the volume used in obtaining the results discussed immediately above. The results are very different in that the pressure drop in the initial rarefaction is very steep. When the time is 200 μ sec, the rarefaction has almost overtaken the shock front. When the time is 250 μ sec, the entire wave has been drastically attenuated. Following this initial attenuation, the wave is oscillatory back of the shock front. From the calculations themselves, there is no way of determining if the oscillatory



EC-5039-28

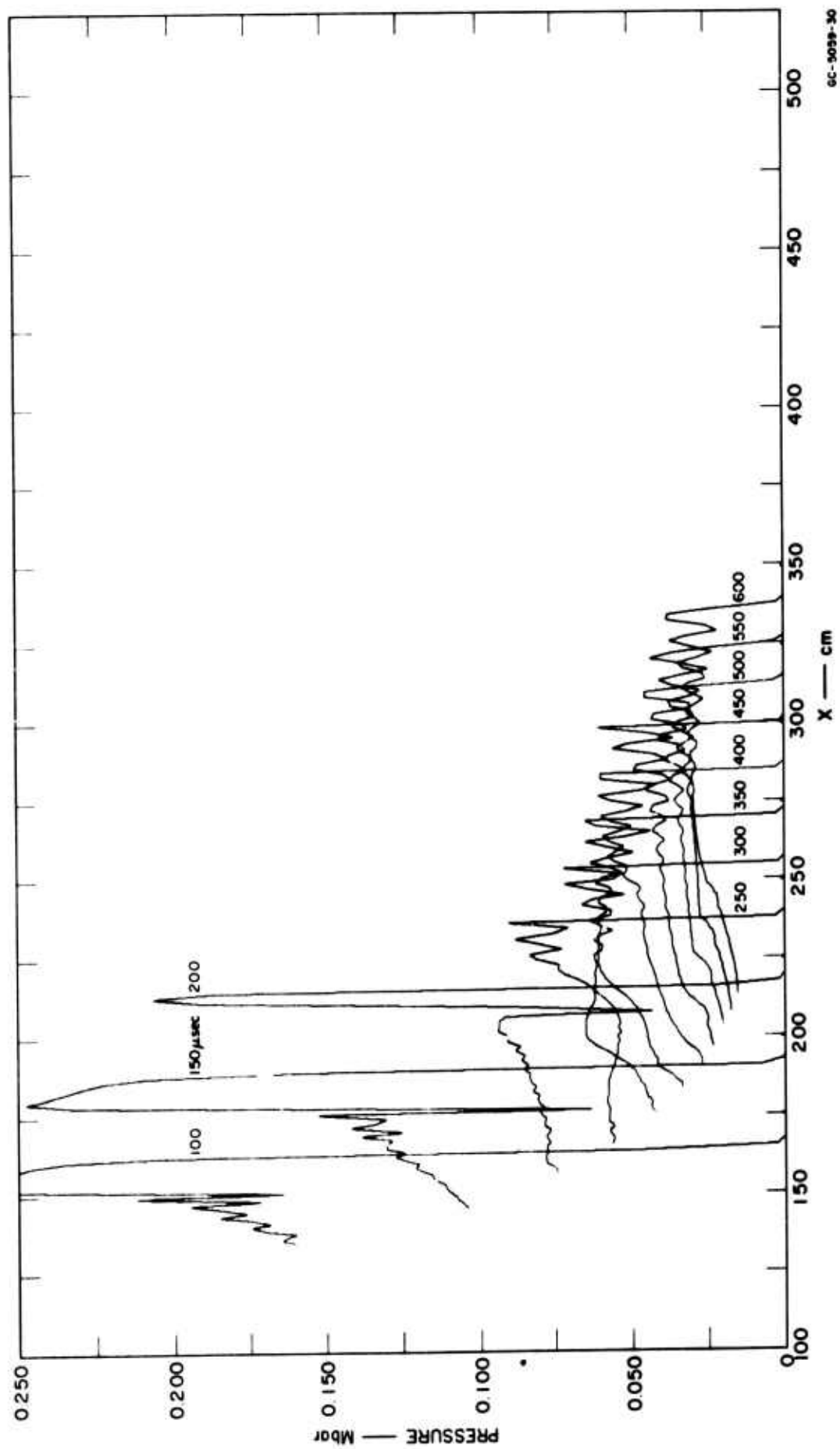
FIG. 6-5(a) PRESSURE vs. DISTANCE FROM CENTER OF CAVITY
Single function phase change, $V_0 = 0.37 \text{ cc/g}$; $\Delta R = 5 \text{ cm}$, Q operated in compression and rarefaction.



ec-5059-29

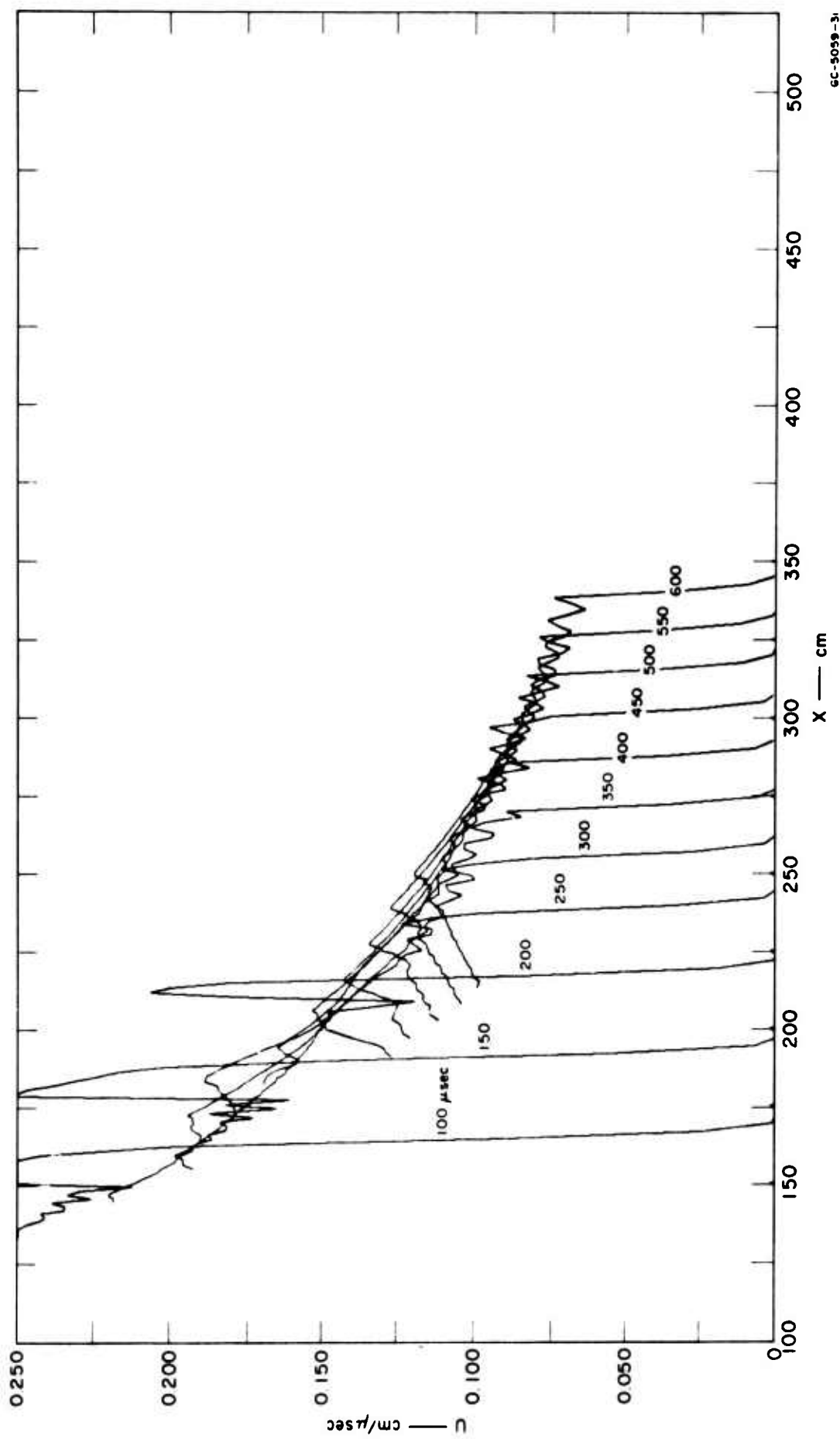
FIG. 6-5(b) PARTICLE VELOCITY vs. DISTANCE FROM CENTER OF CAVITY

Single function phase change, $V_0 = 0.37$ cc/g; $\Delta R = 5$ cm, Q operated in compression and rarefaction.



6C-5039-30

FIG. 6-6(a) PRESSURE vs. DISTANCE FROM CENTER OF CAVITY
Single function phase change, $V_0 = 0.50 \text{ cc/g}$, $\Delta r = 2.5 \text{ cm}$, Q operated in compression only.



6C-5059-31

FIG. 6-6(b) PARTICLE VELOCITY vs. DISTANCE FROM CENTER OF CAVITY
 Single function phase change, $V_0 = 0.50 \text{ cc/g}$, $\Delta r = 2.5 \text{ cm}$, Q operated in compression only.

behavior is due to wave interaction, or if it results from deficiencies in the method of obtaining the solution. The undershoot on the early profiles ($T = 100, 150$ and $200 \mu\text{sec}$) is likewise not understood.

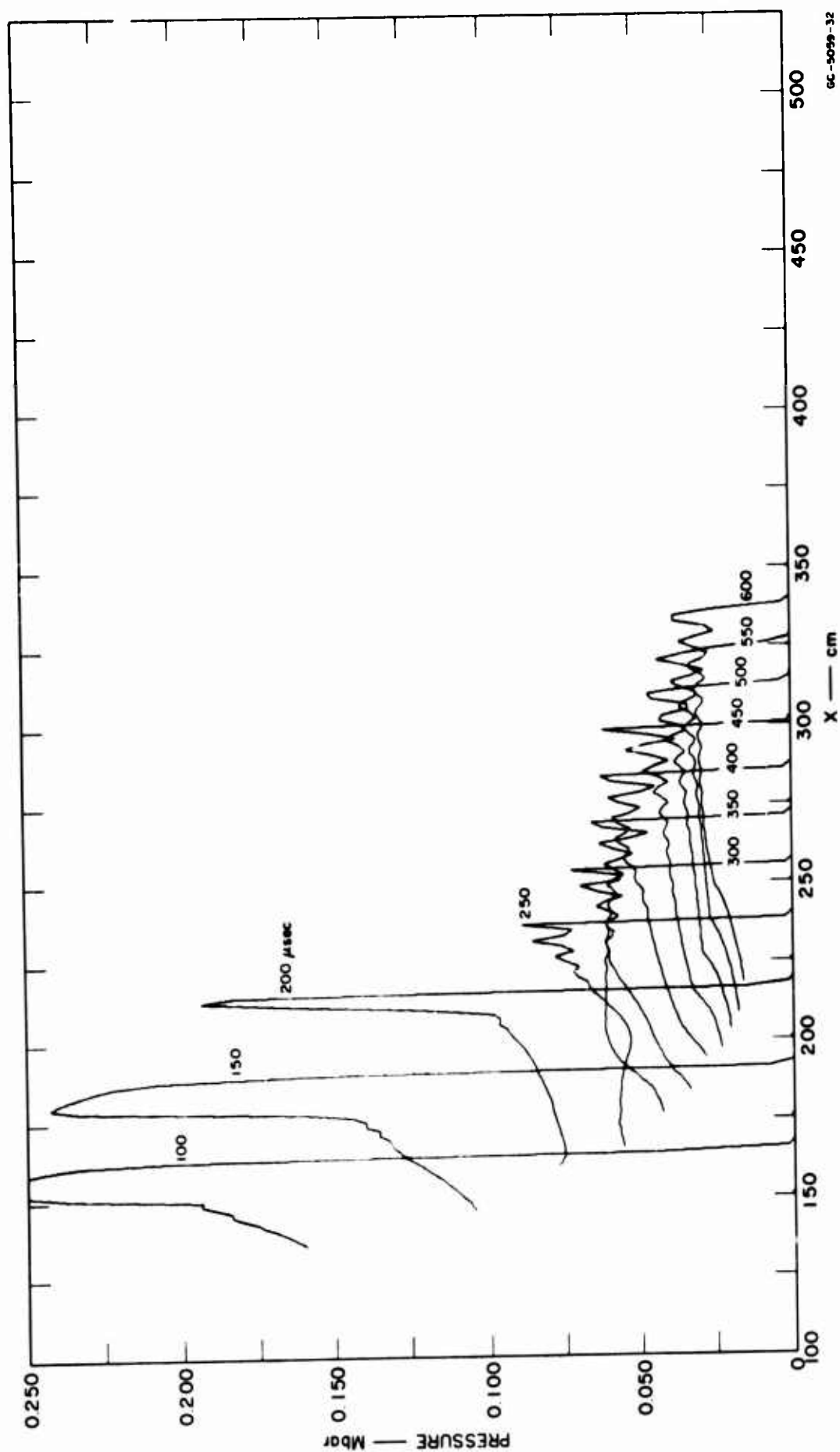
The results presented in Figs. 6-6(a) and 6-6(b) were obtained by using Q in the conventional manner, i. e., in the "cut-off" form so that Q is non-zero only in compression. If Q is used as originally proposed by von Neumann and Richtmyer³⁴ the results shown in Figs. 6-7(a) and 6-7(b) are obtained. For these results, there are no oscillations following the initial large rarefaction. Neither are there undershoots of pressure or of particle velocity immediately following this rarefaction. The profiles are still oscillatory, however, after the pressure has been attenuated below 100 kbar. Hence the significance of these oscillations is still undetermined.

The use of a linear artificial viscosity should have a significant damping effect on oscillations. The term

$$Q = -0.5 \left(u(J+1) - u(J) \right)$$

was used alone, and only in compression in obtaining the results shown in Figs. 6-8(a) and 6-8(B). These results have all the peculiarities first noted in Figs. 6-6(a) and 6-6(b). That is, the solution undershoots following the first large rarefaction and then oscillates. Also, after attenuation to below 100 kbar the profiles are oscillatory.

From the three sets of results as shown in Figs. 6-5(a) through 6-8(b), it appears that interactions between the form of the equation of state and the numerical computation scheme may be causing serious convergence problems. The oscillation and undershooting mentioned above are also observed when the bomb energy is increased to 73.5 Mbar cc/g. Thus these features of the calculated results are not dependent on the pressure in the cavity. If any judgment is to be made, the results shown in Fig. 6-7 are preferable. That is, permitting the artificial viscosity to operate throughout compressions and rarefactions give the preferred results.



GC-5059-32

FIG. 6-7(a) PRESSURE vs. DISTANCE FROM CENTER OF CAVITY
Single function phase change, $V_0 = 0.50 \text{ cc/g}$, $\Delta R = 2.5 \text{ cm}$, Q operated in both compression and rarefaction.

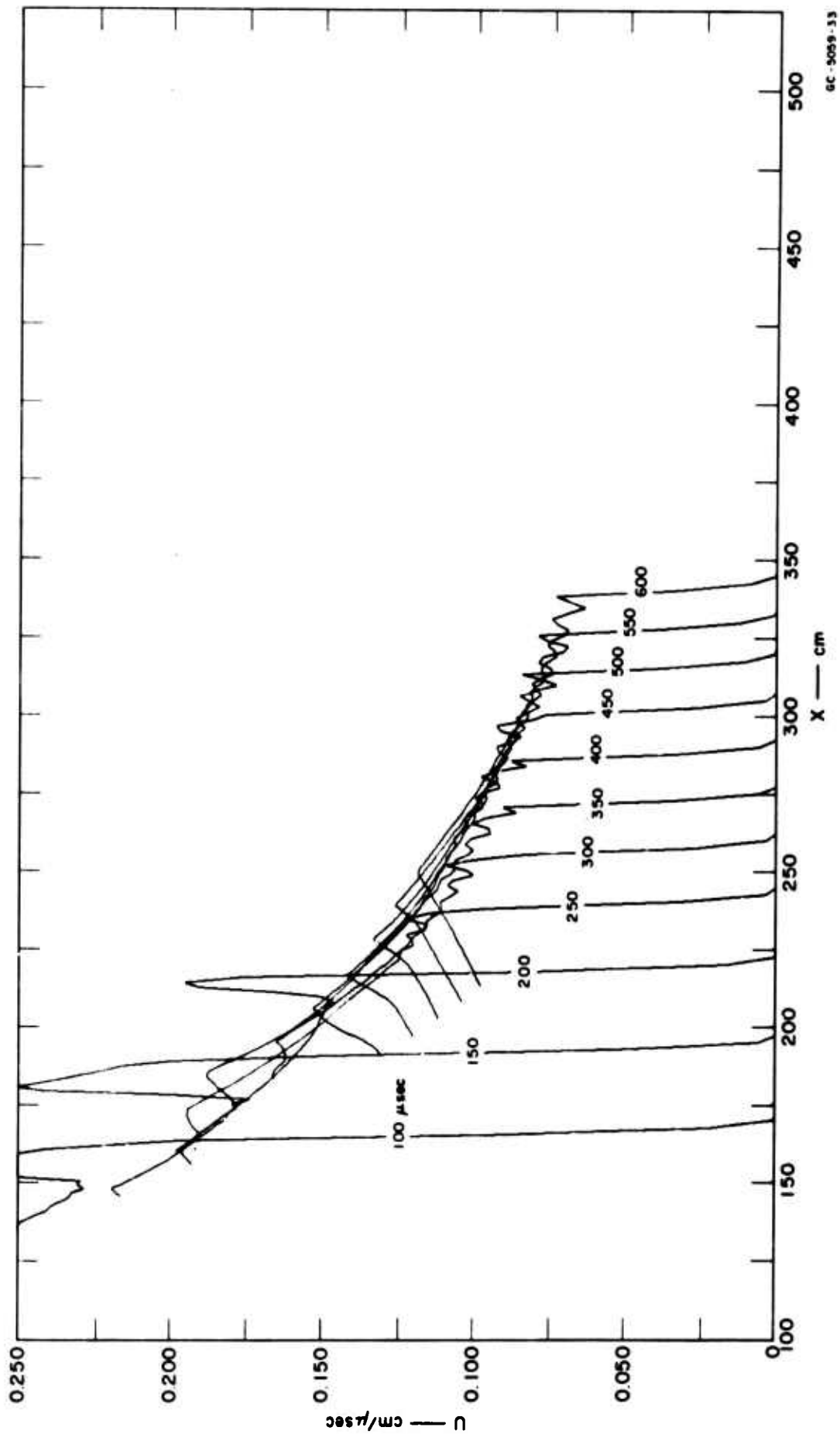
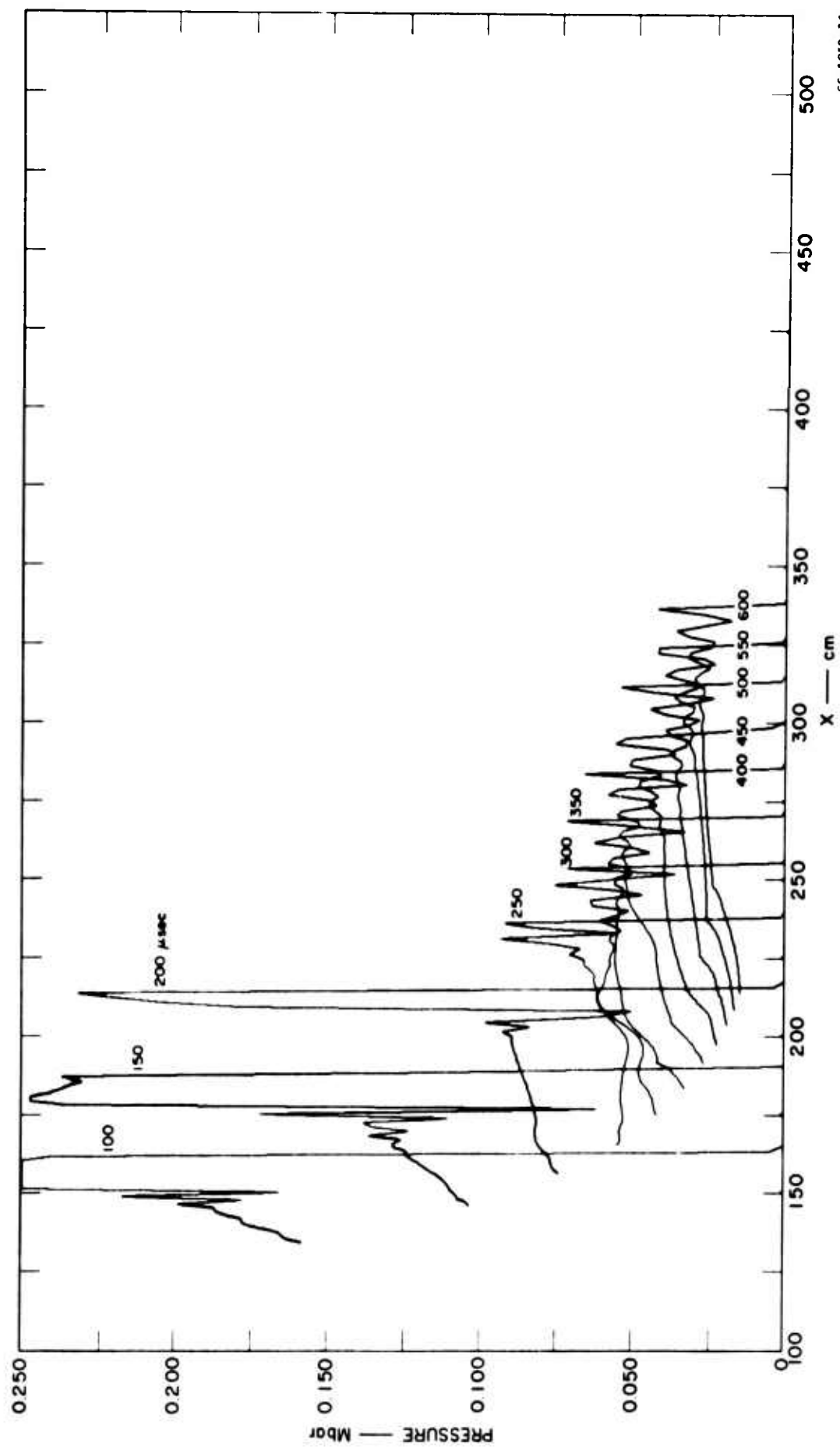


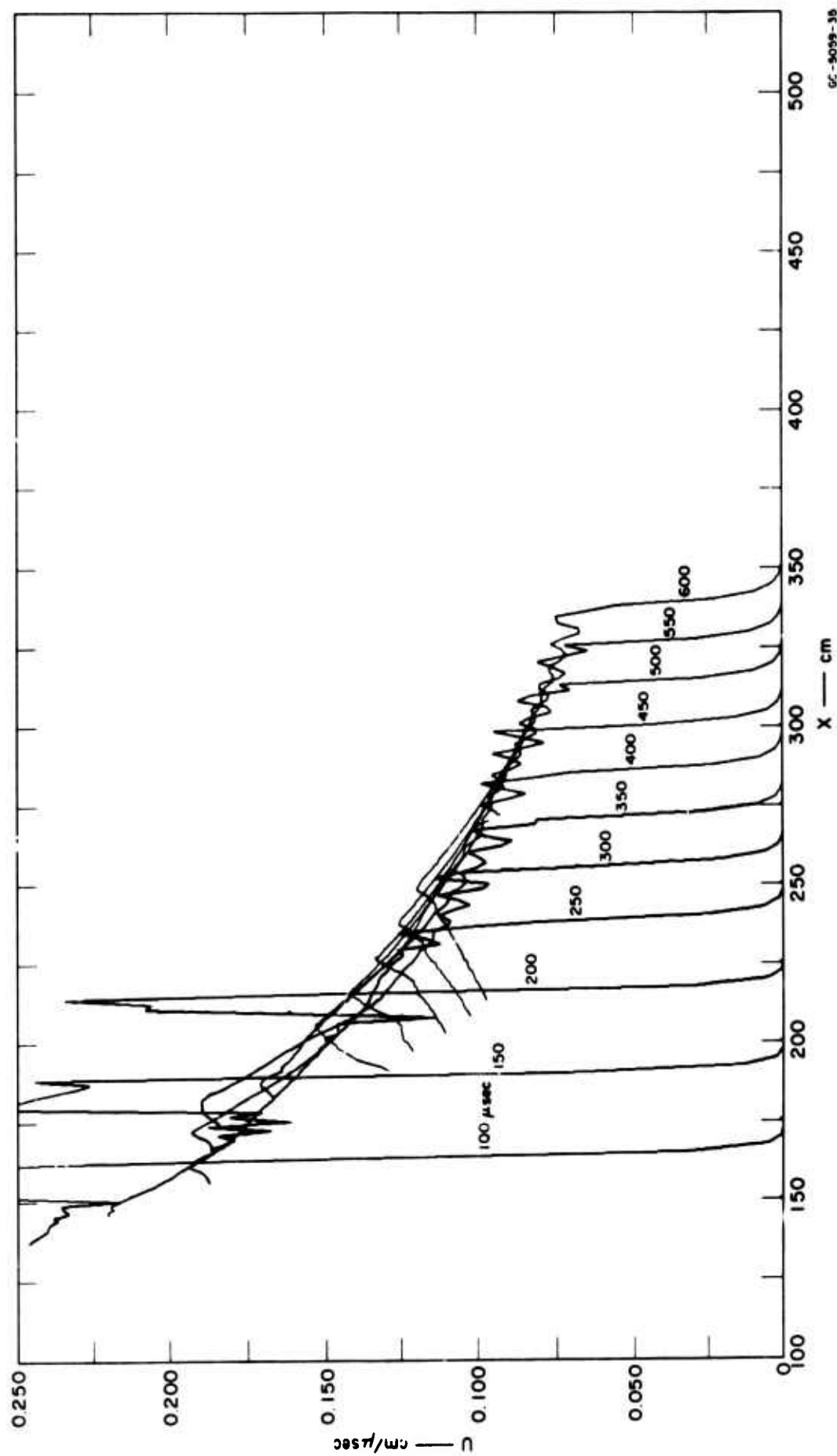
FIG. 6-7(b) PARTICLE VELOCITY vs. DISTANCE FROM CENTER OF CAVITY
Single function phase change, $V_0 = 0.50$ cc/g, $\Delta R = 2.5$ cm, Q operated in both compression and rarefaction.



GC-5059-34

FIG. 6-8(a) PRESSURE vs. DISTANCE FROM CENTER OF CAVITY

Single function phase change, $V_0 = 0.50$ cc/g, $\Delta R = 2.5$ cm, $Q = -0.5 [u(JH) - u(J)]$ in compression only.



GC-9039-38

FIG. 6-8(b) PARTICLE VELOCITY vs. DISTANCE FROM CENTER OF CAVITY

Single function phase change, $V_0 = 0.50$ cc/g, $\Delta R = 2.5$ cm, $Q = -0.5 [u(JH) - u(J)]$ in compression only.

2. Multifunction Representation of a Phase Change

As described in Section B, this representation of the P_k, V relation represents quartz at low pressure and stishovite at high pressure. In this formulation the phase change can be treated as if it were completely reversible, or stishovite may be allowed to expand entirely as stishovite, but no mixed phases are possible in expansion. The critical compression for which alternate relief paths may be chosen corresponds to $V = 0.193 \text{ cc/g}$.

These equations of state relations have been used in calculations for which the original volume is 0.51 cc/g (that is, the material is distended from the solid specific volume of 0.371 cc/g), and for which the cell size is 5 cm . The energy in the cavity is 73.5 Mbar cc/g , giving a maximum pressure of about 7 Mbar in the material near the cavity. The artificial viscosity term is used in both compression and in rarefaction. Results are shown in Figs. 6-9(a) and 6-9(b) for which all elements of the compressed material expand reversibly with respect to the cold isotherm. This model also shows the steep rarefaction (see profiles for 200 and $300 \mu\text{sec}$) discussed above. The particle velocity profiles are perhaps more interesting for this case than are the pressure profiles. As stated above, there is no intent to imply that playa (or any other material) is described by the models discussed here. However, the response of some real material may have features in common with a model such as the one used here.

The results obtained when stishovite is required to expand entirely as stishovite differ very little from the results shown in Fig. 6-9. For this reason, the profiles are not given. The explanation of this small difference is that very little of the material is ever compressed to a volume of 0.193 cc/g or less. Out to about 150 cm from the center of the cavity, some of the material is compressed so that the volume is less than 0.193 cc/g . Slightly further out the wave has attenuated to such an extent that the volume is never reduced to the critical volume. Thus a spherical shell 50 cm thick surrounding the 100-cm radius cavity contains stishovite. Forcing this small amount of material to expand as stishovite, changes the propagation of the wave very little. Using a greater pressure in the cavity would undoubtedly make the results obtained from the use of the two models differ more dramatically in range of distances examined.

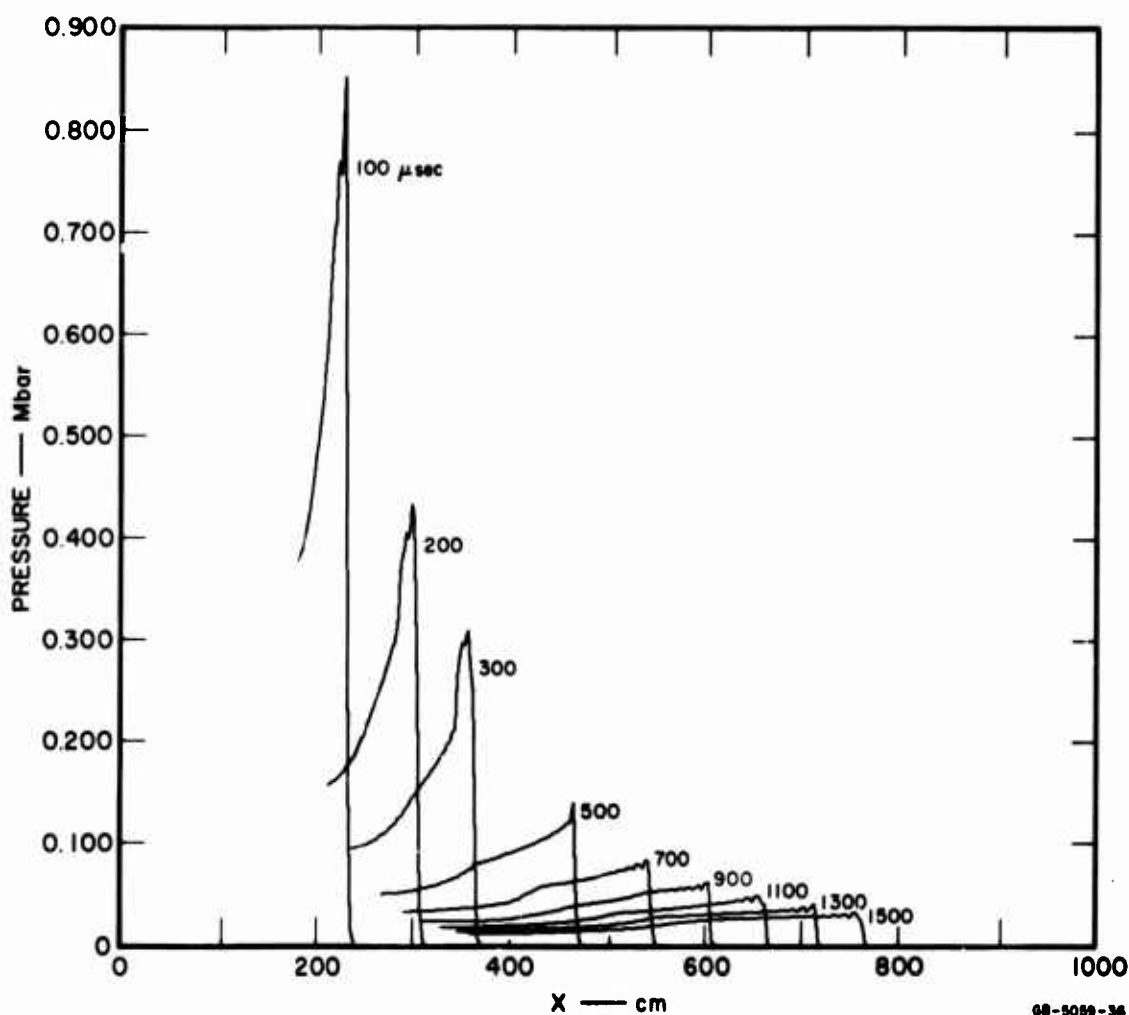


FIG. 6-9(a) PRESSURE vs. DISTANCE FROM CENTER OF CAVITY
Multifunction phase change (reversible) $V_0 = 0.51 \text{ cc/g}$, $\Delta R = 5 \text{ cm}$,
Q in compression and rarefaction.

E. CONCLUSIONS

In this phase of the program, including the previous years effort, some effects due to variations in equation of state on spherical shock propagation have been examined. For this study a particular energy source was chosen to give a rough approximation to a representative nuclear explosion. Pressure and particle velocity pulse shapes and the rates of decay of their peak amplitudes with distance are shown for different models of the equation of state based on different assumptions for the zero-degree isotherm, Grüneisen's ratio, the degree of porosity, and including a reversible phase change. These variations represent reasonable bounds to the uncertainties in knowledge of the equation of state of playa. Because of the particular source function chosen, no claim of generality

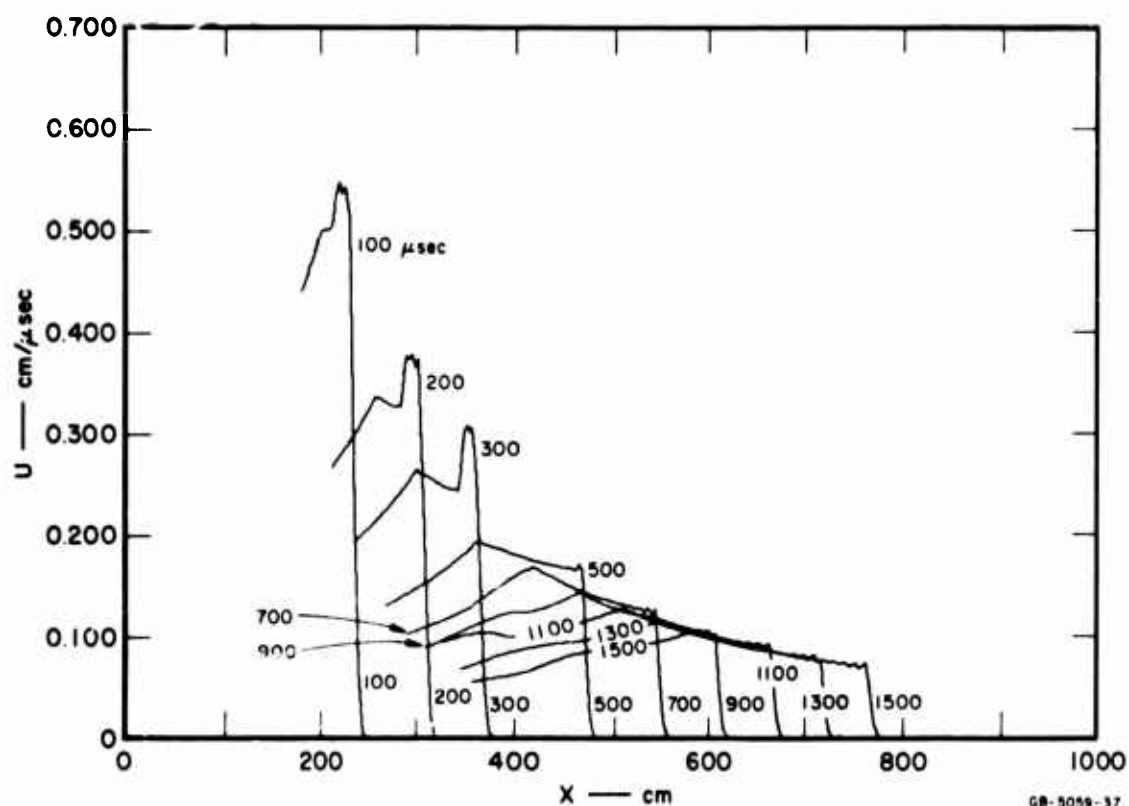


FIG. 6-9(b) PARTICLE VELOCITY vs. DISTANCE FROM CENTER OF CAVITY
Multifunction phase change (reversible) $V_0 = 0.51 \text{ cc/g}$, $\Delta R = 5 \text{ cm}$,
 Q in compression and rarefaction.

of the results can be made. Nevertheless, the results should be useful in indicating the sensitivity of shock propagation to uncertainties in the equation of state.

The effects of changes in chemical composition within the limits of observed variations in the playa were not studied explicitly by shock calculations. Examination of the effects on the equation of state showed that the variation (theoretically) is small and lies within the range of variation already examined by means of other parameters, such as Grüneisen's ratio. It is concluded, therefore, that variations in chemical composition are of lesser importance than the uncertainties to be expected in other parameters.

Unfortunately, experimental data on the effects of moisture on the equation of state (particularly release adiabats) did not become available in time to include such cases in the shock calculations. Moreover, a strictly theoretical approach did not appear likely to be very meaningful. Consequently, the effects of moisture on shock propagation remains an unstudied problem.

The observed differences in the arrival time of the peak pressure are shown in Figs. 6-10 and 6-11. The differences in peak pressure as function of the radial distance amount to a factor of three or less, and are shown in Figs. 6-12 and 6-13. In general the peak pressures assuming a cold isotherm corresponding to stishovite lie below those assuming a quartz isotherm. The direction of this result is clearly proper since there is greater energy dissipation (waste heat) where the release adiabats (and cold isotherm) are steeper.

The effects of varying Grüneisen's ratio are also in the expected direction. Higher values of Grüneisen's ratio correspond to shallower adiabats and, hence, less energy dissipation.

The effects of varying porosity are surprisingly small because porosity drastically effects energy dissipation. The only plausible explanation is that there are two effects that tend to be self-compensating. Higher porosity, and higher dissipation are associated with less mass between the source and a given radius. These two effects cancel to such a degree that the peak pressure at a given radius is not seriously affected. This result is perhaps the most significant one of this phase of the program.

The effect of a phase change is mostly to alter the pulse shape and to cause abrupt changes in the rate of decay of peak pressure. Recognition of such possibilities may be important in understanding field results obtained by short duration pressure gages, or simple time-of-arrival gages.

It was also found that where reversible phase changes occur, the artificial viscosity term in the numerical differencing scheme should be allowed to operate in rarefaction as well as compression in order to accommodate rarefaction shocks.

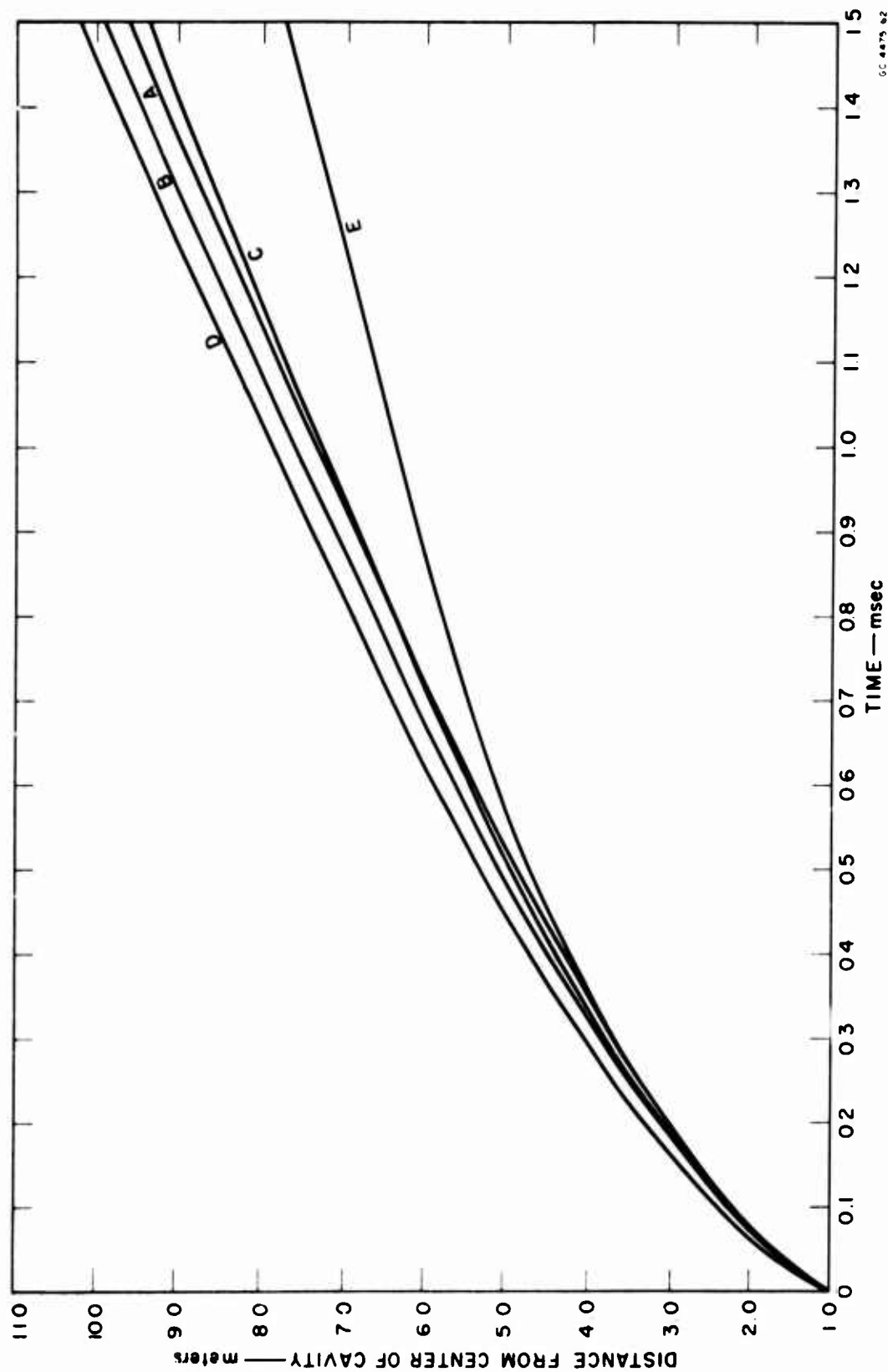


FIG. 6-10 TIME OF ARRIVAL OF PEAK PRESSURE BASED ON QUARTZ EQUATION OF STATE

SYMBOL	INITIAL VOLUME (cc/g)	Γ	DISTENTION RATIO, m
A	0.38	$2/3$	1.0
B	0.38	1.4	1.0
C	0.51	$2/3$	1.34
D	0.51	1.4	1.34
* E	0.51		1.34

* Multifunction representation of reversible phase change.

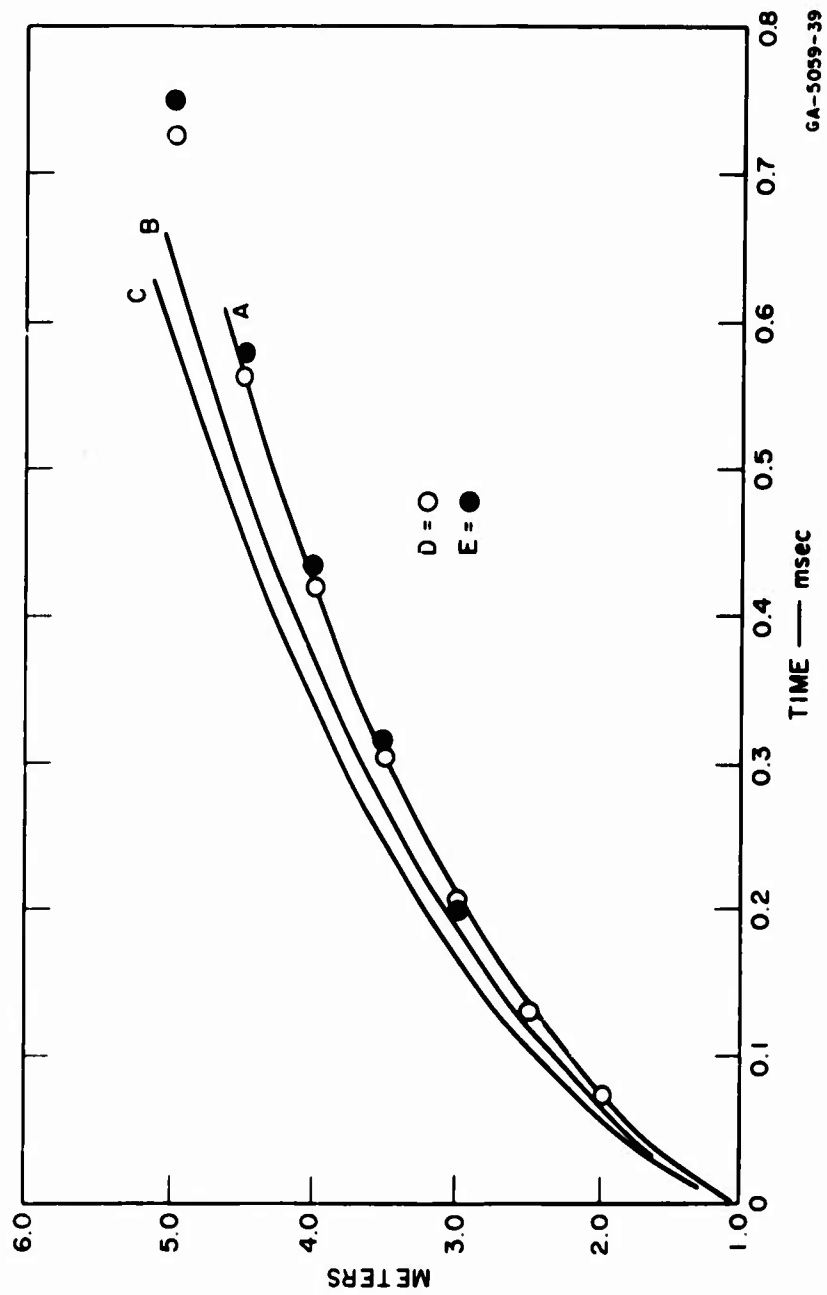


FIG. 6-11 TIME OF ARRIVAL OF PEAK PRESSURE BASED ON STISHOVITE EQUATION OF STATE

SYMBOL	INITIAL VOLUME (cc/g)	Γ	DISTENTION RATIO, m	LINEAR VISCOSITY COEFFICIENT
A	0.38	2/3	1.65	0.2
B	0.38	1.4	1.65	0.2
C	0.51	1.4	2.22	0.2
D	0.38	2/3	1.65	0.1
E	0.51	2/3	2.22	0.2

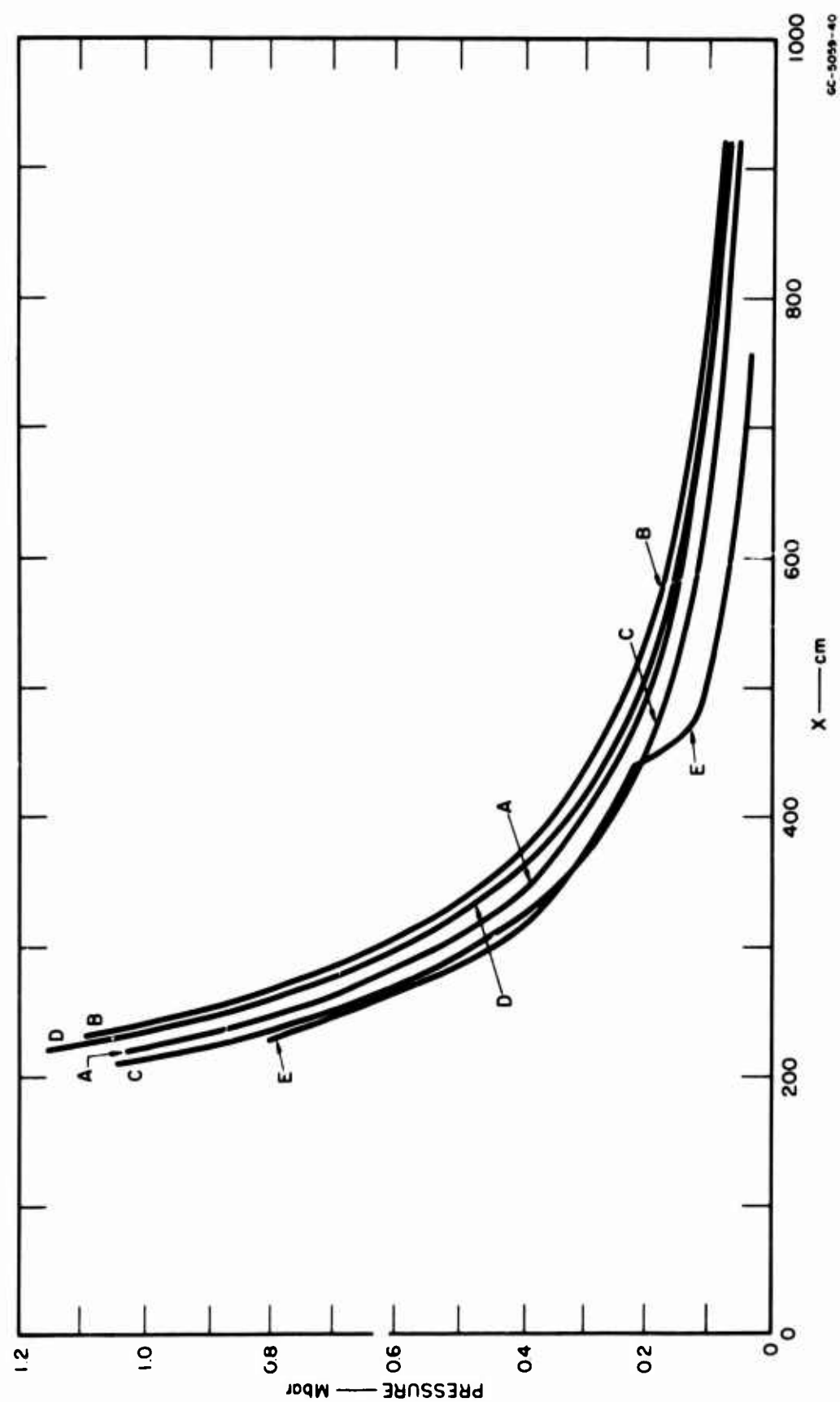


FIG. 6-12 PEAK PRESSURE AS FUNCTION OF RADIUS BASED ON QUARTZ EQUATION OF STATE
(See Fig. 6-10 for definition of symbols)

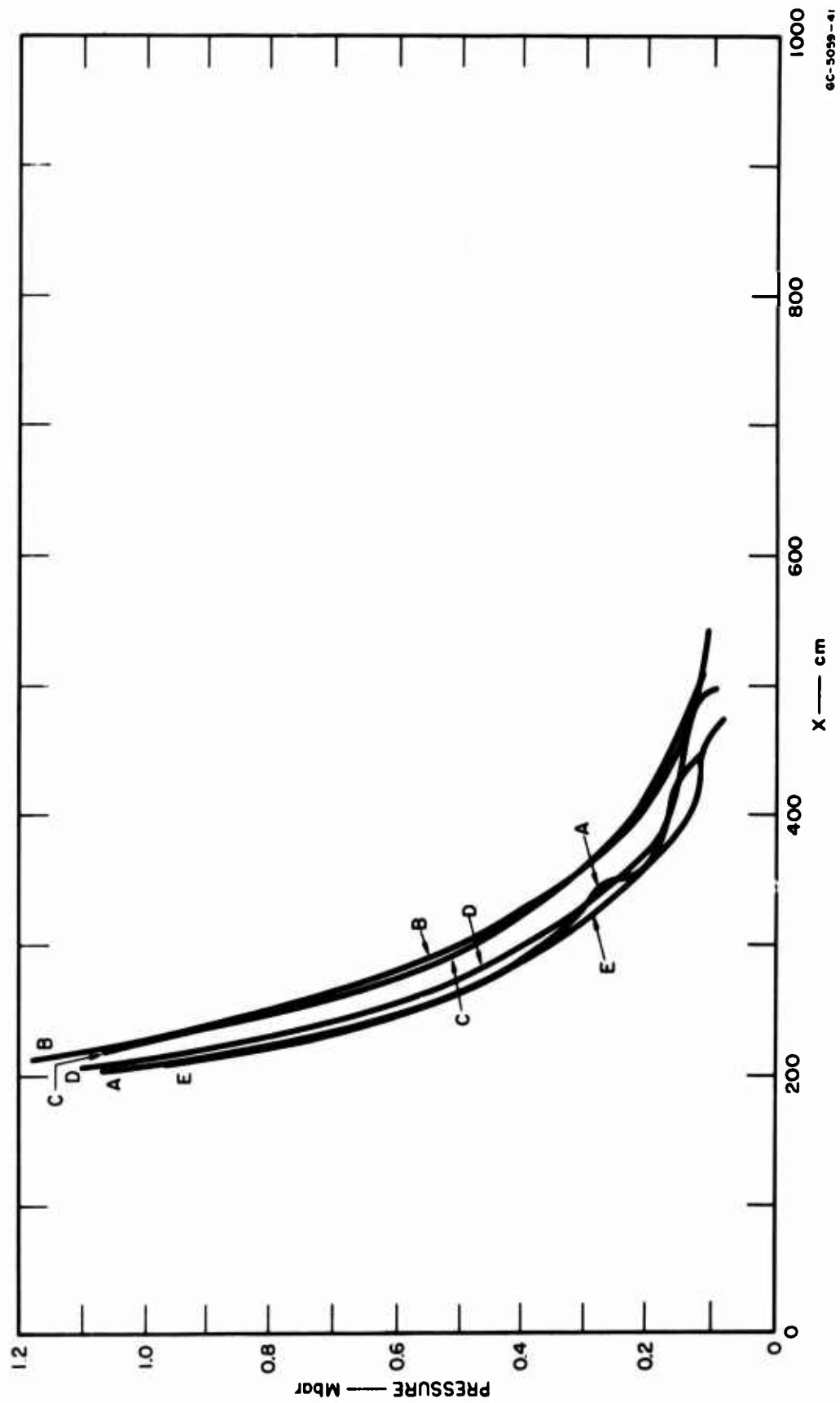


FIG. 6-13 PEAK PRESSURE AS FUNCTION OF RADIUS BASED ON STISHOVITE EQUATION OF STATE
 (See Fig. 6-11 for definition of symbols)

This page intentionally left blank.

APPENDIX

HIGH DENSITY MODELS FOR SEMIEMPIRICAL COLD EQUATIONS OF STATE FOR SOLIDS

Christian Peltzer

I. INTRODUCTION

Various high density models for solids have been introduced to calculate equations of state of materials valid in the pressure range attainable through explosions, high velocity impacts, etc. It is important to realize that the resulting equations of state are "asymptotic model equations of state," not proper mathematical asymptotic forms (in the limit of very high densities) of the exact equation of state of the system. Because of their ad hoc nature it is difficult, if at all possible, to establish their range of validity and to give estimates of the error involved in their use in various density ranges. An answer to such questions can only be obtained within a more general framework that would allow a precise mathematical formulation of the physical assumptions made and a bona fide estimate of the resulting error.

The basic physical assumptions underlying all high density models are that, in the limit of very high densities, all shell structure of individual atoms disappears and that the energy of the electron system tends towards that of a uniform density system.

Here we discuss briefly various high density models* and the corresponding cold equation of state.

* Only nonrelativistic models will be considered.

A general and powerful method for handling the basic, many-body problem of solid state physics has been developed by several authors. An outline of this method, the generalized density operator theory, will be given elsewhere;* there, we will try to show how it allows a unification of various cohesive energy theories and a better understanding of the approximations involved, and why it could lead to new and better computational techniques for obtaining equations of state. Any serious discussion of the validity of the various models used below is best deferred until this formalism has been introduced.

II. SIMPLEST HIGH DENSITY MODELS

A. Perfect Free-Electron Gas

The simplest high density model (Model I) is that of a perfect, free (i. e., noninteracting), electron gas of uniform density in a uniform positive background (necessary for charge neutrality). Such a system possesses only kinetic energy, the constant potential being taken as zero; this energy is a function of the electron density and so, for a fixed number of electrons, of the volume. (The electrons being fermions cannot all lie in the same lowest one-electron energy level even at $T = 0$.)

* Forthcoming ISR report (184531-110).

Let V be the specific volume of the system, M_m the molecular weight, $Z = \sum_i n_i Z_i$ the total number of electrons per molecule, ρ^e the electron density. Then

$$\rho^e = \frac{N_a Z}{M_m V} = \frac{N_a Z}{M_m V_{oo}} \xi^{-1} = \frac{Z}{v_a} \xi^{-1} = \text{const} \quad (1)$$

where N_a is Avogadro's number, $\xi = \frac{V}{V_{oo}}$ the relative specific volume ($V = V_{oo}$ at the reference state $P = 0$, $T = 0$), and v_a the effective atomic volume at the reference state.

The electron kinetic energy density ϵ_k of a perfect free electron gas is well known and is

$$\epsilon_k = \alpha_k \rho^e{}^{5/3} \quad (2)$$

with

$$\alpha_k = \left(\frac{3}{10} \right) \left(3\pi^2 \right)^{2/3} \frac{\hbar^2}{m} = 2.871 e^2 a_o = 3.505 \times 10^{-27} \text{ erg cm}^2 \quad (3)$$

where $a_o = \frac{\hbar^2}{me^2} = \text{Bohr radius} = 0.5292 \times 10^{-8} \text{ cm}$.

The internal energy per gram $E_c^I = V \epsilon_k$ is given by

$$E_c^I = A_k V^{-2/3} = B_k \xi^{-2/3} \quad (4)$$

with

$$A_k = \alpha_k \left(\frac{N_a Z}{M_m} \right)^{5/3} = \alpha_k \left(\frac{Z V_{oo}}{v_a} \right)^{5/3} \quad (5)$$

$$B_k = V_{oo}^{-2/3} A_k = \alpha_k V_{oo} \left(\frac{Z}{v_a} \right)^{5/3}$$

The corresponding cold pressure and bulk modulus are obtained from the thermodynamic relations:

$$P_c = - \frac{dE_c}{dV} = - \frac{1}{V_{oo}} \frac{dE_c}{d\xi} \quad B_c = - V \frac{dP_c}{dV} = - \xi \frac{dP_c}{d\xi} \quad (6)$$

and so

$$P_c^I = \frac{2}{3} A_k V^{-5/3} = \frac{2}{3} V_{oo}^{-1} B_k \xi^{-5/3}, \quad (7)$$

$$B_c^I = \frac{10}{9} A_k V^{-5/3} = \frac{10}{9} V_{oo}^{-1} B_k \xi^{-5/3}$$

is obtained.

The following relations should be noted

$$P_c^I V = \frac{2}{3} E_c^I \quad (\text{Virial theorem})$$

$$B_c^I = \frac{5}{3} P_c^I.$$

This model obviously does not exhibit any binding as E_c^I is a monotonic increasing function of $\rho = 1/V$ in the whole domain $(0, \infty)$. The energy zero chosen here corresponds to an infinitely dilute system, i. e., to the limit $\rho \rightarrow 0$ or $V \rightarrow \infty$.

B. Uniform Electron Gas with Exchange

Apparently, a better model could be that of a uniform density, imperfect, free electron gas in a uniform positive background. By imperfect we mean that the electrons are allowed to interact among themselves; the system will then have, besides its kinetic energy, a volume dependent potential energy.

The total energy density can be written as a sum of three terms

$$\epsilon = \epsilon_k + \epsilon_{ex} + \epsilon_{corr} \quad (8)$$

where the first term is the kinetic energy of the corresponding free electron gas (also often written $\bar{\epsilon}_F$ and called the mean Fermi

energy*), the second term is the exchange energy, and the third one the correlation energy.

The exchange effect is of a repulsive nature; its origin lies in the Pauli exclusion principle that prevents two electrons with parallel spins from occupying the same cell in phase space. (The Fermi statistics only limit the number of electrons per cell to two regardless of their spins.) It follows that an electron effectively will strongly repel all other electrons having parallel spins, and one says that each electron is accompanied by a "Fermi hole."

The exchange energy of a free electron gas has often been calculated and is given by:

$$\epsilon_{ex} = -\alpha_x \rho^{4/3} \quad (9)$$

with

$$\alpha_x = \frac{3}{4} \left(\frac{3}{\pi} \right)^{1/3} e^2 = 0.7386 e^2 = 1.704 \times 10^{-19} \text{ erg cm}.$$

Neglecting the Coulomb correlation effects, the equation of state of Model II is given by

$$E_c^{II} = A_k V^{-2/3} - A_x V^{-1/3} = B_k \xi^{-2/3} - B_x \xi^{-1/3} \quad (10)$$

with

$$A_x = \alpha_x \left(\frac{N_a Z}{M_m} \right)^{4/3} = \alpha_x \left(\frac{Z V_{oo}}{v_a} \right)^{4/3} \quad (11)$$

$$B_x = V_{oo}^{-1/3} A_x = \alpha_x V_{oo} \left(\frac{Z}{v_a} \right)^{4/3}.$$

* One must not confuse the energy at the Fermi level ϵ_F and the mean Fermi energy $\bar{\epsilon}_F$, here equal to $\frac{3}{5} \epsilon_F$. The same remark holds for the correlation energies.

From Eqs. (10) and (6) we obtain

$$P_c^{II} = \frac{2}{3} A_k V^{-5/3} - \frac{1}{3} A_x V^{-4/3} = \frac{2}{3} \frac{B_k}{V_{oo}} \xi^{-5/3} - \frac{1}{3} \frac{B_x}{V_{oo}} \xi^{-4/3}$$

(12)

and

$$B_c^{II} = \frac{10}{9} A_k V^{-5/3} - \frac{4}{9} A_x V^{-4/3} = \frac{10}{9} \frac{B_k}{V_{oo}} \xi^{-5/3} - \frac{4}{9} \frac{B_x}{V_{oo}} \xi^{-4/3}.$$

It is easily verified that the Virial theorem also holds for this model.

$$P_c^{II} V = \frac{2}{3} E_{kin} + \frac{1}{3} E_{pot}$$

where $E_{kin} = E_c^I$ and $E_{pot} = -E_x =$ exchange energy.

Model II corresponds to the Hartree-Fock approximation for a uniform density electron gas; the kinetic energy of the system is the same as that of a perfect electron gas, but this model exhibits some binding because of the repulsive nature of the exchange interaction which is included now. Its equilibrium volume V_{equ}^{II} , i. e., the volume minimizing E_c^{II} , is obtained as the solution of

$$P_c^{II} = 0,$$

and one has

$$V_{equ}^{II} = \left(\frac{2A_k}{A_x} \right)^3 = 41.95 \frac{Z}{M_m} = 69.622 \frac{Z V_{oo}}{v_a \times 10^{24}}$$

(13)

or

$$\xi_{equ}^{II} = 41.95 \frac{Z}{V_{oo} M_m} = 69.622 \frac{Z}{v_a \times 10^{24}}.$$

One sees that ξ_{equ}^{II} is, in general, much larger than 1; the binding is too weak. At the reference state, Model II gives a pressure of the order of the megabar instead of zero.

Using Eqs (10) and (12) as semiempirical equations of state, treating A_x as an adjustable parameter to be determined from the relation

$$\xi_{\text{equ}}^{\text{II}} = \frac{1}{V_{\text{oo}}} \left(\frac{2A_k}{A_x} \right)^2 = 1,$$

is essentially McMillan's empirical procedure applied to the uniform electron gas model instead of the T-F model.

C. Uniform Electron Gas with Exchange and Correlation

The origin of the correlation energy lies in the Coulomb interaction of the electrons; this is a classical two-body interaction given by terms of the form e^2/r_{ij} where r_{ij} is the distance between the i^{th} and j^{th} electrons. It depends on the simultaneous positions of the two electrons, hence the name "correlation effects." The Coulomb interaction between like sign charges being of a repulsive nature and this repulsive energy becoming infinite for $r_{ij} = 0$, one can say that each electron is surrounded by a "Coulomb hole" with respect to all other electrons. As the exchange effect gives rise to a similar effect for each electron with respect to all other electrons with parallel spins, the main part of the Coulomb correlation energy of an electron gas will arise from the interaction between electrons with opposite spins if the exchange effect has already been taken into account. The Coulomb correlations give rise to a change in both the kinetic energy of the electrons (with respect to that of a perfect free electron gas) and their potential energy, the net effect being a lowering of the total energy of the system, i.e., an increase in the binding.

A clear distinction must be kept between a uniform density electron gas and a uniform continuous charge distribution. If we replace the electron gas by such an equivalent (charge wise) continuous distribution, the electrostatic potential energy of the total system (electron and nuclei) would be zero here, each volume element being neutral.

The electrostatic potential energy of the continuous charge distribution equivalent to the electrons can be called the "classical electrostatic potential energy" of the electrons. But in such a replacement the localized nature of the electrons is neglected, and the direct electron-electron interaction is only partly taken into account, appearing as a classical screening effect. The (Coulomb) correlation energy will be defined here* as the difference between the energy calculated on the basis of the Hartree-Fock approximation and the exact one for a given Hamiltonian.

The evaluation of the average Coulomb correlation energy density $\bar{\epsilon}_{\text{corr}}$ is a considerably more difficult problem than that of the exchange energy, and explicit expressions valid for all densities have not yet been obtained. Wigner derived expressions for $\bar{\epsilon}_{\text{corr}}$ in the low density limit, and more recently Macke, Bohm and Pines, and others have given high density limit expressions. Various interpolation formulas have also been used by several authors. Here we shall only consider the high density limit expression in view of the asymptotic nature of the model and its general shortcomings.

One has for $\bar{\epsilon}_c$:

$$\bar{\epsilon}_c = -\alpha_c \rho^e \ln \alpha(\rho^e)^{1/3} - \alpha_d \rho^e \quad (14)$$

with

$$\alpha_c = \frac{1}{\pi^2} (1 - \ln 2) \frac{e^2}{a_o} = 0.0311 \frac{e^2}{a_o} = 1.356 \times 10^{-12} \text{ erg}$$

$$\alpha = \left(\frac{4\pi}{3} \right)^{1/3} a_o = 0.853 \times 10^{-8} \text{ cm}$$

$$\alpha_d = 0.048 \frac{e^2}{a_o} = 2.092 \times 10^{-12} \text{ erg}$$

* Several other definitions of the correlation energy are used in the literature.

Model III is that of a uniform density, imperfect electron gas in a uniform positive background, exchange and correlation effects being taken into account in an approximate way (essentially through a high density perturbation expansion).

One obtains for the cold internal energy per gram E_c^{III} :

$$E_c^{\text{III}} = A_k V^{-2/3} - A_x V^{-1/3} + A_c \ln V - A_d \quad (15)$$

or

$$E_c^{\text{III}} = B_k \xi^{-2/3} - B_x \xi^{-1/3} + B_c \ln \xi - B_d$$

with

$$\begin{aligned} A_c &= \frac{1}{3} \alpha_c \left(\frac{N_a Z}{M_m} \right) & B_c &= A_c \\ A_d &= \alpha_c \left(\frac{N_a Z}{M_m} \right) \ln \alpha \left(\frac{N_a Z}{M_m} \right)^{1/3} + \alpha_d \left(\frac{N_a Z}{M_m} \right) \\ B_d &= A_d - A_c \ln V_{oo} . \end{aligned} \quad (16)$$

The cold pressure and cold bulk modulus are given here by

$$\begin{aligned} P_c^{\text{III}} &= \frac{2}{3} A_k V^{-5/3} - \frac{1}{3} A_x V^{-4/3} - \frac{A_c}{3} V^{-1} \\ &= \frac{2}{3} \frac{B_k}{V_{oo}} \xi^{-5/3} - \frac{1}{3} \frac{B_x}{V_{oo}} \xi^{-4/3} - \frac{1}{3} \frac{B_c}{V_{oo}} \xi^{-1} \end{aligned} \quad (17)$$

and

$$\begin{aligned} B_c^{\text{III}} &= \frac{10}{9} A_k V^{-5/3} - \frac{4}{9} A_x V^{-4/3} - \frac{A_c}{3} V^{-1} \\ &= \frac{10}{9} \frac{B_k}{V_{oo}} \xi^{-5/3} - \frac{4}{9} \frac{B_x}{V_{oo}} \rho^{-4/3} - \frac{1}{3} \frac{B_c}{V_{oo}} \rho^{-1} \end{aligned} \quad (18)$$

The inclusion of the correlation increases the binding, but one can verify that the pressure at the reference state is still of the order of the megabar in general. The equilibrium volume $V_{\text{equ}}^{\text{III}}$ is given by the positive root of the equation $P_c^{\text{III}} = 0$, i.e.,

$$V_{\text{equ}}^{\text{III}} = \left[\frac{4A_k}{A_x + \sqrt{A_x^2 + 8A_k A_c}} \right]^3, \quad (19)$$

and, in general, the corresponding $\xi_{\text{equ}}^{\text{III}}$ is $\gg 1$.

Because of the $(\ln V)$ -term, Eq (17) cannot be used over the whole range $(0, \infty)$ of V . To obtain an expression valid in this whole range one could simply replace the $\bar{\epsilon}_{\text{corr}}$ of Eq (14) by an interpolation formula having (14) as high density asymptotic limit and going over into Wigner's expression, e.g., in the limit of low densities. The validity of such an interpolation formula is, of course, always open to question at intermediate densities. (See II).

D. Uniform Electron Gas with a Positive Lattice Background ^{13,14}

In the previous models, charge neutrality of the system was obtained by assuming the existence of a uniform, continuous, positive charge distribution; such a background differs markedly from that of real matter, and it seems more natural to represent the nuclei system by a positive point charge distribution. The model to be considered now is that of a uniform electron gas with such a positive lattice background.

The essential assumptions made are that the kinetic energy of the nuclei is negligible, that the static approximation is valid (allowing the separation of the electrons and nuclei motions), and that the nuclei form a regular lattice. For simplicity we will consider here only one kind of nuclei and a simple lattice (no basis).

The assumption of a regular lattice is made plausible (for all elements except He and possibly Li) by the fact that the energy associated with the formation of the lattice is negative and by Abrikosov's¹⁴ estimate of the zero point nuclear vibration amplitudes for this model. As Z , the atomic number, factors out in the expression for the lattice binding energy, the geometry of the energetically most favorable lattice is independent of Z (universal for all elements). In principle it should be obtained by strict maximization of this lattice energy, but the energy differences for different lattices are small and within the limits of accuracy of the model one can limit oneself to a cubic one. On the other hand, for polyatomic materials energy differences between various nuclei geometries could be greater, and further study of this point seems worthwhile.

The total energy of the system can be written as a sum of three terms, and in the high density limit the leading one is the kinetic energy of the corresponding perfect free electron gas ϵ_k . In the approximation considered the exchange and correlation energies will be the same as before, up to an additional electron-nuclei correlation energy. But the "classical" electrostatic energy of the electrons, ϵ_{cl} , will no longer be zero (as with a uniform positive background). There are three contributions to ϵ_{cl} : the nuclei-nuclei, the electron-nuclei, and the electron-electron Coulomb interaction energies; but the three must be handled together as each separately would diverge for an infinite solid. We emphasize again that in calculating ϵ_{cl} the electrons are replaced by continuous charge distribution of density $(-e\rho^e)$ and that the electron-electron interaction taken into account is only the classical screening effect of such a charge distribution, i. e., only a partial, average, electron-electron Coulomb interaction.

One obtains* for ϵ_{cl} :

$$\epsilon_{cl} = -\alpha_{cl} \rho e^{4/3} \quad \text{with} \quad \alpha_{cl} \cong 1.44 e^2 Z^{2/3}. \quad (20)$$

This energy results from the formation of the lattice and is sometimes called the "lattice binding energy."

Neglecting correlation terms, we obtain the Model IV equation of state

$$E_c^{IV} = A_k V^{-2/3} - (A_x + A_{cl}) V^{-1/3},$$

or

$$E_c^{IV} = B_k \xi^{-2/3} - (B_x + B_{cl}) \xi^{-1/3}$$

with A_k , A_x , B_k , B_x given as before, and

$$A_{cl} = 1.44 e^2 Z^{2/3} \left(\frac{N_a Z}{M_m} \right)^{4/3} = 1.44 e^2 Z^{2/3} \left(\frac{Z V_{oo}}{v_a} \right)^{4/3}$$

and

$$B_{cl} = A_{cl} V_{oo}^{-1/3} = 1.44 e^2 V_{oo} Z^{2/3} \left(\frac{Z}{v_a} \right)^{4/3}.$$

Comparing (21) and (10) (uniform electron gas with exchange in uniform positive background), one sees that:

- 1) The lattice binding energy E_{cl} is of the same order in V as the exchange energy (in the high density limit).
- 2) E_{cl} is proportional to Z^2 while E_x is proportional to $Z^{4/3}$ only; one has

$$\frac{E_x}{E_{cl}} = \frac{\alpha_x}{\alpha_{cl}} Z^{-2/3} \cong \frac{0.74}{1.44} Z^{-2/3} \cong 0.514 Z^{-2/3} \quad (23)$$

* Abrikosov¹⁴ gives $\alpha_{cl} = 1.3$; we obtained 1.41 for a sc lattice and 1.44 for a fcc and a bcc.

- 3) The binding is considerably greater in this model and the equilibrium volume is now:

$$V_{\text{equ}}^{\text{IV}} = \left(\frac{2A_k}{A_x + A_{cl}} \right)^3 \approx \frac{16.90}{[0.74 + 1.44Z^{2/3}]^3} \frac{Z}{M_m} \quad (24)$$

or

$$\xi_{\text{equ}}^{\text{IV}} \approx \frac{41.73}{[1 + 0.514Z^{2/3}]^3} \frac{Z}{V_{\text{oo}} M_m}.$$

One can verify that, in general, $\xi_{\text{equ}}^{\text{IV}}$ is less than 1 (while $\xi_{\text{equ}}^{\text{III}} \gg 1$). At the reference state Model IV gives a negative pressure, i.e., a tension state rather than a compression state of the order of the megabar.

We can also consider a Model V by introducing here the correlation energy; these corrective terms are of the same form, in the high density limit, as in the case of the uniform background, and their effect is similar (see II).

As we have seen, Models II and III exhibit considerably too weak a binding, while Model IV exhibits too strong a one at normal densities. Although these two models could be used as bounds for the exact cold isotherm E_c , such a property has in no way been proved here. The rigorous derivation of sharp enough upper and lower bounds for E_c , P_c , B_c over an extended range of densities appears to be an almost impossible problem in the frame of the standard approaches to the study of the ground state of most quantum mechanical systems; but we believe that significant progress in obtaining such results can reasonably be expected by rephrasing the problem in the generalized density operator formalism and making better use of the available tools of modern functional analysis. Preliminary studies along this line are presently being conducted here at Stanford Research Institute (ISR-184531-110).

III. THE T-F AND THE T-F-D STATISTICAL MODELS FOR MONO-ATOMIC CRYSTALS

A. Introduction

The semiclassical statistical approach, introduced by Thomas and Fermi in 1927 and developed since by many others, is very simple conceptually but its range of validity and proper estimates of the errors involved (as compared to the Hartree, Hartree-Fock, and/or the exact solution for a given Hamiltonian) have not yet been established, although significant progresses have recently been made in answering such questions, in particular by March, Kirzhnits and others. A discussion of the foundations of the statistical method is best conducted within the frame of the generalized density operator theory and will be given elsewhere. Here we shall give only an heuristic and a variational derivation of the basic equation of the T-F and T-F-D models and shall compare the resulting equations of state for solids with those already obtained.

B. Description of the Models and Heuristic Derivation of the Basic Relation

In the simplest statistical models a solid, represented by a system of electrons in a positive lattice background, is treated in the following manner. The kinetic energy of the nuclei is neglected, and the validity of the static approximation is assumed; furthermore, one argues heuristically that:

- 1) The electron system can be treated locally as a free electron gas--with exchange in the T-F-D model--raised at some position dependent electrostatic potential $V(\vec{r})$.

- 2) The electron system is in a bound state and in statistical equilibrium, i. e., no energy can be gained by transferring an electron from one point to another in the solid.
- 3) The electrostatic potential of the electrons can be taken as that of an equivalent (charge wise) continuous charge distribution $-e\rho(\vec{r})$ satisfying the classical Poisson equation with the usual continuity conditions for $V(\vec{r})$ and $\epsilon_n = -\frac{dV}{dn}$ across any boundary surface.

$$\Delta V^e(\vec{r}) = 4\pi e\rho^e(\vec{r}) \quad (1)$$

+ b. c.

- 4) The total energy of the electron-nuclei system can be obtained, in the T-F model, as the sum of the free electron kinetic energy E_k and the "classical" electrostatic potential energy of the system E_{cl} . In the T-F-D model the Pauli correlation effects are approximately taken into account by adding the free electron gas exchange energy E_x .

From these assumptions, one derives the basic relation of the model, namely, the relation between $\rho^e(\vec{r})$ and the total electrostatic potential $V(\vec{r})$

$$V(\vec{r}) = V_n(\vec{r}) + V_e(\vec{r}) + V_{ext}(\vec{r})$$

where V_n is the potential due to the nuclei, V_e that due to the electrons and V_{ext}^* any external one.

* V_{ext} is assumed null in the sequel.

From 1) and 2) it follows that the energy of an electron at a point \vec{r} is given by

$$\frac{p^2(\vec{r})}{2m} - eV(\vec{r}) - \frac{e^2}{\pi\hbar} p(\vec{r})$$

Since one is considering bound states, one must also have the relation

$$\frac{p^2}{2m} - eV(\vec{r}) - \frac{e^2}{\pi\hbar} p(\vec{r}) \leq -eV_0 \quad (2)$$

where $-eV_0$, the maximum potential energy of an electron at \vec{r} , is position independent (from condition c)).

The maximum momentum $p_{\max}(\vec{r})$ of a free electron gas is related to the electron density by

$$p_{\max}(\vec{r}) = (3\pi^2)^{1/3} \hbar \rho^{1/3}$$

Combining these two relations, one obtains the basic relation of the T-F and T-F-D models:

$$\frac{1}{2m} p_{\max}^2(\vec{r}) - \frac{e^2}{\pi\hbar} p_{\max}(\vec{r}) = e(V - V_0)$$

or

$$e(V - V_0) = (3\pi^2)^{2/3} \frac{\hbar^2}{2m} \rho^{2/3} - \left(\frac{3}{\pi}\right)^{1/3} e^2 \rho^{1/3} \quad (3)$$

$$= \frac{5}{3} \alpha_k \rho^{2/3} - \frac{4}{3} \alpha_x \rho^{1/3}$$

or

$$\rho^{e\vec{r}} = A \left\{ a + [a^2 + (V - V_0)]^{\frac{1}{2}} \right\}^3 \quad (4)$$

with

$$A = \frac{(2em)^{3/2}}{3\pi^2 \hbar^3} = \left(\frac{3e}{5\alpha_k}\right)^{3/2} \quad a = (2em)^{\frac{1}{2}} \frac{e}{\hbar} = \frac{2\alpha_x}{(15e\alpha_k)^{\frac{1}{2}}} \quad (4')$$

(For the T-F model, one sets $a = 0$.)

This relation, of course, holds only in regions where

$$a^2 + (V - V_0) \geq 0$$

and in regions of zero electron density, the Poisson equation is replaced by Laplace's equation. Knowing $\rho^e(\vec{r})$ and $V(\vec{r})$, the total energy of the system is obtained from:

$$\begin{aligned} E = & \int \rho^e(\vec{r}) \epsilon_k(\vec{r}) d\vec{r} + \int \rho^e(\vec{r}) \epsilon_x(\vec{r}) d\vec{r} \\ & + \int \left(V_n + V_e \right) \rho^e(\vec{r}) d\vec{r} + E_{n-n} \end{aligned} \quad (5)$$

C. Variational Derivation of the Basic Relation

It is of interest to note that the basic relations (3) or (4) can also be obtained from a variational principle, namely by minimizing the total energy E --as given by (5)--under variation of the electron density $\rho^e(\vec{r})$ for fixed boundaries (and so fixed nuclei) and subject to the subsidiary condition

$$\int \rho^e(\vec{r}) d\vec{r} = \mathcal{N} = \text{const} \quad (6)$$

(\mathcal{N} = fixed total number of electrons.)

Introducing a Lagrange multiplier V_0 , the extremum condition is is

$$\delta [E + e\mathcal{N}V_0] = 0 . \quad (7)$$

Using the expressions given previously for ϵ_k and ϵ_x and the relation

$$V_e(\vec{r}) = \int \frac{\rho^e(\vec{r}') d\vec{r}'}{|\vec{r}' - \vec{r}|} \quad (8)$$

(i.e., Poisson's equation) one can write the energy in the form:

$$\begin{aligned} E = & \int \left[\alpha_k \rho^{5/3}(\vec{r}) - \alpha_x \rho^e(\vec{r})^{4/3} \right] d\vec{r} + \frac{e^2}{2} \iint d\vec{r} d\vec{r}' \frac{\rho^e(\vec{r}) \rho^e(\vec{r}')}{|\vec{r}' - \vec{r}|} \\ & - e \int V_n(\vec{r}) \rho^e(\vec{r}) d\vec{r} + E_{n-n} \end{aligned} \quad (9)$$

and Eq (7) gives

$$\int \left[\alpha_k \frac{5}{3} \rho^{e^{2/3}}(\vec{r}) - \frac{4}{3} \alpha_x \rho^{e^{1/3}}(\vec{r}) \right] d\vec{r} - e \int (V_n - V_o) d\vec{r} + \frac{e^2}{2} \iint \frac{\rho^e(\vec{r})}{|\vec{r}' - \vec{r}|} d\vec{r} d\vec{r}' + \frac{e^2}{2} \iint \frac{\rho^e(\vec{r}')}{|\vec{r}' - \vec{r}|} d\vec{r} d\vec{r}' = 0$$

or

$$\int \left\{ \frac{5}{3} \alpha_k \rho^{e^{2/3}} - \frac{4}{3} \alpha_x \rho^{e^{1/3}} - e(V - V_o) \right\} d\vec{r} = 0.$$

In view of the bound state condition (2), it follows that the Lagrange multiplier, V_o , is the maximum electron potential and that

$$e(V - V_o) = \frac{5}{3} \alpha_k \rho^{e^{2/3}} - \frac{4}{3} \alpha_x \rho^{e^{1/3}}$$

Q.E.D.

D. Some General Remarks on the T-F and T-F-D Models

The basic quantities in the statistical models are the electron density $\rho^e(\vec{r})$ and the electrostatic potential $V(\vec{r}) = V_n(\vec{r}) + V_e(\vec{r})$ + eventually an external potential. An heuristic argument or an equivalent variational procedure leads to the basic nonlinear relations Eqs (3) or (4) of the T-F and T-F-D theories; the assumption of the validity of Poisson's equation and the usual electrostatic boundary conditions complete the description of the models.

In discussing this approach, one can distinguish two groups of specific assumptions, besides those leading to the corresponding Hamiltonian of the proper quantum mechanical approach:

- 1) The exact energy expression for the given Hamiltonian is replaced by a simpler one where not only the correlation terms are omitted, but also the kinetic energy is simplified by neglecting the effect of density gradients (off diagonal part of $\Gamma(x'_1, x_1)$, the 1st order generalized density matrix).

- 2) The description of the system in terms of the wave function $\Phi(x_1, \dots)$ or the reduced density matrices $\Gamma(x'_1, x_1)$, $\Gamma(x_1 x_2)$ is replaced by a description in terms of $\rho(\vec{r})$ alone, i.e., essentially in terms of the diagonal part only of the first order density matrix, $\Gamma(x'_1, x_1)$.
- 3) The electron density $\rho^e(\vec{r})$ is calculated on the basis of heuristically derived, essentially classical equations, rather than by solving the proper Schrödinger equation.

The difficulties in assessing the exact significance of this approach lie essentially in the last two assumptions. A proper foundation of the statistical method would require not only an estimate of the neglected terms in the energy expression, but also a derivation of Eqs (1), (3), or (4) as a meaningful approximation to the quantum mechanical ones. Although several authors have recently made significant progress in this direction, no complete solution of the problem is yet available. It should also be noted that the statistical approach (T-F, T-F-D suitably modified) is not necessarily limited to the accuracy of the Hartree-Fock approximation but could very well offer in specific problems, a better approximation to the exact solution, especially in view of the difficulties in obtaining any degree of self-consistency in H-F calculations for solids.

E. The T-F and T-F-D Models for Simple Monoatomic Crystals

1. General Equations

For a crystal of lattice given by

$$\vec{R}_{(n)} = \sum_i n_i \vec{a}_i \quad n_i = \pm, 0 \text{ integers}$$

and such that all lattice sites are occupied by identical atoms of atomic number Z , the energy per atom in the T-F-D method can be written as:

$$E_{\Omega} = \lim_{N \rightarrow \infty} \frac{1}{N} \left\{ \int_{N\Omega} \rho^e(\vec{r}) \epsilon_k(\vec{r}) d\vec{r} + \int_{N\Omega} \rho^e(\vec{r}) \epsilon_x(\vec{r}) d\vec{r} - \sum_{(m)} \int_{N\Omega} \frac{Ze\rho^e(\vec{r})}{|\vec{R}_{(m)} - \vec{r}|} d\vec{r} + \frac{1}{2} \sum_{(m)} \sum'_{(n)} \frac{Z^2 e^2}{|\vec{R}_{(m)} - \vec{R}_{(n)}|} + \frac{1}{2} \iint_{N\Omega} \frac{\rho^e(\vec{r}') \rho^e(\vec{r})}{|\vec{r}' - \vec{r}|} d\vec{r} d\vec{r}' \right\}$$

where Ω is the primitive cell of volume $= (\vec{a}_1, \vec{a}_2, \vec{a}_3)$. (For the T-F expression one should take $\epsilon_x \equiv 0$.)

Using the translational invariance of the crystal

$$\rho^e(\vec{r} + \vec{R}_{(m)}) = \rho^e(\vec{r}) \quad V(\vec{r} + \vec{R}_{(n)}) = V(\vec{r})$$

to simplify this energy expression one obtains:

$$E_{\Omega} = \int_{\Omega_0} \left[\alpha_k \rho^{5/3}(\vec{r}) - \alpha_x \rho^{4/3}(\vec{r}) \right] d\vec{r} - eZ \int_{\Omega_0} \frac{\rho^e(\vec{r})}{|\vec{r}|} d\vec{r} + \frac{e^2}{2} \iint_{\Omega_0} \frac{\rho^e(\vec{r}) \rho^e(\vec{r}')}{|\vec{r}' - \vec{r}|} d\vec{r}' d\vec{r} \quad (10)$$

$$+ \frac{1}{2} \sum'_{(m)} \left\{ \frac{e^2 Z^2}{|\vec{R}_{(m)}|} - 2eZ \int_{\Omega_0} \frac{\rho^e(\vec{r})}{|\vec{R}_{(m)} - \vec{r}|} d\vec{r} + e^2 \iint_{\Omega_0} \frac{\rho^e(\vec{r}) \rho^e(\vec{r}')}{|\vec{R}_{(m)} + \vec{r}' - \vec{r}|} d\vec{r} d\vec{r}' \right\}$$

and the boundary value problem giving the electron density reduces to a boundary value problem in a single cell Ω_0 .

For the simple monoatomic solid considered here $\rho^e(\vec{r})$ is to be obtained as a solution of the system of equations:

$$e[V(\vec{r}) - V_0] = \frac{5}{3} \alpha_k \rho^e{}^{2/3}(\vec{r}) - \frac{4}{3} \alpha_x \rho^e(\vec{r})^{1/3} \quad (11)$$

$$\Delta[V(\vec{r}) - V_0] = 4\pi e \rho^e(\vec{r}),$$

with the boundary conditions

$$\lim_{r \rightarrow 0} rV(\vec{r}) = \lim_{r \rightarrow 0} r[V - V_0] = eZ \quad (12)$$

$$\epsilon_n = - \left. \frac{dV}{dn} \right|_{S_\Omega} = 0 \quad S_\Omega = \text{surface of the cell}$$

The first boundary condition states that the total potential converges to that of the nuclei $+Ze$ as $r \rightarrow 0$; the second follows from the lattice translational invariance, the continuity requirement on ϵ_n and the inversion symmetry of Ω and V . One should note that the translational invariance automatically insures the continuity of $V(\vec{r})$ across S (if V is bounded on S).

2. The Sphere Approximation

The "sphere approximation" consists:

a) in replacing the W-S polyhedron cell Ω by a sphere of equal volume, the so-called Wigner-Seitz sphere of radius r_s given by

$$r_s = \left[\frac{3}{4\pi} \Omega_0 \right]^{1/3} = \left(\frac{3v_a}{4\pi} \right)^{1/3} \quad (13)$$

where v_a = atomic volume ;

b) in assuming that the electron density and electrostatic potential are spherically symmetric

$$\rho^e = \rho^e(r) \quad \text{and} \quad V = V(r) \quad r = |\vec{r}| ; \quad \text{and}$$

c) in neglecting the overlap of the "equivalent spheres" in calculating the energy of the system.

With these supplementary assumptions the equations for ρ^e take the form

$$e[V(r) - V_0] = \frac{5}{3} \alpha_k \rho^e(r)^{2/3} - \frac{4}{3} \alpha_x \rho^e(r)^{1/3} \quad (14)$$

$$\frac{1}{r} \frac{d^2}{dr^2} (rV(r)) = 4\pi \rho^e(r)$$

with the boundary conditions

$$\lim_{r \rightarrow 0} r[V(r) - V_0] = eZ \quad (15)$$

$$-\left. \frac{dV}{dr} \right|_{r=r_s} = 0 \quad (\text{and } V(r_s) = 0)$$

and the energy expression reduces to

$$E_\Omega = 4\pi \int_0^{r_s} \left[\alpha_k \rho^e(r)^{5/3} - \alpha_x \rho^e(r)^{4/3} \right] r^2 dr \quad (16)$$

$$- 4\pi e \int_0^{r_s} \left[\frac{Z}{r} - 2\pi \int_0^r \frac{\rho^e(r') r'^2 dr'}{|r' - r|} \right] \rho^e(r) r^2 dr,$$

i.e., to that of an "equivalent spherical atom." The only difference between a free atom problem and that of a solid in the sphere approximation is that in the later case $\rho^e(r_s)$ is not equal to zero in general, so the pressure at the atom boundary due to the electrons is also different from zero (compressed atoms).

Note that the overlap correction terms neglected are of the form

$$N \xrightarrow{\lim} \frac{1}{N} \left\{ \sum_{(m)}' \frac{e^2 Z^2}{2 |\vec{R}_{(m)}|} - 4\pi eZ \int_0^{r_s} \frac{\rho^e(r) r^2 dr}{|\vec{R}_{(m)} - \vec{r}|} + \right.$$

$$\left. + (4\pi)^2 \frac{e^2}{2} \int \int_0^r r'^2 r^2 \frac{\rho^e(r) \rho^e(r')}{|\vec{r}' - \vec{r} + \vec{R}_{(m)}|} dr' dr \right\} \quad (16)$$

and were included in the calculation of the energy of the uniform electron gas in a positive lattice background.

F. Some Remarks on the Sphere Approximation and on the Inclusion of Correlation Effects in the T-F-D Model

Clearly the sphere approximation is in no way justified for solids and is made solely for convenience to reduce the 3-dimensional boundary value problem giving ρ^e to a 1-dimensional one. Some of the physical consequences of this approximation are that:

1) The crystallographic structure of the solid is almost completely washed away, the volume of the cell being the only remaining geometrical parameter.

2) Since the solid is replaced by a collection of neutral spheres with spherical symmetric charge distributions, no energy is involved in forming the solid--only in compressing the individual atoms, and this model cannot offer any resistance to shear stresses.

3) The extension of such a model to nonsimple crystals, in particular to polyatomic ones, can be done only in a very artificial way (such as the smoothing technique) or by introducing "effective mono-atomic models," i.e., through largely artificial and arbitrary averaging procedures.

4) Calculation of the electronic structure of the solid in this approximation is almost meaningless.

If, at the time of the development of the T-F, T-F-D models, the available mathematical tools seemed to leave little hope of dealing successfully with the 3-dimensional problem, the recent developments

in mathematical techniques for handling such nonlinear problems--in particular variational ones--have completely altered the picture, and it appears that approximate solutions and proper error estimates could be obtained for the actual problem.

This is one direction along which further research at this time is possible. Within the limits of the statistical approach it would allow one to obtain a more complete and realistic model for monoatomic and polyatomic solids at high pressures including the pressure dependence of the elastic coefficients, dielectric tensor and degree of anisotropy; possible high pressure phase transformations could be better handled and eventually the electronic structure of different types of materials could also be studied over an extended density range by solving the Bloch problem with the 3-dimensional statistical crystal potential.

Correlation effects can be introduced in the T-F-D model in the same approximate way as the exchange effect in the T-F model, namely, by adding to the energy expression a term arising from the correlation energy of the locally free electron gas:

$$E_{\text{corr}} = \int \rho^e(\vec{r}) \bar{\epsilon}_{\text{corr}}[\rho^e] d\vec{r}.$$

This has been done by Gombas, Lewis, and Erma. The resulting basic relation between ρ^e and $V(r)$ becomes quite involved, and a straightforward numerical treatment in the line of those applied to the T-F-D model is almost prohibitive. Also the value of this extension of the statistical method is very doubtful for it still leaves out completely the inhomogeneity corrections* which can be at least of the same order as the Coulomb correlation one.

A second direction along which profitable work on the statistical approach could be done presently is in obtaining meaningful extensions

* These are essentially kinetic energy correction terms that take partly into account the effect of potential (or electron density) gradients.

of the T-F-D models; these should incorporate both inhomogeneity corrections and correlation effects in a consistent fashion--at least to the same order in a perturbation expansion--and should include a practical computational scheme. Various formal extensions¹⁰ have been proposed in the last few years by several authors, but little numerical work is available outside free atom calculations.

These different schemes are being presently evaluated, partly in conjunction with basic work on the statistical and generalized density operator theory, and we shall eventually report later on their possible use in deriving improved equations of state for solids.

This page intentionally left blank.

REFERENCES

1. Fowles, G. R. , Investigation of Equation of State of Porous Earth Media, Stanford Research Institute, Project GSU-4475, Final Report, Technical Documentary Report No. WL TDR-64-59 August 1964.
2. Rice, M. H. , R. G. McQueen, and J. M. Walsh, Compression of Solids by Strong Shock Waves, Solid State Physics, Vol. 6, Seitz, F. and D. Turnbull, eds. , Academic Press, New York, 1958.
3. Gregson, Jr. , V. G. , Driver Plate Pressures, Stanford Research Institute, Poulter Laboratories Internal Report 003-64.
4. Al'tshuler, L. V. , A. A. Bakanova, and R. F. Trunin, Phase Transformations of Water Compressed by Strong Shock Waves, Soviet Physics/Doklady 3, 761-763 (1958).
5. Wiedermann, A. H. and O. E. Curth, Shock Unloading Characteristics of Crushable Rocks, Air Force Weapons Laboratory Report, WL-TDR-64-52, August 1964.
6. Graham, R. A. , F. W. Nielson, and W. B. Benedick, Piezoelectric Current from Shock-Loaded Quartz - A Submicrosecond Stress Gauge, J. Appl. Phys. 36, 1775 (1965).
7. Chabai, A. J. , Synthesis of Shock Hugoniot for Rock Materials, Rock Mechanics, (Proceedings of 5th Symposium on Rock Mechanics, U. of Minnesota, May 1962), ed. by C. Fairhurst, MacMillan Company, New York, 1963.
8. Tillotson, J. H. , Metallic Equations of State for Hypervelocity Impact, General Atomic Report GA-3216, July 18, 1962.
9. Brush, S. G. , Equation of State: A Survey of the Thermodynamic Properties of Matter at High Pressures and Temperatures, UCRL-7437, June 12, 1964.

10. Balazs, Nandor L. , Thomas-Fermi Theory of the Atom as a Solution of the Density-Matrix Hierarchy, *Phys. Rev.* 134, A841-852 (May 18, 1964).

Golden, Sidney, Statistical Theory of Electronic Energies, *Revs. Modern Phys.* 32, 322-327 (April 1960).

Kirzhnits, D. A. , Quantum Corrections to the Thomas-Fermi Equation, *Sov. Phys/JETP* 5, 64-71 (August 1957).

Kirzhnits, D. A. , The Limits of Applicability of the Quasi-Classical Equation of State of Matter, *Sov. Phys/JETP* (35)8, 1081-1089 (June 1959).

Kirzhnits, D. A. , Internal Structure of Super-Dense Stars, *Sov. Phys/JETP* 11, 365-368 (August 1960).
11. Kormer, S. B. , A. I. Funtikov, V. D. Urlin, and A. N. Kolesnikova, Dynamic Compression of Porous Metals and the Equation of State with Variable Specific Heat at High Temperatures, *Sov. Phys/JETP* 15, 477-488 (September 1962).

Kormer, S. B. , M. V. Sinitsyn, A. I. Funtikov, V. D. Urlin, and A. V. Blinov, Investigation of the Compressibility of Five Ionic Compounds at Pressures Up to 5 Mbar, *Sov. Phys/JETP* 20, 811-819 (April 1965).
12. Al'tshuler, L. V. , S. B. Kormer, M. I. Brazhnik, L. A. Vladimirov, M. P. Speranskaya, and A. I. Funtikov, "The Isentropic Compressibility of Aluminum, Copper, Lead, and Iron at High Pressures," *Sov. Phys/JETP* 11, 766-775 (October 1960).

Al'tshuler, L. V. , S. B. Kormer, A. A. Bakanova, and R. F. Trunin, Equation of State for Aluminum, Copper, and Lead in the High Pressure Region, *Sov. Phys/JETP* 11, 573-579 (September 1960).
13. Bellemans, A. and M. de Leener, Advances in Chemical Physics, VI, Interscience, 1964, p. 85--and references given here.
14. Abrikosov, A. A. , "Some Properties of Strongly Compressed Matter. I, *Sov. Phys/JETP* 12, 1254-1259 (June 1961).

15. Rayleigh, J. , Aerial Plane Waves of Finite Amplitude, Proc. Roy. Soc. 84, 247-284 (1910).
16. Bethe, H. A. , Theory of Shock Waves for an Arbitrary Equation of State, OSRD Report No. 545 (1942). Republished as Poulter Laboratories Report No. G-320, Stanford Research Institute.
17. Minshall, Stanley, Investigation of a Polymorphic Transition in Iron at 130 k.b. , Bull. Am. Phys. Soc. 29, No. 8, 23 (December 28, 1954).
18. Drummond, W. E. , Multiple Shock Production, J. Appl. Phys. 28, 998-1001 (September 1957).
19. Rice, M. H. , R. G. McQueen, and J. M. Walsh, Compression of Solids by Strong Shock Waves, Solid State Physics, Vol. 6, Seitz, F. and D. Turnbull, eds. , Academic Press, New York, 1958.
20. Duvall, George E. , Shock Wave Stability in Solids, Les Ondes de Detonation, Editions du Centre National de la Recherche Scientifique, 15 Quai Anatole-France - Paris (VII^e), 1962, pp. 337-352.
21. Bridgman, P. W. , Polymorphic Transitions of 35 Substances to 50,000 kg/cm² , Am. Acad. Proc. 72, No. 2, 45-136 (July 1937).
22. Slater, J. C. , Introduction to Chemical Physics, McGraw-Hill, 1939. p. 220 ff.
23. Courant, R. and K. O. Friedrichs, Supersonic Flow and Shock Waves, Interscience Publishers, New York, 1948, p. 143.
24. Duff, Russell, E. and F. Stanley Minshall, Investigation of a Shock-Induced Transition in Bismuth, Phys. Rev. 108, 1207-1212 (December 1, 1957).
25. Bancroft, Dennison, Eric L. Peterson, and Stanley Minshall, Polymorphism of Iron at High Pressure, J. Appl. Phys. 27, 291-298 (March 1956).
26. Johnson, P. C. , B. A. Stein, and R. S. Davis, Temperature Dependence of Shock-Induced Phase Transformations in Iron, J. Appl. Phys. 33, 557-561 (February 1962).
27. Bridgman, P. W. , Polymorphism, Principally of the Elements, up to 50,000 kg/cm² , Phys. Rev. 48, 893-906 (December 1, 1935).

28. Wackerle, Jerry, Shock-Wave Compression of Quartz, J. Appl. Phys. 33, 922-937 (March 1962).
29. Ahrens, Thomas J. and V. G. Gregson, Jr., Shock Compression of Crustal Rocks: Data for Quartz, Calcite, and Plagioclase Rocks, J. Geophys. Research 69, 4839-4874 (November 15, 1964).
30. Stishov, S. M., Equilibrium Lines between Coesite and a Rutile-like Modification of Silica, Dokl. Acad. Nauk SSSR 148, No. 5, 1186-1188 (1963).
31. Balchan, A. S. and H. G. Drickamer, High Pressure Electrical Resistance Cell, and Calibration Points above 100 kilobars, Rev. Sci. Instr. 32, 308-313 (March 1961).
32. Duvall, George E., Propagation of Plane Shock Waves in a Stress-Relaxing Medium, Stress Waves in Anelastic Solids, Kolsky, Herbert and William Prager, eds., Springer-Verlag, 1964.
33. Chao, E. C. T., J. J. Fahey, Janet Littler, and D. J. Milton, Stishovite, SiO_2 , a Very High Pressure New Mineral from Meteor Crater, Arizona, J. Geophys. Research 67, 419-421 (January 1962).
34. von Neumann, J. and R. D. Richtmyer, A Method for the Numerical Calculations of Hydrodynamic Shock, J. Appl. Phys. 21, 232-237 (1950).
35. Drummond, W. E., Multiple Shock Production, J. Appl. Phys. 28, 998-1001 (September 1957).
36. Erkman, J. O., Smooth Spalls and the Polymorphism of Iron, J. Appl. Phys. 32, 939-944 (1961).
37. Zel'dovich, Ya. B., On the Possibility of Rarefaction Shock Waves, J. Experimental and Theoretical Physics 16, #4, Moscow, 1946, p. 363-364; available in translation from U. S. Joint Publications Research Service, 1636 Connecticut Ave., N.W., Washington 25, D. C.
38. Nucholls, J. H., A Computer Calculation of Rainier (The First 100 Milliseconds), UCRL-5675, TID 4500, UC-35 (15th ed.), 1959.

Unclassified

Security Classification

DOCUMENT CONTROL DATA - R&D

(Security classification of title, body of abstract and indexing annotation must be entered when the overall report is classified)

1 ORIGINATING ACTIVITY (Corporate author) Stanford Research Institute Menlo Park, California		2a REPORT SECURITY CLASSIFICATION Unclassified	
		2b GROUP	
3 REPORT TITLE INVESTIGATION OF EQUATION OF STATE OF POROUS EARTH MEDIA			
4 DESCRIPTIVE NOTES (Type of report and inclusive dates) Final Report 15 June 1964 to 26 July 1965			
5 AUTHOR(S), (Last name, first name, initial) Anderson, G. D.; Duvall, G. E.; Erkman, J. O.; Fowles, G. R.; and Peltzer, C. P.			
6 REPORT DATE February 1966	7a TOTAL NO. OF PAGES 186	7b NO. OF REFS 38	
8a CONTRACT OR GRANT NO. AF29(601)-6427	9a. ORIGINATOR'S REPORT NUMBER(S) AFWL-TR-65-146		
b. PROJECT NO. 5710			
c. Subtask No. 13.144	9b. OTHER REPORT NO(S) (Any other numbers that may be assigned this report) SRI Project No. GSU-5059		
d			
10 AVAILABILITY/LIMITATION NOTICES Distribution of this document is unlimited.			
11. SUPPLEMENTARY NOTES		12. SPONSORING MILITARY ACTIVITY Air Force Weapons Laboratory (WLDC) Kirtland AFB, New Mexico 87117	
13 ABSTRACT Earlier experimental work has been extended to evaluate the effect of moisture on the Hugoniot of playa. For engineering applications the Hugoniot of moist playa can be predicted with sufficient accuracy from the Hugoniot of dry playa and water and the assumption of pressure equilibrium. Isentropic release data were obtained for moist and dry playa. The steep release curve (in the P-V plane) from high pressure implies an irreversible phase change. Some low pressure data in the elastic-plastic region are presented. A theoretical discussion of various forms of the Mie-Grüneisen equation and the physical basis of asymptotic statistical models is presented. Shock stability is reviewed. Phase transitions in which $\Delta V < 0$ are classified according to the signs of the slopes of the coexistence curves. Relative slopes of Hugoniots and isentropes in the mixed phase region are calculated. The results of the theoretical discussion are applied to transitions in bismuth, iron, and quartz. Agreement of values of dP/dT deduced from shock data and measured directly are good for bismuth and poor for quartz and iron. Calculations of spherical shock propagation in a hypothetical medium that undergoes a phase change are presented. The calculations show qualitatively some types of pulse shapes that may be expected in a transforming medium. It is concluded that the proper treatment of phase changes is an outstanding problem in predicting equations of state for earth materials.			

14. KEY WORDS	LINK A		LINK B		LINK C	
	ROLE	WT	ROLE	WT	ROLE	WT
Equation of State (EOS) Hugoniot Experiments Nevada Test Site Playa Isentropic Release Data Effect of Moisture Content Mie-Grüneisen Equation Thermodynamics Shock Stability Phase Transitions Spherical Shock Propagation High Density Models EOS for High Temperatures and Pressures						

INSTRUCTIONS

1. **ORIGINATING ACTIVITY:** Enter the name and address of the contractor, subcontractor, grantee, Department of Defense activity or other organization (*corporate author*) issuing the report.

2a. **REPORT SECURITY CLASSIFICATION:** Enter the overall security classification of the report. Indicate whether "Restricted Data" is included. Marking is to be in accordance with appropriate security regulations.

2b. **GROUP:** Automatic downgrading is specified in DoD Directive 5200.10 and Armed Forces Industrial Manual. Enter the group number. Also, when applicable, show that optional markings have been used for Group 3 and Group 4 as authorized.

3. **REPORT TITLE:** Enter the complete report title in all capital letters. Titles in all cases should be unclassified. If a meaningful title cannot be selected without classification, show title classification in all capitals in parenthesis immediately following the title.

4. **DESCRIPTIVE NOTES:** If appropriate, enter the type of report, e.g., interim, progress, summary, annual, or final. Give the inclusive dates when a specific reporting period is covered.

5. **AUTHOR(S):** Enter the name(s) of author(s) as shown on or in the report. Enter last name, first name, middle initial. If military, show rank and branch of service. The name of the principal author is an absolute minimum requirement.

6. **REPORT DATE:** Enter the date of the report as day, month, year; or month, year. If more than one date appears on the report, use date of publication.

7a. **TOTAL NUMBER OF PAGES:** The total page count should follow normal pagination procedures, i.e., enter the number of pages containing information.

7b. **NUMBER OF REFERENCES:** Enter the total number of references cited in the report.

8a. **CONTRACT OR GRANT NUMBER:** If appropriate, enter the applicable number of the contract or grant under which the report was written.

8b, 8c, & 8d. **PROJECT NUMBER:** Enter the appropriate military department identification, such as project number, subproject number, system numbers, task number, etc.

9a. **ORIGINATOR'S REPORT NUMBER(S):** Enter the official report number by which the document will be identified and controlled by the originating activity. This number must be unique to this report.

9b. **OTHER REPORT NUMBER(S):** If the report has been assigned any other report numbers (*either by the originator or by the sponsor*), also enter this number(s).

10. **AVAILABILITY/LIMITATION NOTICES:** Enter any limitations on further dissemination of the report, other than those

imposed by security classification, using standard statements such as:

- (1) "Qualified requesters may obtain copies of this report from DDC."
- (2) "Foreign announcement and dissemination of this report by DDC is not authorized."
- (3) "U. S. Government agencies may obtain copies of this report directly from DDC. Other qualified DDC users shall request through _____."
- (4) "U. S. military agencies may obtain copies of this report directly from DDC. Other qualified users shall request through _____."
- (5) "All distribution of this report is controlled. Qualified DDC users shall request through _____."

If the report has been furnished to the Office of Technical Services, Department of Commerce, for sale to the public, indicate this fact and enter the price, if known.

11. **SUPPLEMENTARY NOTES:** Use for additional explanatory notes.

12. **SPONSORING MILITARY ACTIVITY:** Enter the name of the departmental project office or laboratory sponsoring (*paying for*) the research and development. Include address.

13. **ABSTRACT:** Enter an abstract giving a brief and factual summary of the document indicative of the report, even though it may also appear elsewhere in the body of the technical report. If additional space is required, a continuation sheet shall be attached.

It is highly desirable that the abstract of classified reports be unclassified. Each paragraph of the abstract shall end with an indication of the military security classification of the information in the paragraph, represented as (TS), (S), (C), or (U).

There is no limitation on the length of the abstract. However, the suggested length is from 150 to 225 words.

14. **KEY WORDS:** Key words are technically meaningful terms or short phrases that characterize a report and may be used as index entries for cataloging the report. Key words must be selected so that no security classification is required. Identifiers, such as equipment model designation, trade name, military project code name, geographic location, may be used as key words but will be followed by an indication of technical context. The assignment of links, rules, and weights is optional.